2007

Characterization and Functional Analysis of Astrotactin 2 Reveals a Role for Endocytosis in Glial-guided Neuronal Migration

Perrin Megan Wilson

Characterization and Functional Analysis of Astrotactin 2 Reveals a Role for Endocytosis in Glial-Guided Neuronal Migration

A Thesis Presented to the Faculty of
The Rockefeller University
in Partial Fulfillment of the Requirements for
the degree of Doctor of Philosophy

by
Perrin Megan Wilson
June 2007

To my rock, my family: Mom, Dad, Bri-Anne, and Christopher

Acknowledgements

First, I would like to thank my advisor and mentor, Mary Beth Hatten for her continual support, guidance, and enthusiasm. I am also grateful for the encouragement, unique insight, and thoughtful discussions of my faculty committee: Leslie Vosshall, Cori Bargmann, Bob Darnell, and Peter Scheiffele. I would like to thank the entire Hatten Lab, especially Jee Hae Kim, David Solecki, Yung Lie, and Bob Fryer for their intellectual guidance, enlightening conversations, critical reading of this manuscript, and continuous support, Eve Govek for her thoughtful dialogue, Toshi Tomoda, Niels Adams, and Paul Matteson for their insightful discussions and practical advice, and Yin Fang, Caixin Zhang, and Michael Morris for their expert technical assistance. Additionally, I am grateful to Alison North and the Rockefeller University Bioimaging Facility for use of the spinning disk confocal microscope and technical advice, and Svetlana Mazel and the Rockefeller University Flow Cytometry Resource Center for the use of the FACSort Analyzer and expert assistance and advice. I would also like to recognize the Rockefeller University Dean's office, including Kristen Cullen, Marta Delgado, Emily Harms, and Sid Strickland for their technical assistance and support. Finally, I would like to thank my friends and family for their endless love, support, and understanding; I am eternally grateful and share this achievement with all of you.

The anti-ASTN1 antibody used in this work was generated by Jee Hae Kim and constructs were generously supplied by Franck Polleux (pCIG2-iresEGFP, pCIG), Peter Scheiffele (pNICE-Neuroligin-1-EYFP), David Solecki (pMSCXβ-Venus-αTubulin, pCX-I-BSR-Venus Clathrin Light Chain, pCX-I-BSR-Venus-Numb) and Jonathan Cooper (Fred Hutchinson Cancer Research Center, Seattle, Washington (pCMX-Dab1-EGFP, pGL1-SuperC-GFP-Dab2). This work was supported by NSRA Training Grant GM07524 and US National Institutes of Health grant 2RO1 NS015429-27 to M.E.H.

Table of Contents

List of Figures

Characterization and Functional Analysis of Astrotactin 2 Reveals a Role for Endocytosis in Glial-Guided Neuronal Migration

Perrin Megan Wilson, Ph.D.
The Rockefeller University 2007

The cerebellum is essential for learning coordinated movements, balance, eye movements, and aspects of sensory cognition. The remarkably uniform array of the principal neurons of the cerebellar circuitry, granule cells and Purkinje cells, develops by glial-guided migrations that position these cell types in specific neuronal layers. Classical EM studies and real time imaging of the migration of granule neurons along glial fibers established the mode of movement of migrating neurons, including the formation of an interstitial junction beneath the cell soma. Biochemical and molecular biological experiments demonstrated that neuronal protein astrotactin (ASTN1) functions as a neuron-glial ligand during migration. This thesis presents the cloning and biochemistry of a second member of the *Astn* gene family, *Astn2*. Although the peptide sequence of ASTN1 and ASTN2 is highly conserved, we demonstrate that different domains of ASTN1 and ASTN2 are exposed on the cell surface. Immunoprecipitation experiments show that ASTN1 associates with ASTN2 and flow cytometry analysis reveals that coexpression with ASTN2 alters the cell surface localization of ASTN1. Thus, implying that ASTN1 forms a complex with ASTN2.

Recent evidence indicates the polarity complex mPar6α regulates forward movement of the neuron along the glial fiber by coordinating the forward translocation of the centrosome and nucleus. Studies presented in this thesis

provide evidence that the junction beneath the cell soma is released by endocytosis of the ASTN1:ASTN2 complex. Real time imaging of labeled ASTN1 shows a flow of protein to the front of the cell and base of the leading process as the neuron moves along the glial guide. Double labeling with fluorescently tagged Clathrin light chain suggests that the endocytosis of ASTN1 and ASTN2 occurs by a clathrin-related mechanism. Based on these results we present a model whereby the endocytosis of the neuron-glial ligands, ASTN1 and ASTN2, releases adhesion to the glial guide, after which the neuronal soma moves along the glial fiber until a new adhesion junction forms. Thus, studies on ASTN2 in this thesis show a mechanism for the termination of neuron-glial adhesion required for neuronal movement along the glial fiber.

Chapter 1: Introduction

Classic patterns of vertebrate central nervous system development include morphogenetic movements, the formation of ganglionic structures, and the establishment of neuronal layers (Hatten and Heintz, 1995). The wide-ranging, orchestrated cell movements that occur during development result in promoting the differentiation of a multitude of cell types and fashioning of the complex laminar cytoarchitecture of the brain (Galaburda and Christen, 1997). Migration of neurons from germinal zones to regions where they establish functional synaptic connections is a key step in creating the brain's characteristic architectonic features. Defects in neuronal migration have been linked to human neuronal disorders, including childhood epilepsies (Kuzniecky, 1994), lissencephaly, and Zellweger syndrome (Dobyns, 1995). The discovery and characterization of genes involved in these migratory processes are an initial move towards the clarification and interpretation of the molecular basis of brain development and will begin to elucidate the causes of these human developmental disorders. This thesis work focuses on the characterization of the newly identified *Astrotactin* family member, *Astrotactin 2*. Our data suggest that Astrotactin 2 plays a unique role during glial-guided neuronal migration and is responsible for inducing the endocytosis of the neuron-glial adhesion ligand, Astrotactin 1. Based on our results we propose a new model for glial-guided neuronal migration, which incorporates a role for receptor recycling and endocytosis in the formation and disassembly of adhesion sites between the neuronal cell soma and radial glial fibers as the neuron locomotes along the glial substrate.

The Cerebellar Cortex as a Model System for Neuronal Migration

The cerebellum is essential for learning coordinated movements (Boyden et al., 2004), balance, eye movements (De Zeeuw and Yeo, 2005), and aspects of sensory cognition (Fiez, 1996), and is organized into a remarkably uniform array of the two principal neurons of the cerebellar circuitry, granule cells and Purkinje neurons (Eccles et al., 1967; Ito, 1984; Palay and Chan-Palay, 1974). The laminar structure of the cerebellum is established through the coordinated, wide-ranging movements of precursor cells and the directed migrations of differentiated neurons; thus, the cerebellar cortex presents an excellent model system to examine some of the key issues in central nervous system development. The cerebellar cortex has a relatively simple, well-characterized structure, a limited number of cell types, and its organization is stereotyped among the different vertebrate species (Gao et al., 1991; Rakic et al., 1974). In addition, the cerebellar granule neuron is the most abundant neuronal type in the brain, and it can be easily studied due to its postnatal development (Rakic, 1971) and its ability to be isolated and purified *in vitro* (Hatten and Heintz, 1995). The cerebellar granule neuron undergoes a well-characterized, yet highly unusual developmental scheme (Ramon y Cajal, 1911) involving periods of proliferation, differentiation, and both tangential and glial-guided radial migration (Hatten and Heintz, 1995; Zheng et al., 1996).

The glial-guided neuronal migration of cerebellar granule neurons can be directly observed by imaging purified cells in *in vitro* migration assays (Edmondson and Hatten, 1987) and imaging labeled cells in *in situ* organotypic cerebellar slice culture systems (Gao and Hatten, 1993; Solecki et al., 2004). Through the use of time-lapse video microscopy, migration rates can be

determined (Edmondson and Hatten, 1987) and cell motility can be examined (Rivas and Hatten, 1995). *In vitro* studies of glial-guided neuronal migration of cells from heterotypic brain regions demonstrated that the mode of migration and dynamics of motion is common amongst cerebellar and hipppocampal granule neurons (Gasser and Hatten, 1990) and, in addition, extensive electron microscopy studies have demonstrated that the glial-guidance mechanism of cerebellar granule neurons appears to be very similar to that of neurons in the cerebral cortex (Sidman and Rakic, 1973), thereby making the cerebellum an appealing model system to diagnose the mechanics and key issues surrounding the establishment of the complex architectonics of the vertebrate brain.

Embryonic Development of the Cerebellum

Much like the organization of the cerebrum, the cerebellum has a core nuclear region with an overlying cortical structure. During embryogenesis, combinatorial codes of transcription factors, including mammalian homologues of LIM homeodomain-containing proteins, basic helix-loop-helix proteins, and three amino acid loop-containing proteins, play a critical role in defining the fundamental structure of the cerebellum (Shirasaki and Pfaff, 2002). Ultimately, the differential patterns of expression of these transcriptions factors in the developing cerebellar anlage serve to delineate the three principal neuron types of the cerebellum: neurons of the cerebellar nuclei, and Purkinje and granule cells of the cerebellar cortex, and demonstrate that a complex pattern of both histogenesis and migration set forth the architecture of the murine cerebellum (Morales and Hatten, 2006).

The cerebellum is formed entirely from rhombomere 1, a region whose maintenance and expansion is regulated by signals from the midbrain and hindbrain (Wingate, 2001; Wingate and Hatten, 1999). The murine cerebellar anlage begins to form at embryonic day 11 (E11) with a widespread proliferation of cells derived from the dorsal region of rhombomere 1, the roof of the IVth ventricle, to create the rhombic lip (Hatten and Heintz, 1995). Neuronal precursor cells proliferate at the dorsal edge of the neuroepithelium (rhombic lip) and then stream across the lip rostrally, via tangential migration to create a displaced, secondary germinal zone on the surface of the anlage termed the external germinal layer (EGL) (Figure 1.1, left) (Galaburda and Christen, 1997; Hatten, 1999; Hatten and Heintz, 1995; Wingate, 2001). The cells which form the EGL are wholly derived from neuronal precursor cells which previously occupied the rhombencephalic, dorsal ridge of the cerebellar anlage (Alvarez Otero et al., 1993; Galaburda and Christen, 1997; Hatten, 1999; Hatten and Heintz, 1995; Millet et al., 1996; Wingate, 2001; Wingate and Hatten, 1999). Experiments have shown that the cells that migrate from the rhombic lip to occupy the EGL are of one sub-class of cerebellar cells, the cerebellar granule neuron (Alder et al., 1996; Hatten, 1993; Hatten et al., 1997; Rakic, 1971; Wingate, 2001).

Postnatal Development of the Cerebellum: Glial-Guided Neuronal Migration

After granule cell precursors reached the EGL, they undergo an extended period of proliferation in the superficial layer that lasts through the first two postnatal weeks. This clonal expansion results in the production of an extremely large population of granule neuron precursors that expand the EGL from one to

Figure 1.1. Development of the Cerebellar Cortex.

During embryogenesis (left) both of the principal classes of cerebellar neurons are specified. As Purkinje cells (filled cells) become postmitotic and migrate through the cerebellar anlage, granule neuron precursors (unfilled circles) stream across the roof of the anlage to form the secondary germinal zone of the cerebellum, the EGL. Throughout the first two postnatal weeks, granule neurons in the EGL proliferate, become postmitotic, and migrate along Bergmann glial fibers into the underlying layers of the cerebellar cortex. As the granule neurons migrate inward, they extend parallel fibers, and migration continues until they reach a position deep to the Purkinje cell layer (PC). In the adult, granule neurons form synaptic connections with the dendrites of the Purkinje cells. (Figure from Hatten. Annu. Rev. Neurosci. 1999. EGL=external granule layer; VZ=ventricular zone; WM=white matter; IZ=intermediate zone; ML=molecular layer; IGL=internal granule layer).

Figure 1.1

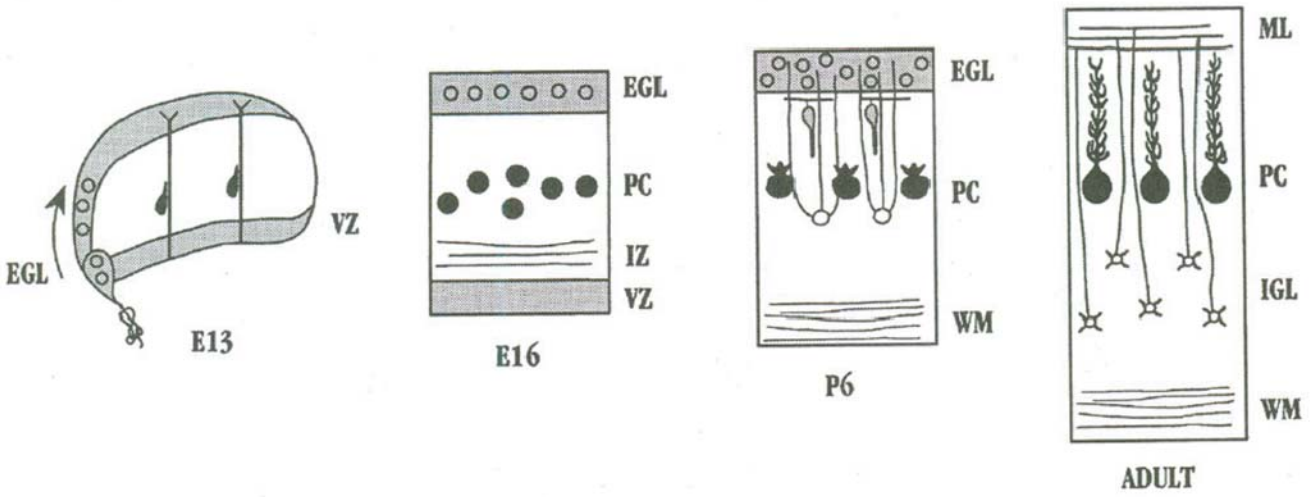

eight cell layers in thickness (Galaburda and Christen, 1997; Hatten et al., 1997). As proliferation in the EGL continues, some neurons begin to differentiate, which results in a subdivision of the EGL into two separate zones, a superficial region of proliferating cells and an inner region of differentiating neurons (Galaburda and Christen, 1997). Local interactions and differential gene expression in these two zones allow the proliferation of precursors to continue superficially while, more internally, neurons begin to undergo differentiation (Galaburda and Christen, 1997; Hatten, 1993; Hatten, 1999; Hatten et al., 1997; Kuhar et al., 1993).

During the first and second postnatal week, differentiated, postmitotic granule neurons being to migrate inward into the underlying cerebellar cortex to form the internal granule cell layer (IGL) and complete the layered architecture of the cerebellum. As shown in Figure 1.1, the granule neurons migrate along glial fibers through a region of differentiating Purkinje cells to form three layers (as described by Ramón y Cajal, 1911): the outer molecular layer (ML) composed of granule cell axons and Purkinje cell dendrites, a middle layer of Purkinje cells, and an innermost layer of granule neuron cell bodies, the IGL. As the granule neurons reach the outer border of the molecular layer and prepare to migrate, the cell body changes from the round shape it had during proliferative stages to a tear drop shape and begins to extend horizontal bipolar axons (parallel fibers) oriented longitudinally to the cerebellar folium (Rakic, 1971). After this cell-shape change and parallel fiber extension, the cell body develops a thin "leading process" oriented in direction of migration resulting in a T-shape morphology characteristic of migrating granule neurons (Edmondson and Hatten, 1987; Rakic, 1971; Sidman and Rakic, 1973). The migration of neurons is saltatory, with a motion phase, characterized by an advance of the cell soma, followed by a

period when the neuron pauses. *In vitro*, both the motion and rest phases lasts for periods of 4-5 minutes, with the average speed of neuronal migration during the motion phase ranging from 20-60 μm/hour (Edmondson and Hatten, 1987; Gasser and Hatten, 1990). The glial guided migration of the cerebellar granule neurons continues until about postnatal day 15 (P15), after which the EGL disappears owing to the complete repositioning of the differentiated neurons into the IGL where they proceed in making synaptic connections and establishing neuronal circuitry (Hatten and Heintz, 1995).

Neuron-Glial Apposition During Neuronal Migration

Throughout the duration of their migration into the IGL, young granule neurons move along the processes of Bergmann glia, a specialized type of astrocyte whose thick, radial processes extend from deep within the cerebellar cortex to the pial surface, providing a scaffold-like support system in the same plane as the migrating neurons (Gasser and Hatten, 1990; Rakic, 1971; Sidman and Rakic, 1973). Rakic's detailed Golgi impregnation and electron microscopy examinations of the developing brain of Rhesus monkeys (1971) describe the constant and close association between the migrating granule cell and the Bergmann glial process and he contends that the migrating neuron and the glial cell appear to form a dynamic cytophysiologic unit. Extensive *in vitro* and correlated electron microscopy studies of purified granule neurons and Bergmann glia have confirmed that Bergmann glial processes are the substrate for granule cell migration and have described a specialized junction between the migrating neuron and glial fiber, in which the neuronal cell soma and leading process are tightly apposed to the glial fiber (Figure 1.2) (Edmondson and

Figure 1.2. Neuron-Glial Apposition in Migrating Granule Neurons.

Bergmann glial fibers provide the substrate for granule cell migration in the cerebellum. (**A**) Schematic of migrating granule neurons demonstrates the tight apposition of the neuronal cell soma and leading process with the radial glial fiber during glial-guided migration. (Figure from Hatten. JCB. 2005)
(**B**) *In vitro*, purified cerebellar granule neurons migrate along Bergmann glial fibers. After 24 hours, the neurons form specialized junctions with the glial fibers and extend a leading process in the direction of migration. (Adapted from Gasser and Hatten. Proc. Natl. Acad. Sci. USA. 1990.)

Figure 1.2

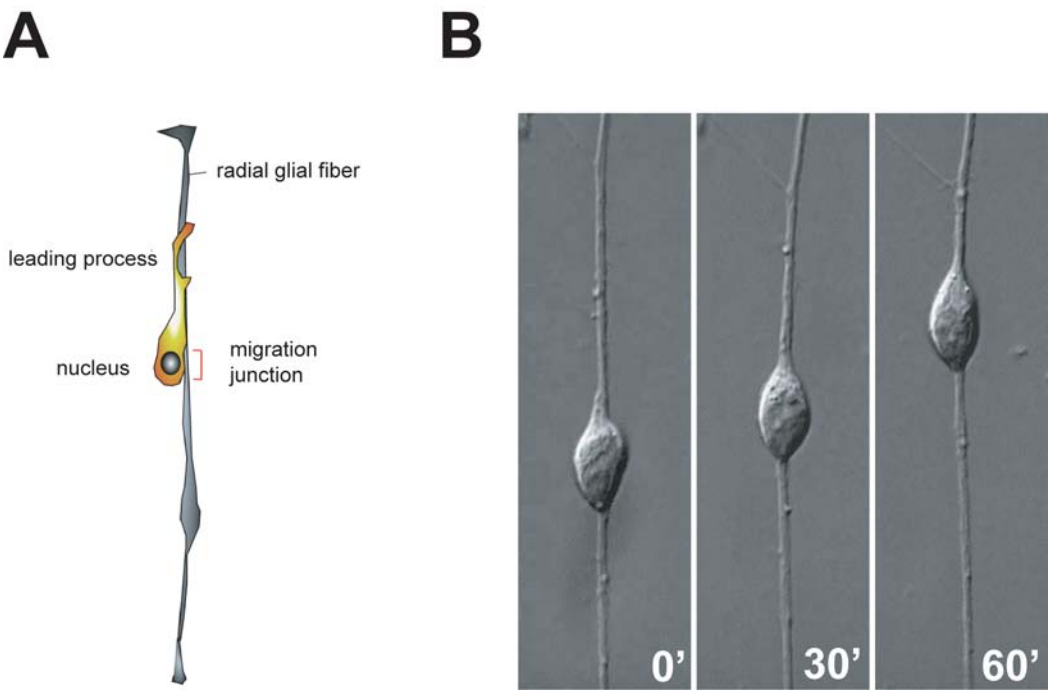
A
B
radial glial fiber
leading process
nucleus
migration
junction
0'
30'
60'

Hatten, 1987; Gasser and Hatten, 1990; Gregory et al., 1988; Hatten, 1990; Hatten et al., 1984; Hatten and Mason, 1990; Hatten, 1986; Mason et al., 1988). In addition, time-lapse microscopy studies have demonstrated that granule neurons move along the radial glial fiber in a saltatory manner, continuing to maintain close contact with the glial guide while extending filipodia in all directions along the length of the leading process (Edmondson and Hatten, 1987; Hatten, 1990; Hatten and Mason, 1990; Powell et al., 1997). Forward movement of the neuron is characterized by the extension of the leading process along the glial fiber and a contraction of the cell soma followed by the extension of the cell soma as the underlying adhesion junction is released (Edmondson and Hatten, 1987). The intimate association of migrating granule neurons with the radial glial fibers suggests a role for membrane adhesion receptor systems in the molecular basis of glial-guided neuronal migration (Gregory et al., 1988; Hatten, 1993; Hatten and Mason, 1990) and extensive studies have identified Astrotactin (Adams et al., 2002; Edmondson et al., 1988; Fishell and Hatten, 1991; Fishman and Hatten, 1993; Stitt and Hatten, 1990), Neuregulin (Anton, 1997; Rio et al., 1997), Tenascin (Husmann et al., 1992), and Thrombospondin (O'Shea, 1990) as regulators of glial-guided migrations in cortical brain regions.

Identification of Astrotactin as a Principal Receptor System In Glial-Guided Neuronal Migration in the Cerebellum

Astrotactin was originally identified in an *in vitro* assay in which antisera to granule cells added to migration cultures blocked glia-guided neuronal migration (Edmondson et al., 1988). *In vitro* antibody perturbation studies demonstrated a role for the cell surface antigen, Astrotactin, in neuron-glial

contact mediation (Stitt and Hatten, 1990) and additional antibody perturbation studies of granule neurons migrating on glial fibers *in vitro* (Fishell and Hatten, 1991) and on glass fibers coated with glial membranes (Fishman and Hatten, 1993) confirmed that Astrotactin plays a major role in neuron-glial adhesion and migration. Further analysis demonstrated that the addition of anti-Astrotactin antibodies resulted in abnormal morphological changes in the migrating granule neurons including the absence of a leading process, loss of filopodial extension, and disruption of the specialized junction between the neuronal soma and glial fiber (Fishell and Hatten, 1991). Interestingly, the migration studies by Stitt and Hatten (1990) revealed that other classic cell adhesion molecules, including N-CAM, L1, and TAG-1, do not mediate neuron-glial binding. Moreover, the binding of granule neurons to glia was shown to be calcium independent, excluding calcium-dependent receptor systems including N-cadherin from a role in neuron-glial interactions. *In vitro* assays also illustrated that of the three general classes of receptor systems: Astrotactin, the neural cell adhesion molecules of the IgG superfamily (N-CAM, L1, and TAG-1), and the β1 subunit of the integrin family, Astrotactin is the principal receptor system in glial-guided neuronal migration (Fishell and Hatten, 1991).

Müller and colleagues demonstrated that integrin β1 is critical for the proliferation of granule neuron precursors (Blaess et al., 2004), and while β1 integrin is a universal adhesion molecule critical for signaling in a variety of biological processes, studies show integrin-mediated cell migrations are calcium dependent (Lawson and Maxfield, 1995; Pierini et al., 2000). This evidence argues against a role for integrins in the calcium-independent migrations of

neurons along glial fibers. Moreover, loss of function evidence from knockout animals reveals no role for β1 integrin in neuron-glial interaction or glial-guided migration (Graus-Porta et al., 2001). By contrast, the targeted disruption of Astrotactin in mice leads to slowed neuronal migration, and granule neurons isolated from Astrotactin null P6 cerebella have reduced glial binding (Adams et al., 2002). Other molecules known to be important for glial-guided neuronal migration, such as Neuregulin, appear to be signals from neurons to promote and maintain glial differentiation, which, in turn, is required for proper neuronal migration (Rio et al., 1997). In light of this evidence, and the failure to identify alternate adhesion systems involved in glial-guided migration, studies of this process have focused on the neuron-glial adhesion ligand, Astrotactin.

New Models of Neuronal Migration

Recent advances have been made in understanding the mechanisms of glial-guided neuronal migration. *In vitro* studies of the polarity protein, mPar6α, have provided insight into the mechanism of somal translocation and established a model involving the coordinated two-stroke movement of the nucleus and centrosome, whereby the centrosome moves forward before the perinuclear microtubule cage and nucleus (Solecki et al., 2004). In addition, mPar6α, dynein, and dynactin loss of function experiments (Solecki et al., 2004) along with actin disruption experiments (Rivas and Hatten, 1995) and the genetic analyses of human migration disorders, (Gleeson et al., 1999; Hirotsune et al., 1998; Smith et al., 2000), have confirmed a key role for the neuronal cytoskeleton in glial-guided neuronal migration. However, at this time, the exact mechanism of forward

movement of the neuronal soma during glial-guided migration remains unclear, with the key question being the means of the formation and release of the specialized adhesion sites formed between the neurons and Bergmann glial fibers.

Vesicle Dynamics and Presence of Coated Vesicles at Neuron-Glial Adhesion Sites

Time-lapse video microscopy and correlated electron microscopy studies have described, in detail, the specialized junction that exists between the migrating neuronal cell soma and the apposing glial fibers. Gregory et al. (1988) noted the presence of coated endo/exocytic figures and coated vesicles adjacent to the interstitial densities in the migrating granule neurons, which indicates ongoing membrane turnover at these sites. In addition these studies described both coated vesicles within the cytoplasm of the leading process and coated endo/exocytic figures on the plasma membrane of the leading process. Coated vesicles were also found surrounding the Golgi apparatus, which is located just in front of the nucleus in the soma of migrating neurons. These descriptions confirmed the previous video observations (Edmondson and Hatten, 1987), which revealed the flow and extension of intracellular vesicles from the nuclear indentation into the leading process. In addition, later studies (Rivas and Hatten, 1995) demonstrated an area of dense dicarbocyanine dye staining of membranous organelles in the juxtanuclear area in the cell soma of migrating neurons. Taken together, this evidence suggests roles for membrane turnover, intracellular trafficking, and endocytosis in the creation and release of adhesion sites at the neuron-glial junctions formed during neuronal migration.

De-adhesion, Endocytosis, and Migration

Endocytosis is a highly coordinated process through which cells internalize plasma membrane components from the cell surface into internal membrane compartments to control the composition of the plasma membrane, downregulate signaling receptors, and recycle transmembrane proteins (Le Roy and Wrana, 2005; Maldonado-Baez and Wendland, 2006; Sorkin, 2004; Szymkiewicz et al., 2004). During development, the endocytosis and intracellular trafficking of cell surface molecules plays key roles in maintaining gradients and long-range distribution of morphogens, controlling asymmetric cell divisions, and restricting signaling outputs (Gonzalez-Gaitan and Stenmark, 2003). While there is evidence for the role of receptor turnover and endocytosis in growth cone collapse and motility (Fournier et al., 2000) and in the de-adhesion step required for forward migration of neutrophils and macrophages (Fan and Malik, 2003; Lawson and Maxfield, 1995; Pierini et al., 2000), the role of endocytosis in glial-guided neuronal migration has just recently been considered.

Studies by Thelen et al. (2002), demonstrate a role for the cell adhesion molecule L1 in the potentiation of neuronal migration toward extracellular matrix proteins though β1 integrin, a process which is dependent on receptor-mediated endocytosis. In addition, they demonstrated that L1 and β1 integrin antibodies can induce endocytosis and that this induced endocytosis has an inhibitory effect on migrating neurons in acute cerebellar slices, suggesting that endocytosis of receptors can inhibit neuronal migration. The endocytosis of L1 has also been shown to occur in the rear of growth cones, suggesting that internalization of adhesion receptors could contribute to the de-adhesion steps

that occur during axon growth and motility (Kamiguchi et al., 1998). Since the *in vitro* studies of glial-guided granule neuron migration did not demonstrate a dominant role for either L1 or β1 in migration in the cerebellum, our attention turns to the Astrotactin family proteins. Interestingly, the perturbation of migration in living cells by the addition of anti-Astrotactin antibodies caused a cessation of organelle and vesicle flow into the leading process suggesting that Astrotactin is in some way connected to cytoskeletal dynamics and vesicle trafficking (Fishell and Hatten, 1991).

Discovery of a Novel Astrotactin Family Member

The *Astrotactin* gene encodes a neural glycoprotein protein of approximately 100kD with three epidermal growth factor (EGF) repeats, one MAC/Perforin (MAC/PF) domain, and one fibronectin III (FNIII) domain (Zheng et al., 1996). Northern analysis demonstrates that *astrotactin* is a brain-specific transcript that is developmentally regulated. During the early postnatal period when granule cell migration is at its peak, *astrotactin* is expressed in Purkinje cells as well as in postmitotic and migrating granule neurons moving along the glial fiber scaffold (Zheng et al., 1996). Recently, a new *Astrotactin* family member has been identified, hereafter referred to as *Astrotactin 2* (*Astn2*) (T. Tomoda and M.E. Hatten, unpublished observations). *Astn2* was discovered through a BLAST search of the mouse EST database using *Astrotactin* (now referred to as *Astrotactin 1*, *Astn1*) sequence. A partial sequence, containing the first three EGF repeats of a homologous protein, was initially found and a subsequent cDNA library screen generated more of the sequence of the *Astn2* gene. ASTN2 is 65% homologous at the amino acid level to ASTN1 and contains

the same functional domains. Due to the high homology between the proteins, and the incomplete disruption of migration in the Astn1 knockout mouse (as compared with the early antibody perturbation studies), we hypothesized that ASTN2 may also have a role in radial, glial-guided neuronal migration in the cerebellum. This thesis characterizes the newly identified *Astn* family member, *Astn2*, and reveals a novel role for ASTN2 in the endocytosis of ASTN1, resulting in a new model in which the processes of receptor turnover and endocytosis are key mechanisms for de-adhesion of the neuronal cell soma from the glial fiber during neuronal migration.

Chapter 2: Identification and Characterization of Astrotactin 2

Introduction

Several lines of *in vitro* antibody perturbation studies have demonstrated a role for Astrotactin in neuron-glial adhesion and glial-guided neuronal migration. Addition of anti-Astrotactin antibodies prevented the positioning of neurons along glial fibers (Edmondson et al., 1988). In cultures treated with Astrotactin antibodies, fewer than 50% of neurons were within 20 μm of a glial process as opposed to more than 90% of neurons in control conditions being positioned within 20 μm of a glial fiber (Edmondson et al., 1988). Further antibody perturbation investigations (Stitt and Hatten, 1990) revealed that anti-Astrotactin antibodies inhibited the binding of granule cell membranes to astroglia by 60-70%, but had no effect on homotypic granule cell adhesion, suggesting that Astrotactin functions only in heterotypic neuron-glial binding. In addition, perfusion of anti-Astrotactin antibodies was shown to rapidly arrest glial-guided neuronal migration *in vitro* by 60%, reducing both the rate and frequency of migration (Fishell and Hatten, 1991). Studies by Stitt and Hatten (1990) suggest that Astrotactin is the neuronal factor in neuron-glial adhesion, since antibody treatment of the neuronal membranes, but not the glia, inhibited neuron-glial binding. The presence of anti-Astrotactin antibodies resulted in the migrating neurons losing the characteristic features of migration, including the extension of a leading process and the formation of the specialized adherens junction between the neuronal cell soma and the glial fiber (Fishell and Hatten, 1991).

The targeted disruption of Astrotactin in mouse confirms a role for astrotactin in neuron glial binding and glial-guided neuronal migration (Adams et al., 2002). *In vitro* assays demonstrate that Astrotactin null granule neurons have a 60% reduction in neuron-glial binding and slower average migration rates (9.5 μm/hour) as compared with wild-type neurons (which migrated at an average rate of 12 μm/hour). Slice culture assays also revealed a slower migration of the Astrotactin null granule neurons, but histological examination shows that although migration is slowed, the columnar organization of the cerebellum is still established. As compared to the antibody perturbation studies, the disruption of migration in the Astrotactin knockout is less severe. Adams et al. conjectured that this could be due to the Astrotactin function blocking antibodies also binding the newly identified Astrotactin family member, Astn2. With the hope of further advancing the understanding of the mechanisms involved in glial-guided migration and the role of the Astrotactin family, we embarked on a characterization and examination of Astn2.

Identifying Mouse *Astn2* Genomic Sequence

Mouse *Astn2* was originally identified through a BLAST search of the mouse EST database using mouse *Astn1* cDNA sequence and the sequence resulting from the search was verified to be in the mouse genome using the Celera database. *Astn1* and *Astn2* reside on different chromosomes in the mouse and have very different genomic structures. In the mouse, *Astn1* is located in the qH1 region of chromosome 1 and *Astn2* is located in the qC1 region of chromosome 4 (UCSC Genome Browser, http://genome.ucsc.edu). Mouse *Astn1* consists of 23 exons over 329.430 kB of genomic sequence, whereas mouse *Astn2* contains 23 exons, has two splice forms, and spans 1023.680 kB (Figure 2.1 A; UCSC Genome Browser, http://genome.ucsc.edu). RT-PCR analysis of demonstrates that both *Astn2* splice forms are present in cerebellar granule neurons (data not shown). In humans, both *Astn1* and *Astn2* have 23 exons and multiple splice forms, but the genes are located on different chromosomes (human chromosome 1 and 9 respectively) and, as in mouse, *Astn2* spans a larger genomic region (UCSC Genome Browser, http://genome.ucsc.edu). Both *Astn1* and *Astn2* are vertebrate-specific genes with putative homologs in *Homo sapiens* (human), *Pan troglodytes* (chimp), *Canis familaris* (dog), and *Mus musculus* (mouse) (NCBI Homologene, http://www.ncbi.nlm.nih.gov). *Astn1* also has a putative homolog in *Gallus gallus* (chicken) and, collectively, the *Astn* proteins have similarity with groups of transcribed sequences found in other vertebrates including *Rattus norvegicus* (rat), *Bos Taurus* (cow), *Oryctolagus cuniculus* (rabbit), *Danio rerio* (zebrafish), and *Xenopus tropicalis* (frog) (NCBI Homologene, http://www.ncbi.nlm.nih.gov).

Figure 2.1. *Astn2* Genomic and Protein Structure.

(**A**) Schematic representation of *Astn2* genomic and protein structure. Orange, signal sequence; green, transmembrane domain; dark blue, EGF Repeat; red, MAC/Perforin Domain; purple, Fibronectin III Domain; light blue, anti-ASTN2 antibody recognition site; pink, *astn2* Northern/*in situ* probe location; arrow, N' linked glycosylation site. (**B**) ASTN2 amino acid sequence.

Figure 2.1

A

Astn2 Genomic Structure

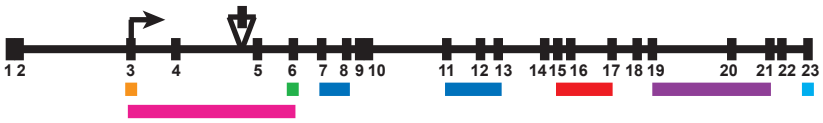

ASTN2 Protein Structure

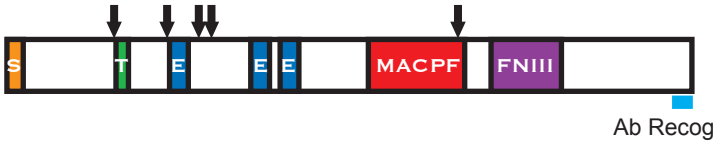

- Signal Sequence
- Transmembrane Domain
- EGF Repeat
- MAC/Perforin Domain
- Fibronectin III Domain
- ASTN2 Antibody Recognition
- *astn2* Northern/*In Situ* Probe
- N-Linked Glycosylation

B

ASTN2 Protein Sequence

```
MGGLIALLLLLLVFTVALYAQRRWQKRRRIPQKSASAEATHEIHYIPSVLLGPQARESFRSSRLQTHNSVIGVPI   75
RETPILDDYDYEEEEEPPRRANHVSREDEFGSQMTHALDSLGRPGEEKVEFEKKGGISFGRTKGTSGSEADDETQL  151
TFYTEQYRSRRRSKGLLKSPVNKTALTLIAVSSCILAMVCGNQMSCPLTVKVTLHVPEHFIADGSSFVVSEGSYLD  227
ISDWLNPAKLSLYYQINATSPWVRDLCGQRTTDACEQLCDPDTGECSCHEGYAPDPVHRHLCVRSDWGQSEGPWPY  303
TTLERGYDLVTGEQAPEKILRSTFSLGQGLWLPVSKSFVVPPVELSINPLASCKTDVLVTEDPADVREEAMLSTYF  379
ETINDLLSSFGPVRDCSRNNGGCTRNFKCVSDRQVDSSGCVCPEELKPMKDGSGCYDHSKGIDCSDGFNGGCEQLC  455
LQQTLPLPYDTTSSTIFMFCGCVEEYKLAPDGKSCLMLSDVCEGPKCLKPDSKFNDTLFGEMLHGYNNRTQHVNQG  531
QVFQMTFRENNFIKDFPQLADGLLVIPLPVEEQCRGVLSEPLPDLQFLTGDIRYDEAMGYPMVQQWRVRSNLYRVK  607
LSTITLSAGFTNVLKILTKESSRDELLSFIQHYGSHYIAEALYGSELTCIIHFPSKKVQQQLWLQYQKETTELGSK  683
KELKSMPFITYLSGLLTAQMLSDDQLISGVEIRCEEKGRCPSTCHLCRRPGKEQLSPTPVLLEINRVVPLYTLIQD  759
NGTKEAFKNALMSSYWCSGKGDVIDDWCRCDLSAFDASGLPNCSPLPQPVLRLSPTVEPSSTVVSLEWVDVQPAIG  835
TKVSDYILQHKKVDEYTDTDLYTGEFLSFADDLLSGLGTSCVAAGRSHGEVPEVSIYSVIFKCLEPDGLYKFTLYA  911
VDTRGRHSELSTVTLRTACPLVDDNQAEEIADKIYNLYNGYTSGKEQQTAYNTLMEVSASMLFRVQHHYNSHYEKF  987
GDFVWRSEDELGPRKAHLILRRLERVSSHCSSLLRSAYIQSRVDTIPYLFCRSEEVRPAGMVWYSILKDTKITCEE 1063
KMVSMARNTYGETKGR*                                                             1079
```

Generation of the *Astrotactin 2* Full-Length cDNA and ASTN2 Protein Sequence Characterization

The mouse EST database contained a partial sequence with the first three EGF repeats of *Astn2*. A subsequent P7 mouse brain cDNA library screen provided more of the *Astn2* sequence (T. Tomoda and M.E. Hatten, unpublished observations). Using the 5′ sequence of that original *Astn2* coding sequence we searched the TIGR Gene Indices (now the Dana Farber Gene Index Project, http://compbio.dfci.harvard.edu/tgi/) and identified additional upstream gene sequence (about 750 nucleotides). The upstream region of the *Astn2* cDNA was generated by 5′RACE and PCR walking using E17 brain cDNA as a template. The resulting PCR products were then verified by DNA sequencing. We produced the full-length *Astn2* cDNA by joining this upstream *Astn2* DNA fragment with the existing partial cDNA by restriction enzyme digestion. The newly identified *Astn2* sequence yielded a longer open reading frame containing a putative start site that would produce a protein of 1079 amino acids (Figure 2.1 B). Sequence analysis of the new open reading frame predicts a protein that contains a signal sequence, transmembrane domain, three epidermal growth factor-like (EGF) repeats, a MAC/Perforin (MAC/PF) domain, a fibronectin type III (FNIII) domain, and five N-linked glycosylation sites (Figure 2.1 A). These results demonstrate that ASTN2 contains all the same conserved domains as ASTN1. A complete alignment of the ASTN1 and ASTN2 protein sequences using the BLOSUM 30 matrix is shown in Figure 2.2; the alignment illustrates that ASTN1 and ASTN2 are 48% identical and 65% homologous overall. Homologene analysis of *Astn1* and *Astn2* gene sequence demonstrates that the

Figure 2.2. ASTN1 and ASTN2 Homology.

Alignment of the ASTN1 and ASTN2 proteins generated by pairwise alignment using the BLOSUM 30 matrix (Open Gap Penalty=10, Extend Gap Penalty=0.1). Homologous amino acids are shown in grey, and the antibody recognition sites for the ASTN1- and ASTN2-specific carboxyl terminal antibodies are indicated by the red box. (Ab=antibody; Recog=recognition).

Figure 2.2

most highly conserved domain among different vertebrate species is the MAC/PF domain, which is conserved from *Gallus gallus* to *Homo sapiens* (NCBI, http://www.ncbi.nlm.nih.gov).

Characterization of *astrotactin 2* mRNA Expression:

***Astrotactin 2* is Expressed in the Developing and Adult Brain**

RT-PCR experiments demonstrate that *astn2* mRNA is expressed early in development, in the E8.5 whole embryo and in the brain and whole embryo at E10 (Figure 2.3 A). Using a 634 base pair probe against the beginning of the coding region of the gene (Figure 2.1 A, pink), the developmental time course of *astn2* expression was assayed by Northern Blot. *Astn2* is expressed during embryonic development in the brain at E10 and E12.5, in the cerebellum at E14.5, and in the cerebellum and cortex at E16.5 (Figure 2.3 B, arrows). Compared with embryonic ages, expression of *astn2* mRNA increases in the postnatal brain. Postnatally, *astn2* is expressed in the cerebellum and cortex from birth to adulthood, although it is most highly expressed in the cerebellum at each time point. Northern blotting reveals that there are two *astn2* transcripts (4.2 kB and 5.8 kB), which may be due to alternative splicing in an untranslated region. GAPDH (Figure 2.3 B, bottom panel) was used as a loading control ensuring an equal amount of RNA was loaded per lane.

***Astrotactin2* is Expressed in Neurons in the Developing and Adult Cerebellum**

To further characterize the localization of *astn2*, we performed in situ hybridization on 60μm P6, P10, and adult brain sections using the same 634 base pair probe from the beginning of the *Astn2* gene (Figure 2.1 A, pink) as in the

Figure 2.3. *Astn2* is Expressed in the Developing and Adult Brain.

(**A**) RT-PCR shows early expression of *astn2* mRNA. *Astn2* transcripts are present in E8.5 and E10.5 embryos and E10.5 brain. GAPDH loading control is shown in the bottom panel. (**B**) Northern Blot demonstrates that *astn2* is expressed in the developing and adult brain. The developmental time course shows that *astn2* mRNA (arrows) is present early in development, and expression is strong in the cerebellum by E14.5 and continues through adulthood. GAPDH loading control is shown in the bottom panel. (cb=cerebellum; ctx=cortex).

Figure 2.3

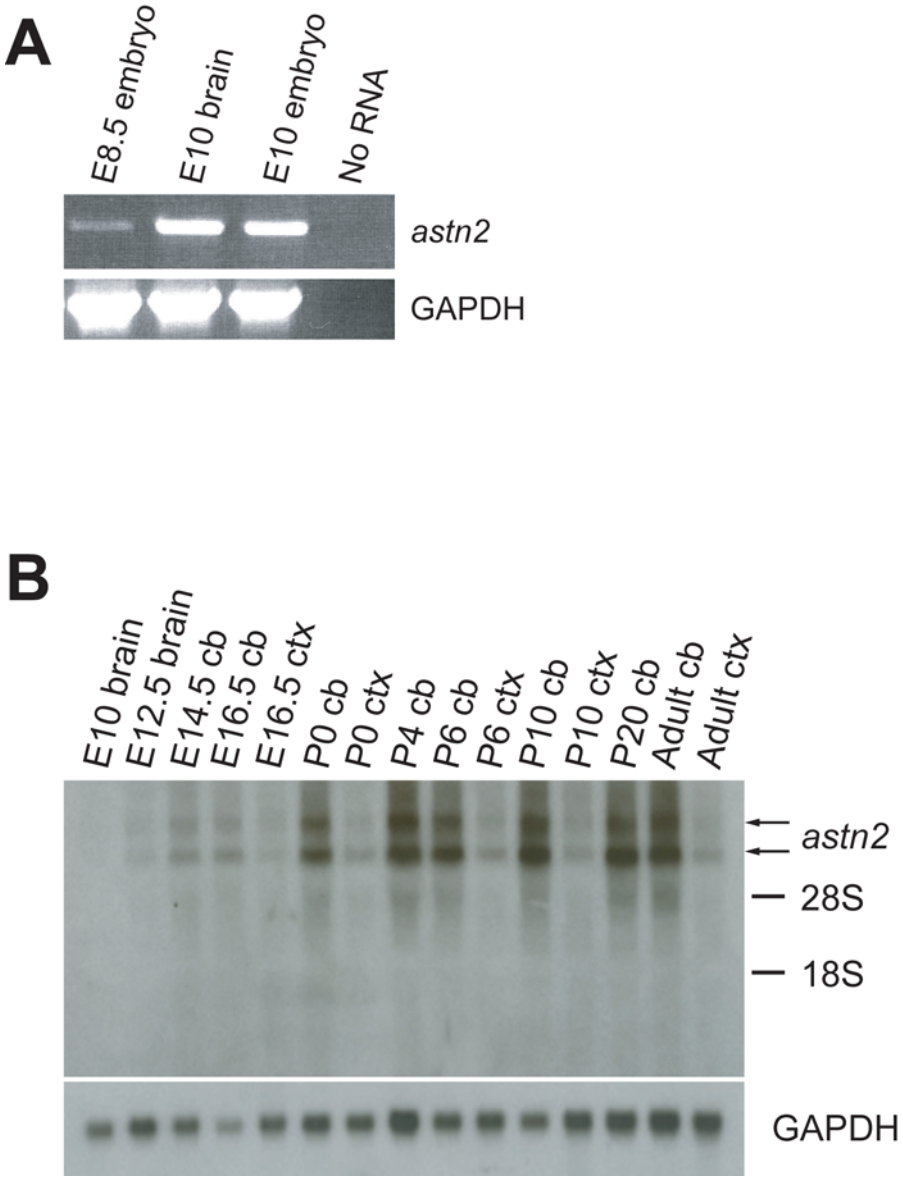
A
E8.5 embryo
E10 brain
E10 embryo
No RNA
astn2
GAPDH
B
E10 brain
E12.5 brain
E14.5 cb
E16.5 cb
E16.5 ctx
P0 cb
P0 ctx
P4 cb
P6 cb
P6 ctx
P10 cb
P10 ctx
P20 cb
Adult cb
Adult ctx
astn2
28S
18S
GAPDH

Northern Blot analysis. *In situ* analysis shows that postnatally, *astn2* is expressed primarily in the cerebellum, but is also expressed in the cortex, olfactory bulb, hindbrain, and dentate gyrus of the hippocampus at P6, P10, and adult stages (Figure 2.4 A, D, and G). At P6 and P10, during which neuronal migration is occurring in the cerebellum, *astn2* transcripts are expressed in Purkinje neurons, cerebellar granule cells in both the external germinal layer and forming internal granule layer, as well as in migrating granule cells in the molecular layer (Figure 2.4 B, E, and M). By adulthood, when the external germinal layer has disappeared, *astn2* expression is limited to the granule neurons of the internal germinal layer and the Purkinje neurons (Figure 2.4 H). In comparison, *astn1* transcripts are expressed in a more widespread pattern throughout the brain, with the highest level of expression in the cortex, olfactory bulb, hindbrain, dentate gyrus of the hippocampus, and cerebellum (Figure 2.4 J). In the P6 cerebellum *astn1* is expressed in the Purkinje neurons, in migrating granule neurons and in the granule neurons of the newly forming internal granule layer (Figure 2.4 K), however the expression level is significantly weaker than that of *astn2*. Sense controls performed for each probe at each age do not show any signal (Figure 2.4 C, F, I and L). Our results were confirmed by quantitative radioactive *in situ* hybridization experiments performed by the Curran laboratory as part of the GENSAT project (http://www.ncbi.nlm.nih.gov/projects/gensat/). Their analysis also demonstrates that during development, *astn2* is expressed predominately in the granule neurons and Purkinje cells in the cerebellum, as well as in the olfactory bulb, cortex, and dentate gyrus of the

Figure 2.4. Expression of *astn2* mRNA *in situ*.

In situ hybridization of sagittal brain sections reveals that *astn2* is expressed in the cerebellum, cortex, olfactory bulb, hindbrain, and hippocampus at (**A**) P6, (**D**) P10, and (**G**) adult stages. Magnification (5x) of the cerebellum reveals that at (**B**) P6 and (**E** and **M**) P10 *astn2* is expressed in granule neurons in the EGL, IGL, ML, and Purkinje neurons. At adult stages (**H**), *astn2* expression is localized to Purkinje neurons and granule neurons in the IGL. *In situ* hybridization of *astn1* at P6 illustrates that *astn1* is ubiquitously expressed throughout the brain (**J**) and is expressed in the granule neurons and Purkinje neurons of the cerebellum (**K**). **C**, **F**, and **I** show the sense control of *astn2* at P6, P10, and adult stages, respectively, and **L** shows the sense control of *astn1* at P6. **N** and **O** illustrate quantitative, radioactive *in situ* hybridization of *astn2* performed with an independent probe by the Gensat project and confirm our expression analysis. Scale bar represents 1000 μm in **A**, **C**, **J**, and **L**, 400 μm in **B**, **E**, **H** and **N**, 1200 μm in **D** and **F**, 1500 μm in **G** and **I,** and 200 μm in **M**. (EGL=external granule layer; ML=molecular layer; IGL=internal granule layer).

Figure 2.4

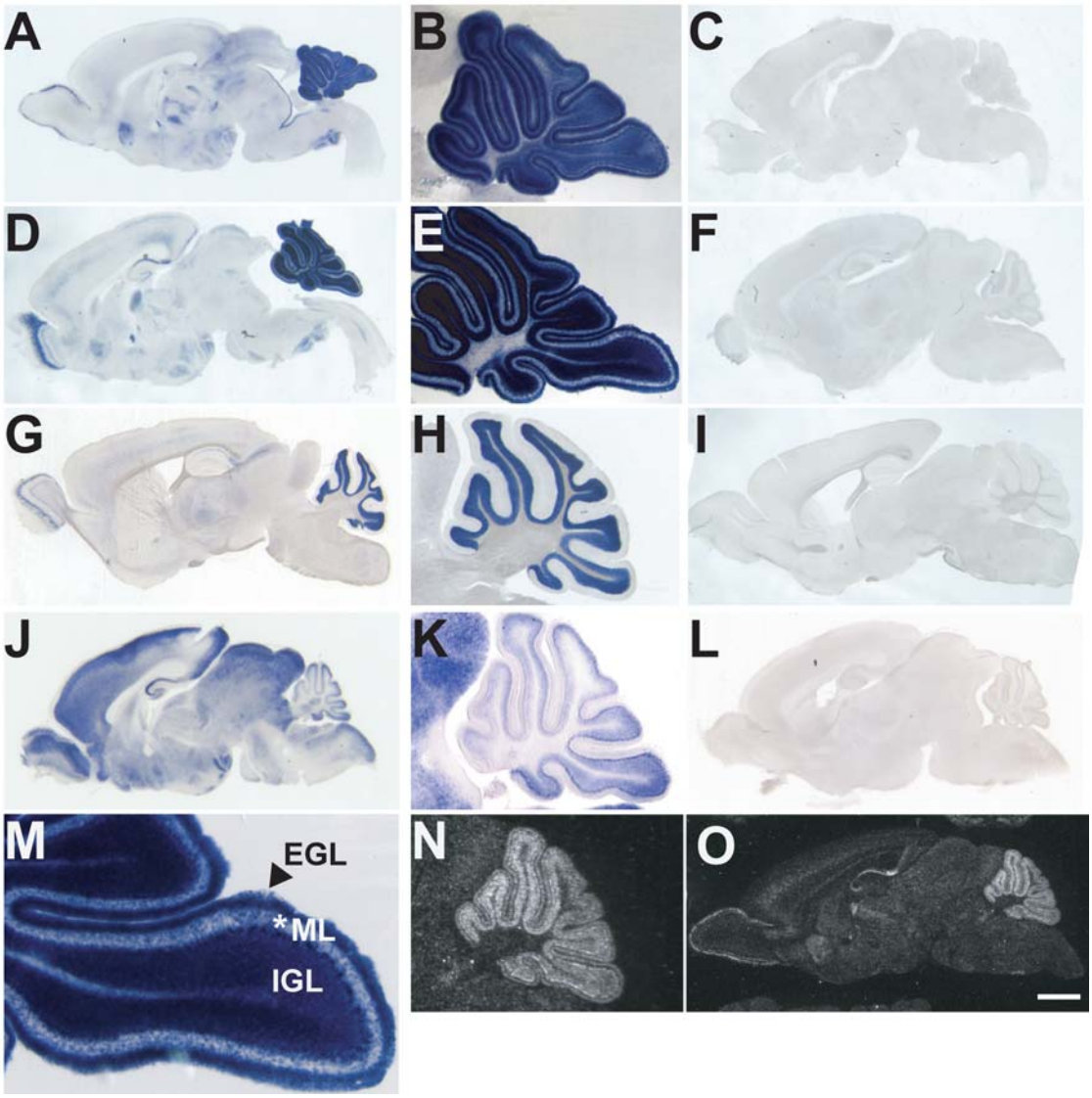

hippocampus (Figure 2.4 N and O). Since *astn2* has a similar cerebellar expression profile as *astn1*, these results suggest that ASTN2 may also play a role in neuronal migration in the cerebellum.

Generation and Characterization of an anti-ASTN2 Specific Antibody:

Purification of anti-ASTN2 Antibodies

In order to assay ASTN2 protein expression, we generated an anti-ASTN2 specific antibody. We identified the carboxy-terminus of ASTN2 to be the most antigenic region and least homologous to ASTN1 and, therefore, chose to target this area to create an anti-ASTN2 specific antibody. A polyclonal antibody was raised in New Zealand white rabbits against the ASTN2 peptide (KITCEEKMVSMARNTYGETKGR; Figure 2.2, red box). Rabbit serum was subsequently column purified and the low pH glycine and high salt $MgCl_2$ eluates were tested for specificity by Western blot against P10 cerebellar homogenate (chosen based on *astn2* mRNA expression data) and ASTN2 transfected cell lysate. The Western blots in Figure 2.5 A of P10 cerebellar homogenate show a prominent band at ~110kD in the anti-ASTN2 serum probed lane which subsequently disappears in the flow-through demonstrating that all specific antibodies were bound to the column. The 110kD band is present in the blots probed with both the anti-ASTN2 glycine and $MgCl_2$ eluates showing that the anti-ASTN2 specific antibodies were eluted under both conditions. The blotting of the ASTN2 transfected cell lysate (Figure 2.5 B) demonstrates the same pattern, confirming the antibodies eluted are indeed recognizing ASTN2 protein. To further confirm the specificity of the antibodies, both the anti-ASTN2 glycine and $MgCl_2$ eluates were blocked with the peptide against which they

Figure 2.5. Biochemical Analysis of the Anti-ASTN2 Antibody.

The rabbit serum, flow-through, and glycine and $MgCl_2$ eluates from the antibody affinity purification process were tested for specificity by Western blot against P10 cerebellar homogenate (**A**) and *Astn*2-transfected cell lysate (**B**). The predominant band at 110 kD in the glycine and $MgCl_2$ eluate probed lanes demonstrates that antibodies were specifically eluted under both conditions. Western blot recognition of ASTN2 in P10 cerebellar homogenate by the purified glycine (**C**) and $MgCl_2$ (**D**) eluates was blocked by pre-absorption with the peptide against which the antibodies were raised. (**E**) Illustration of the specificity of the anti-ASTN antibodies by Western blot. Anti-ASTN1 and anti-ASTN2 antibodies recognize endogenous proteins in P10 cerebellar homogenate and their respective transfected cell lysates. Neither the anti-ASTN2 glycine (upper left) nor $MgCl_2$ (upper right) antibodies cross-react with ASTN1 transfected cell lysate and likewise, the anti-ASTN1 antibody (bottom left and right) does not cross-react with ASTN2 transfected cell lysate. (cb=cerebellum; homog=homogenate; A1=ASTN1; A2=ASTN2; pep=peptide).

Figure 2.5

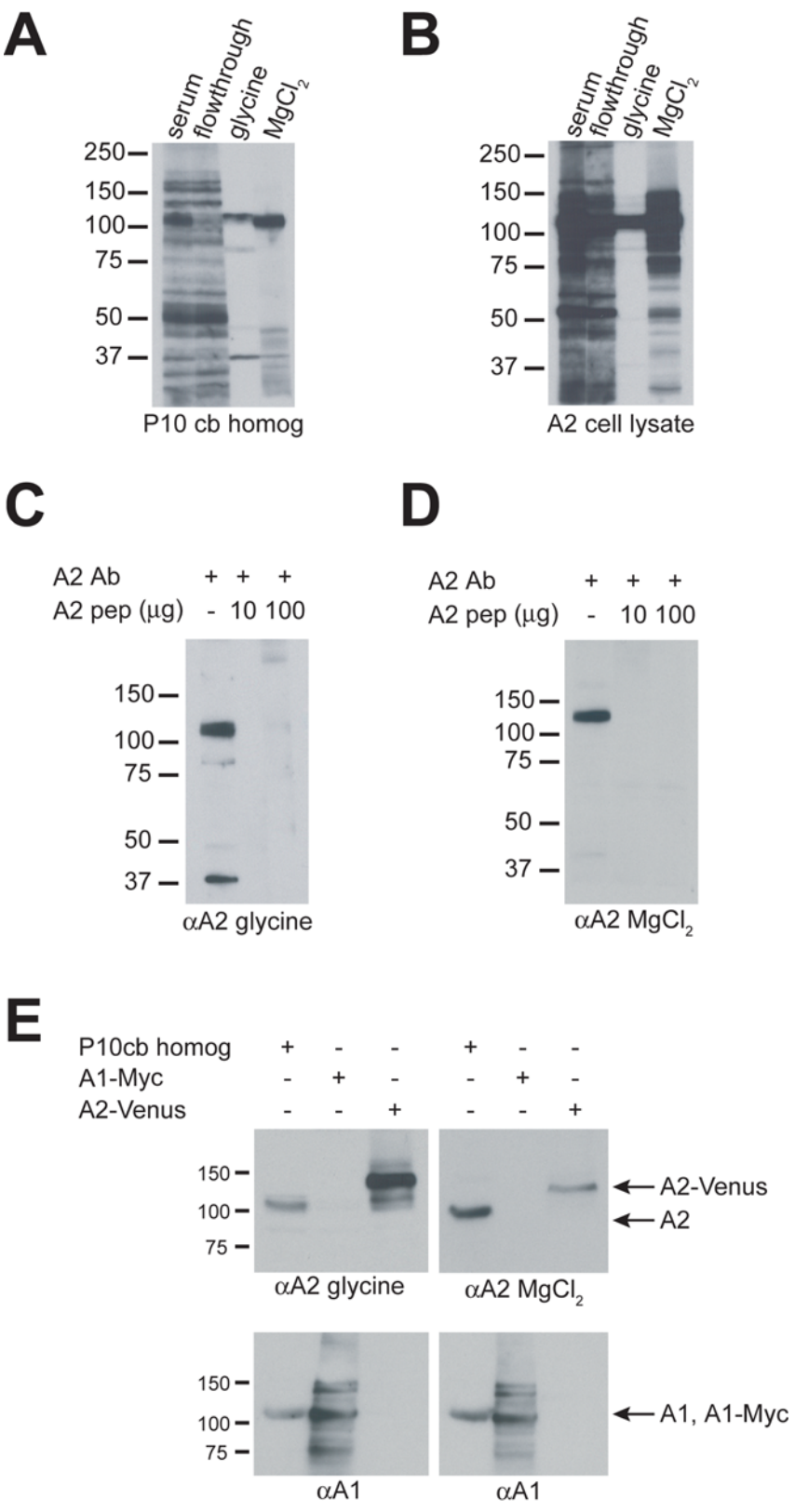
A
serum
flowthrough
glycine
MgCl2
250
150
100
75
50
37
P10 cb homog
B
serum
flowthrough
glycine
MgCl2
250
150
100
75
50
37
A2 cell lysate
C
A2 Ab + + +
A2 pep (μg) - 10 100
150
100
75
50
37
αA2 glycine
D
A2 Ab + + +
A2 pep (μg) - 10 100
150
100
75
50
37
αA2 MgCl2
E
P10cb homog + - - + - -
A1-Myc - + - - + -
A2-Venus - - + - - +
150
100
75
αA2 glycine
αA2 MgCl2
A2-Venus
A2
150
100
75
αA1
αA1
A1, A1-Myc

were raised and then used in a Western blot against P10 cerebellar homogenate (Figure 2.5 C and D). In both cases the 110kD ASTN2 band is present in the first lane probed with the antibody alone, but not in the subsequent lanes which were probed with the antibody pre-absorbed with 10 μg and 100 μg of peptide respectively, illustrating that the anti-ASTN2 antibodies are specifically recognizing the peptide against which they were raised.

Anti-ASTN2 Antibodies Do Not Cross-react with ASTN1

We next wanted to confirm that the anti-ASTN2 antibody did not cross-react with ASTN1. To do so, a Western Blot containing P10 cerebellar homogenate and ASTN1-Myc and ASTN2-Venus transfected cell lysates was probed with both the anti-ASTN2 and anti-ASTN1 antibodies. The top panel of Figure 2.5 E shows that the anti-ASTN2 purified antibodies (glycine, top left; $MgCl_2$, top right) recognize only the P10 cerebellar homogenate and the ASTN2-Venus transfected cell lysate, and do not cross-react with the ASTN1-Myc cell lysate. The bottom panel (Figure 2.5 E) verifies the presence of the ASTN1-Myc transfected cell lysate and demonstrates that the anti-ASTN1 antibody also generated against the carboxy-terminal peptide (J.H. Kim and M.E. Hatten, unpublished data; Figure 2.2, red box) is specific and does not cross react with ASTN2. To further confirm this finding, HEK293T cells were transiently transfected with ASTN2-Myc or ASTN1-Flag and immunostained with anti-ASTN2 or anti-ASTN1 antibodies. As shown in Figure 2.6 A, anti-ASTN2 antibody recognizes the ASTN2-Myc transfected cells (top panel) but does not recognize the ASTN1-Flag transfected cells (second panel from top). Likewise, the anti-ASTN1 antibody recognizes the ASTN1-Flag transfected cells (Figure

Figure 2.6. Immunocytochemistry Analysis of the Anti-ASTN2 Antibody.

(**A**) Demonstration of the specificity of the anti-ASTN antibodies via immunocytochemistry. Transfected HEK293T cells were fixed after 24 hour culture *in vitro* and immunostained with anti-ASTN2, anti-ASTN1, anti-Myc, and anti-Flag antibodies. Anti-ASTN2 antibodies specifically recognize ASTN2-Myc in transfected cells (top), but do not cross-react with ASTN1-Flag (third from top). Likewise, anti-ASTN1 antibodies specifically recognize ASTN1-Flag in transfected cells (bottom), but do not cross-react with ASTN2-Myc (second from top). (**B**) Anti-ASTN2 antibodies recognize endogenous ASTN2 in cerebellar granule neurons. Purified cerebellar granule neurons were fixed after 24 hours of culture *in vitro* and immunostained with anti-ASTN2 antibodies (left) and anti-ASTN2 antibodies pre-absorbed with 10 μg of the peptide against which the antibody was raised (right). Pre-absorption of the antibody blocks recognition of endogenous ASTN2 (right). Scale bar represents 10 μm. (Tf=transfection; A1=ASTN1, A2=ASTN2; pep=peptide).

Figure 2.6

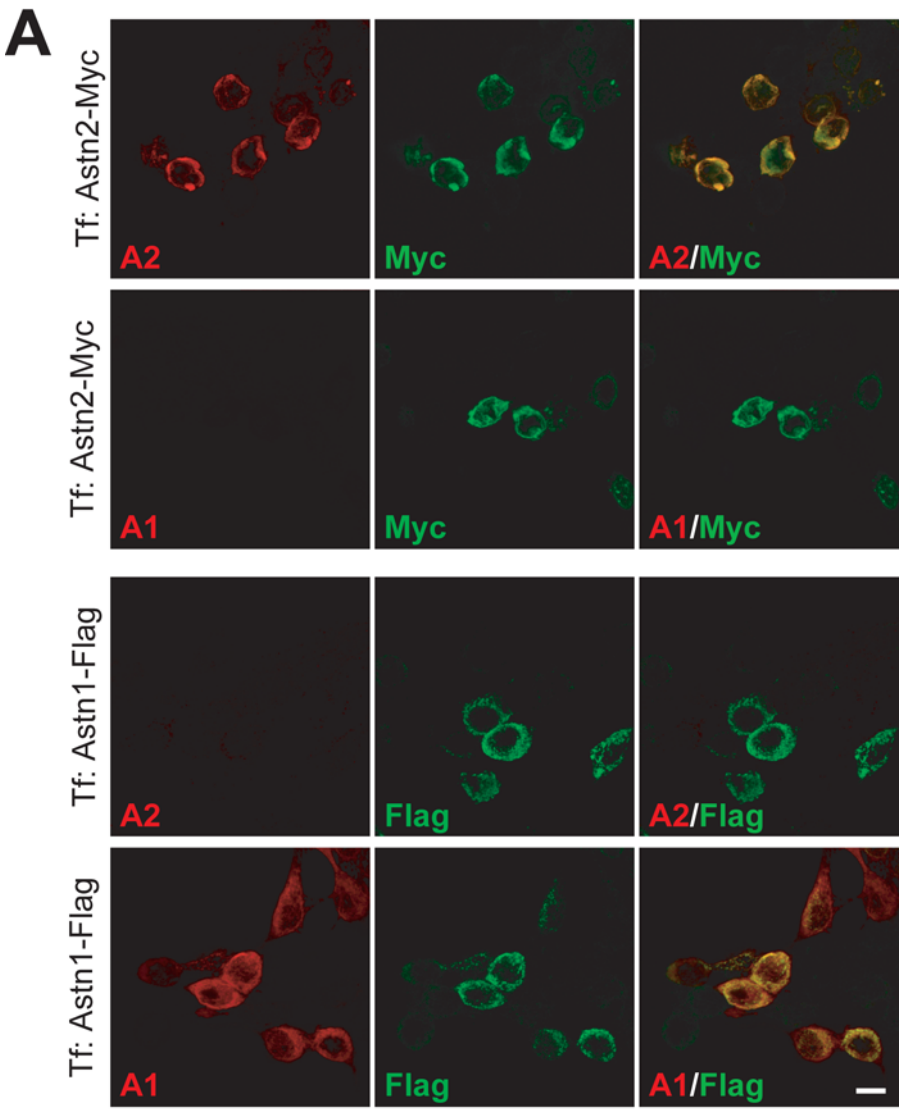
A
Tf: Astn2-Myc
A2
Myc
A2/Myc
Tf: Astn2-Myc
A1
Myc
A1/Myc
Tf: Astn1-Flag
A2
Flag
A2/Flag
Tf: Astn1-Flag
A1
Flag
A1/Flag

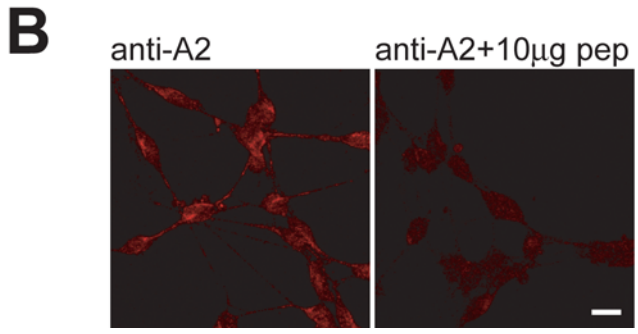
B
anti-A2
anti-A2+10µg pep

2.6 A, bottom panel) but does not recognize the ASTN2-Myc transfected cells (Figure 2.6 A, third panel from top). Taken together these experiments demonstrate the specificity of both the anti-ASTN2 and anti-ASTN1 antibodies.

Anti-ASTN2 Antibodies Recognize Endogenous ASTN2

After determining that the anti-ASTN2 antibody specifically recognized ASTN2 protein in P10 cerebellar homogenate and transfected HEK293T cells, we verified the antibody's recognition of endogenous ASTN2 in cerebellar granule neurons. Purified cerebellar granule neurons were grown in culture for 24 hours and then immunostained with anti-ASTN2 antibodies or anti-ASTN2 antibodies that had been pre-absorbed with the ASTN2 peptide to which the antibodies were raised (Figure 2.6 B). These results demonstrate that anti-ASTN2 antibodies do recognize ASTN2 protein and that ASTN2 is expressed in a punctate pattern in the cerebellar granule neuron, suggestive of vesicular expression (Figure 2.6 B, left). The peptide blocking (Figure 2.6 B, right) shows that the anti-ASTN2 immunostaining is specific since the punctate staining is eliminated by pre-absorption of the antibody with the peptide against which it was raised. After verifying its recognition and specificity, the anti-ASTN2 antibody will now be utilized as a tool to characterize ASTN2 protein expression and localization.

Biochemical Characterization of ASTN2 Protein Expression:

ASTN2 is Expressed in the Developing and Adult Brain

Using the anti-ASTN2 specific antibody, we assayed the expression of ASTN2 protein in various neonatal mouse tissues via Western blot. ASTN2 is highly expressed in P7 brain, eye, heart, and lung and expressed at lower levels

in the liver and kidney (Figure 2.7 A). Little to no expression of ASTN2 was seen in the spleen or skin. The blot was also probed for GAPDH (bottom panel) to illustrate that an equal amount of protein was added to each lane. Since ASTN2 expression is highest in the brain, the developmental time course of ASTN2 expression was assayed by Western blot in this tissue. This analysis demonstrated that ASTN2 is expressed in both the developing and adult brain and that the expression is developmentally regulated (Figure 2.7 B). Although ASTN2 is weakly expressed in the head at E10 and brain at E12, E14 and E16, expression peaks during the first two postnatal weeks and continues into adulthood (Figure 2.7 B). The developmental analysis also illustrates that ASTN2 and ASTN1 are differentially regulated. ASTN1 is more highly expressed than ASTN2 embryonically, during the time of migration of cortical pyramidal neurons and cerebellar precursors (blue bar). Furthermore, ASTN1 expression is diminished by P10 when the migration of granule neurons along Bergmann glia (red bar) is still ongoing. In comparison, ASTN2 expression peaks and is consistently expressed during the entire period of granule neuron migration (red bar), and continues into adulthood when expression of ASTN1 has ceased. GAPDH expression demonstrates that an equal amount of protein was loading per lane (bottom panel). The results of the developmental assay suggest that ASTN2 may play a slightly different role than ASTN1 during migration, and may possibly serve an alternate function in adulthood.

ASTN2 is an Integral Membrane Protein

Cell fractionation experiments demonstrate that ASTN2 is enriched in membranes and is an integral membrane protein (Figure 2.7 C). P10 cerebellar

Figure 2.7. Biochemical Characterization of ASTN2 Protein Expression.

(**A**) Tissue distribution of ASTN2 protein in neonatal mouse was examined using the anti-ASTN2 antibody. GAPDH loading control is shown in the bottom panel. (**B**) The expression of ASTN1 and ASTN2 in the brain is developmentally regulated. ASTN2 (top) is expressed in the embryonic, postnatal, and adult brain, and the peak of expression occurs during the radial migration of the granule neurons into the IGL (red bar). ASTN1 (middle) is expressed in the embryonic and postnatal brain and its expression overlaps with both the tangential migration of the granule cell precursors in the cerebellar anlage (blue bar) and the radial migration of the granule neurons into the IGL (red bar). The bottom panel shows the GAPDH loading control. (**C**) ASTN2 (top) and ASTN1 (second from top) are integral membrane proteins. Cell fractionations and membrane sub-fractionations were made from P10 cerebellar homogenate. The blot was probed for integral membrane (ErbB4, third from top) and peripheral membrane (MMP9, bottom) proteins as a control. (**D**) Anti-ASTN1 and anti-ASTN2 antibody probing of the membrane fraction from P10 cerebellar homogenate under reducing and non-reducing conditions demonstrates that the ASTN proteins multimerize (arrowhead). (cb=cerebellum; MMP=matrix metallopeptidase; A1=ASTN1; A2=ASTN2; red=reducing).

Figure 2.7

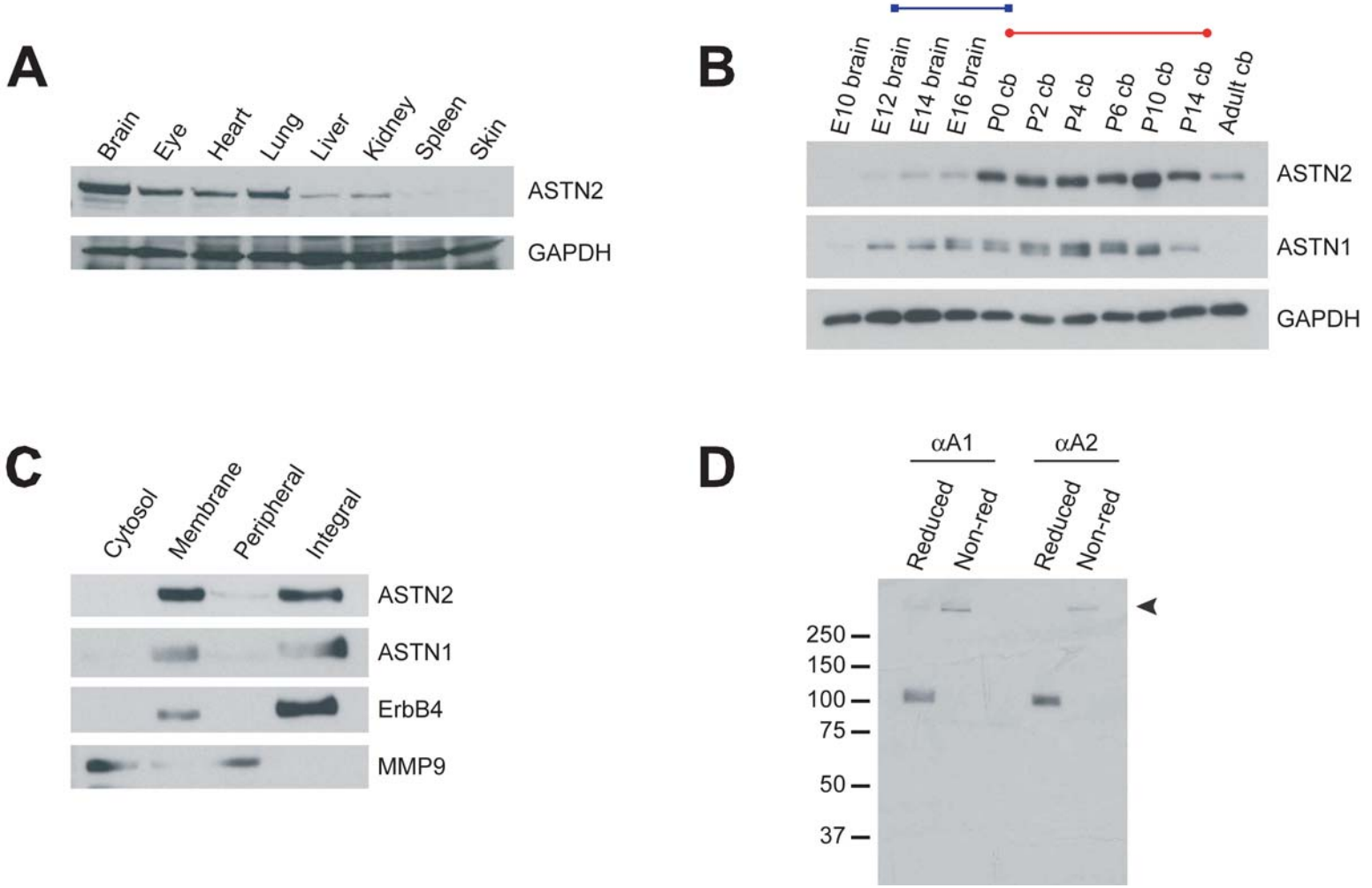
A
Brain
Eye
Heart
Lung
Liver
Kidney
Spleen
Skin
ASTN2
GAPDH
B
E10 brain
E12 brain
E14 brain
E16 brain
P0 cb
P2 cb
P4 cb
P6 cb
P10 cb
P14 cb
Adult cb
ASTN2
ASTN1
GAPDH
C
Cytosol
Membrane
Peripheral
Integral
ASTN2
ASTN1
ErbB4
MMP9
D
αA1
αA2
Reduced
Non-red
Reduced
Non-red
250
150
100
75
50
37

homogenate was separated into cytosolic and membrane fractions, and a portion of the membrane fraction was then further sub-fractionated into peripheral membrane and integral membrane fractions. The Western blot in Figure 2.7 C demonstrates that ASTN2 is predominately expressed in the membrane and integral membrane fractions, although a small amount of ASTN2 was also found in the peripheral membrane fraction. ASTN1 shows an identical sub-cellular expression pattern as ASTN2. As a control, the blot was probed for peripheral membrane (matrix metallopeptidase 9, MMP9) and integral membrane (ErbB4) proteins to demonstrate that the fractionations were complete. Additional Western blotting experiments show that the ASTN proteins multimerize (Figure 2.7 D). ASTN1 and ASTN2 were detected in P10 cerebellar membrane fractions under reducing and non-reducing conditions. Under reducing conditions both ASTN1 and ASTN2 are ~110 kD in size and the super-shifting of the band under non-reducing conditions (arrowhead) indicates that these proteins multimerize in either homomers or heteromers with other proteins.

In vitro Characterization of ASTN2 Protein Expression:

ASTN2 is Expressed in a Speckled Pattern in Transfected HEK293T and Cerebellar Granule Cells

Immunostaining of ASTN2-Venus expression in the HEK293T heterologous cell system demonstrates that ASTN2 is expressed in a speckled pattern. Figure 2.8 A shows a high power confocal *z*-stack of ASTN2-Venus expression in a transfected HEK293T cell. This imaging reveals that ASTN2-Venus is expressed in a speckled pattern throughout the cytoplasm and along the cell membrane but is not present in the nucleus. Furthermore, in cells that have a

Figure 2.8. Immunocytochemistry Characterization of ASTN2 Protein Expression.

(**A**) Expression of ASTN2-Venus in transfected HEK293T cells. Confocal microscopy demonstrates that ASTN2-Venus is expressed in discrete speckles throughout the cell and along the cell processes (arrowheads).
(**B**, **C**) Immunocytochemistry reveals that ASTN2 is expressed in a punctate pattern in cerebellar granule neurons with an accumulation of protein at one edge of the cell (arrowhead). Purified cerebellar granule neurons were fixed after 36 hours culture *in vitro* and immunostained with the anti-ASTN2 antibody.
(**D**-**I**) Immunocytochemistry shows that ASTN2 is expressed in cerebellar granule neurons, but not astroglia. The percoll purified small cell fraction (95% granule neurons, 5% glia) was fixed after 36 hours *in vitro* and immunostained with the anti-ASTN2, anti-Tag-1 and anti-GFAP antibodies. The anti-ASTN2 antibody costains Tag-1 positive cerebellar granule neurons (**F**), but not GFAP astroglia (**I**, arrowheads). **(J**-**M**) Cell surface staining of transfected HEK293T cells. After 36 hours *in vitro*, transfected HEK293T cells were live stained with the anti-ASTN1 and anti-ASTN2 antibodies to detect surface expression. Surface staining reveals that while carboxy-terminus of ASTN1 is expressed on the cell surface (**K**, arrowheads), the carboxyl terminus of ASTN2 is not (**M**). Mock transfected cells were stained with the (**J**) anti-ASTN1 and (**L**) anti-ASTN2 antibodies to control for non-specific reactivity. Scale bar represents 5 μm in **A** and **C**, 10 μm in **B** and **F**, and 20 μm in **I** and **M**. (A2=ASTN2; Tf= transfection; Ab=antibody).

Figure 2.8

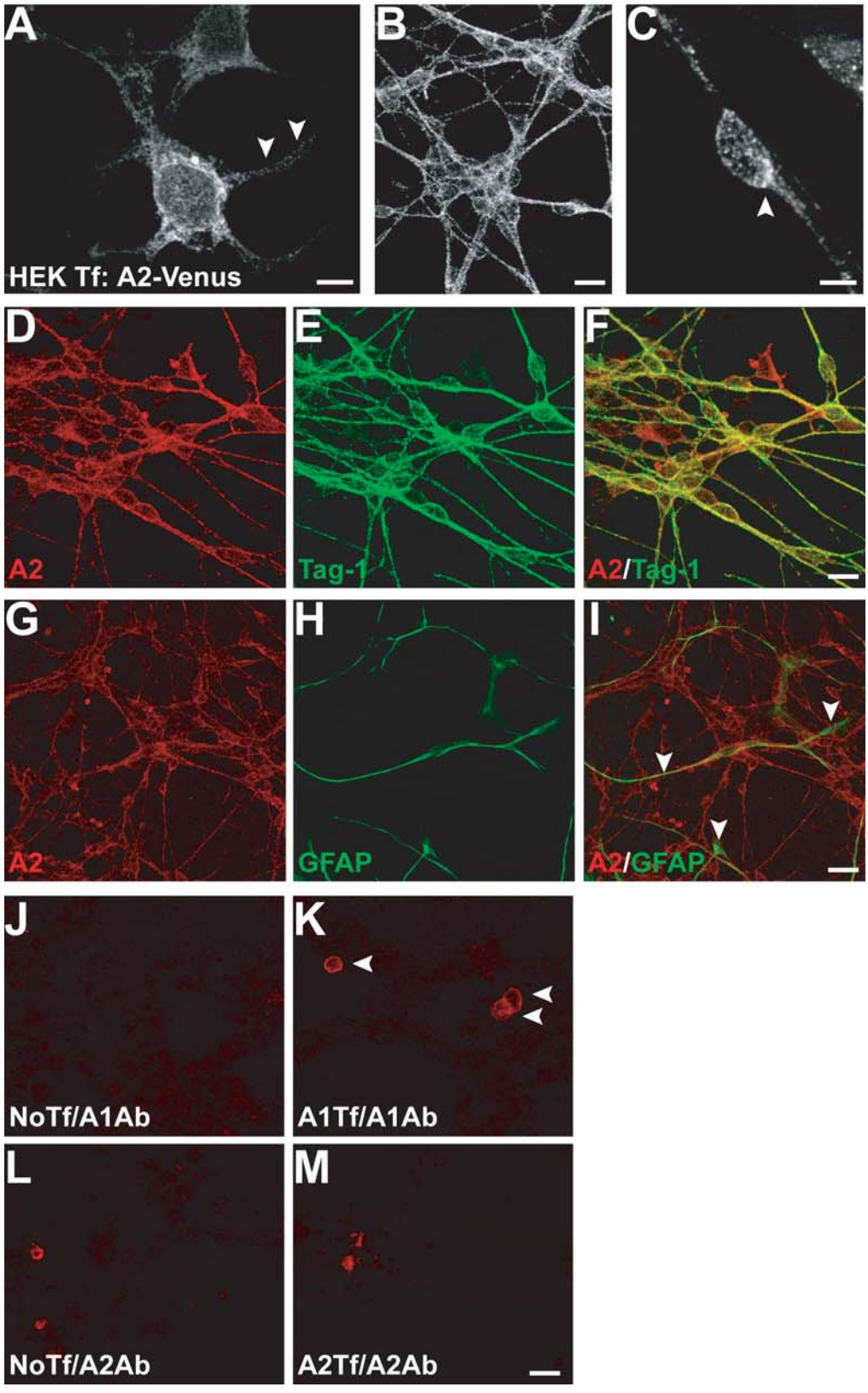
A
HEK Tf: A2-Venus
B
C
D
A2
E
Tag-1
F
A2/Tag-1
G
A2
H
GFAP
I
A2/GFAP
J
NoTf/A1Ab
K
A1Tf/A1Ab
L
NoTf/A2Ab
M
A2Tf/A2Ab

process extended, ASTN2 is expressed in a speckled pattern along the cell process (arrowheads). Immunostaining of endogenous ASTN2 in cerebellar granule cells shows a similar pattern of expression (Figure 2.8 B and C). Confocal microscopy reveals that in granule neurons, ASTN2 is expressed in a punctate fashion throughout the cytoplasm and along the cell membranes, as well as along the neurites (Figure 2.8 B), with an accumulation of ASTN2 protein frequently appearing along one side of the cell (Figure 2.8 C, arrowhead). The staining pattern of both transfected ASTN2-Venus in HEK293T cells and endogenous ASTN2 in granule neurons is suggestive of vesicular/membrane expression.

ASTN2 is Expressed in Neurons, but Not Astroglia

In order to verify the results of the *in situ* hybridization analysis which show ASTN2 is a neuronal protein and not expressed in glia, the small cell fraction of a percoll purification of cerebellar cells containing 95% granule neurons and 5% glia was plated and grown in culture for 48 hours, and then immunostained with anti-ASTN2, anti-Tag-1, and anti-GFAP antibodies. ASTN2 colocalizes in cells that express Tag-1, a granule neuron marker (Figure 2.8 D-F), but is not expressed in cells that express GFAP, a marker of astroglia (Figure 2.8 G-I, arrowheads). The results of this experiment confirm that like ASTN1, ASTN2 is expressed in cerebellar granule neurons and not astroglia.

ASTN1 and ASTN2 are Differentially Exposed on the Cell Surface

Since previous work illustrated that FNIII domain of ASTN1 is expressed on the cell surface of cerebellar granule neurons (Fishell and Hatten, 1991;

Zheng, 1996) and could therefore interact with potential binding partners on Bergmann glial fibers to create adherence junctions during neuronal migration in the postnatal cerebellum, we were interested to see if ASTN2 was similarly localized on the surface of the cell. Live staining experiments using the anti-ASTN1 antibody confirmed the localization of the carboxy-terminus of ASTN1 on the cell surface of transfected HEK293T cells (Figure 2.8 K, arrowheads), while live staining using the anti-ASTN2 antibody failed to detect the carboxy-terminus of ASTN2 on the cell surface (Figure 2.8 M). In Figure 2.8, panel L demonstrates that the immunoreactivity in the ASTN2 transfected cells is comparable to the non-transfected control stained with the anti-ASTN2 antibody and is therefore non-specifically reacting with what appear to be dead cells in the culture.

To further characterize the expression of ASTN2 on the cell surface, we generated Venus tagged constructs containing serial deletions of the ASTN2 protein (Figure 2.9). These constructs were transfected into HEK293T cells and live staining experiments were performed and surface expression was quantified using flow cytometry. In this experiment, Venus-αTubulin (Figure 2.10A, top panel, left) was used as a negative control for surface staining because it is a cytoplasmic protein and therefore contains no extracellular domains, and Neuroligin-1-EYFP (NLG1-EYFP), (Figure 2.10A, top panel, middle) was used as a positive control for surface staining because it is an integral membrane protein that contains domains which are expressed on the cell surface of neurons (Scheiffele et al., 2000). Our results demonstrate that although a portion of the ASTN2 protein may be exposed to the cell surface, as indicated by the positive

Figure 2.9. Schematic of Astn2 Deletion Constructs.

Deletions of Astn2 were created to further characterize ASTN2 protein expression and interactions with ASTN1. Dashed lines represent deleted regions. (Top) Full length Venus tagged Astn2 construct. (Middle) Venus tagged Astn2 individual domain deletions. (Bottom) Venus tagged Astn2 serial domain deletions. (A2=Astn2; Indiv=individual; S=signal sequence; T=transmembrane domain; E=EGF repeat; MACPF=MAC/Perforin domain; FNIII=fibronectin III domain).

Figure 2.9

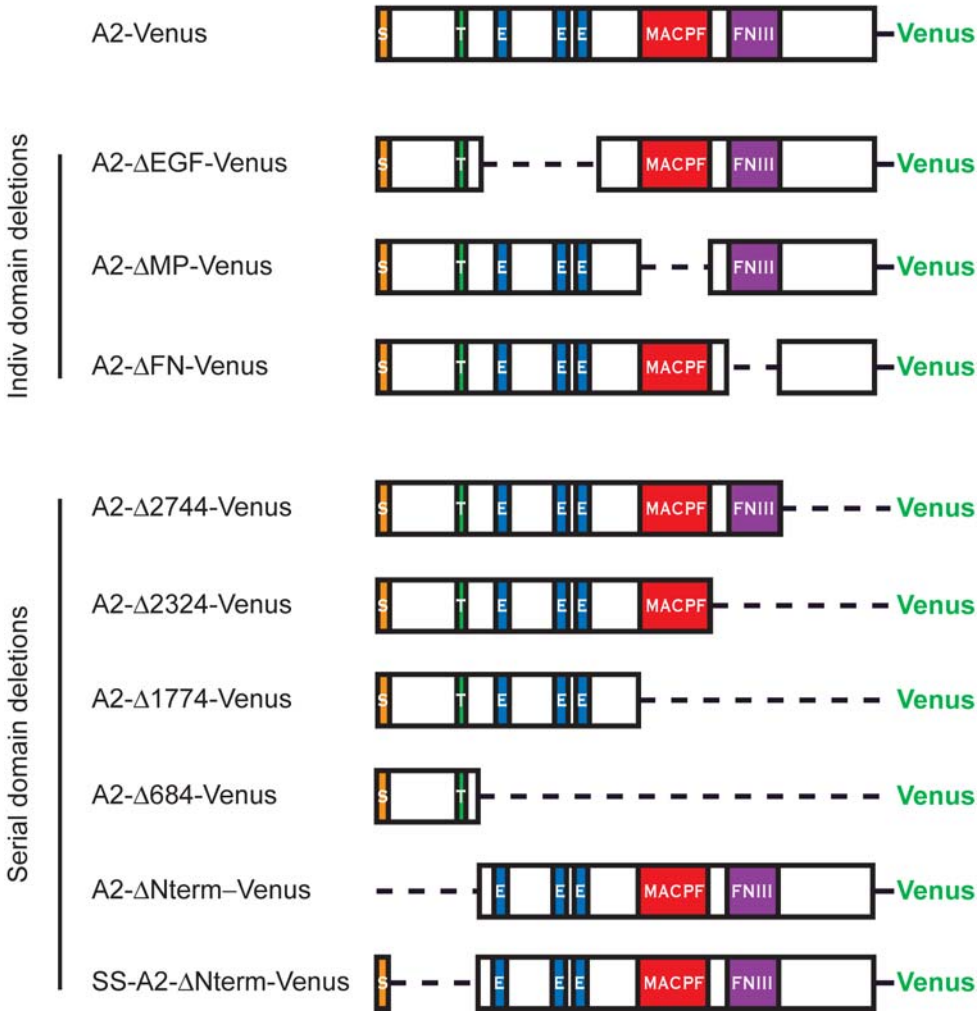
A2-Venus
S
T
E
E
E
MACPF
FNIII
Venus
Indiv domain deletions
A2-ΔEGF-Venus
A2-ΔMP-Venus
A2-ΔFN-Venus
Serial domain deletions
A2-Δ2744-Venus
A2-Δ2324-Venus
A2-Δ1774-Venus
A2-Δ684-Venus
A2-ΔNterm–Venus
SS-A2-ΔNterm-Venus

Figure 2.10. Surface Expression of ASTN2.

Flow cytometry analysis of cell surface staining of transfected HEK293T cells. After 36 hours *in vitro,* transfected HEK293T cells were live stained with an anti-GFP antibody and surface expression was detected with a FACSort Analyzer. (**A**) Surface labeling demonstrates that the A2Δ684-Venus construct is exposed to the cell surface (bottom right dot plot) but full length A2-Venus is not (top right dot plot). Dot plots of surface labeling represented as FL4 (Alexa 647 signal on X-axis) vs. FL1 (Venus/EYFP signal on Y-axis). Upper left quadrant values represent single/transfection (Venus/EYFP) positive cells, and upper right quadrant values represent double positive/surface labeled cells (Venus/EYFP expression positive and Alexa 647 live stain positive). (**B**) Quantification of surface labeling from **A**. Average surface labeling from two experiments was calculated and Student t-test was performed. (Ven=Venus; Tub=Tubulin; NLG1=Neuroligin-1; A2=ASTN2).

Figure 2.10

A

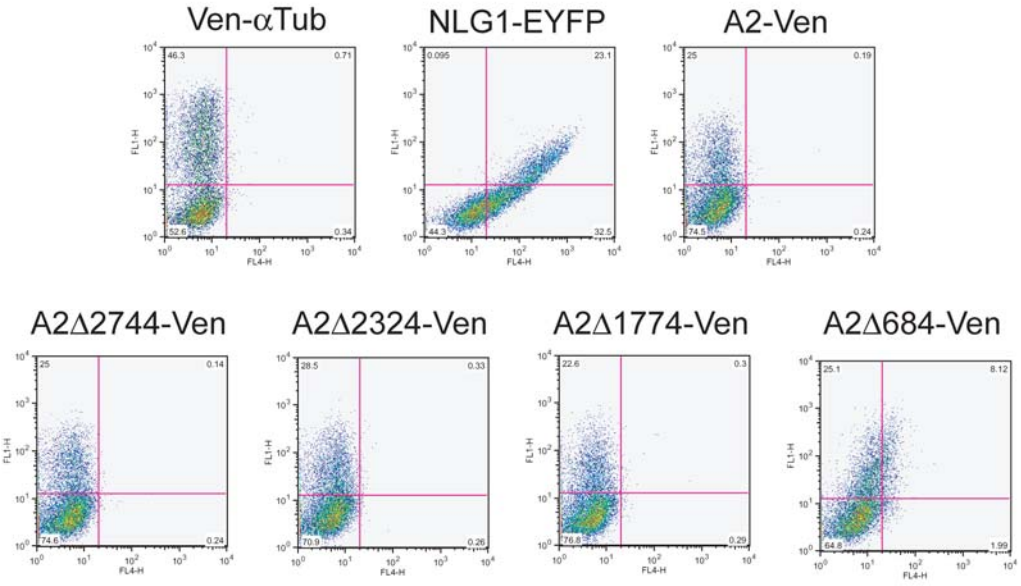

B

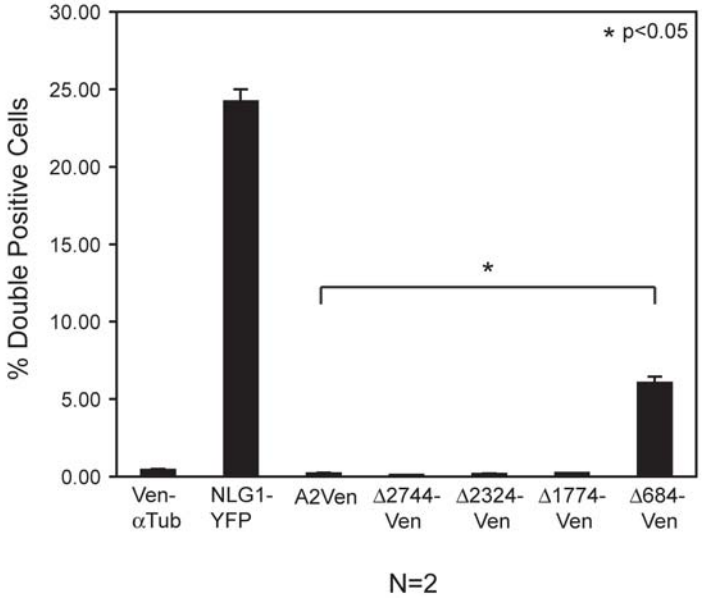

surface labeling detected with the ASTN2-Δ684-Venus construct, a majority of the protein is not exposed on the cell surface (Figure 2.10 A and B). These data are statistically significant as determined by Student t-test. The differential surface expression amongst the ASTN proteins suggests that perhaps ASTN2 may have a distinct role in neuronal migration.

Modeling ASTN2 Membrane Topology

Previous studies (Fishell and Hatten, 1991; Zheng, 1996) and work illustrated in this thesis shows that ASTN1 is located in the plasma membrane as well as in internal membrane compartments, and the carboxy-terminus and FNIII domain of the protein are exposed on the cell surface. However, our live staining results demonstrate that these (and many other) regions of ASTN2 are not exposed on the cell surface (Figure 2.10). These data have two alternate interpretations: 1) ASTN1 and ASTN2 have the same membrane topology but are localized to different cellular compartments or 2) ASTN1 and ASTN2 actually have different orientations in the membrane. To examine these possibilities we analyzed the protein sequence of ASTN2 to identify relevant domains and residues to predict the topology of ASTN2 in the membrane (G. von Heijne, personal communications). Sequence analysis of ASTN2 (Figure 2.11 A) reveals the presence of a putative signal sequence (orange) and transmembrane domain (green), as well as two stretches of positively charged residues (brown) in the amino-terminus. Commonly, an accumulation of positively charged amino acids are found in the cytosolic edge of membrane spanning domains of integral membrane proteins (Alberts, 1994). In light of our sequence analysis and live

Figure 2.11. Models of ASTN2 Membrane Topology.

(**A**) Sequence analysis of ASTN2 reveals a putative signal sequence (orange) and transmembrane domain (green) and two regions of positively charged residues (brown). Locations of the conserved domains are shown: blue, EGF Repeat; red, MAC/Perforin Domain; purple, Fibronectin III Domain. (**B**) Models of ASTN2 membrane topology (orange bar=signal sequence, green bar=transmembrane domain, red bar=MAC/Perforin domain, blue rectangle=cell/ER membrane).

Figure 2.11

A


MGGLIALLLLLLVFTVALYAQRRWQKRRRIPQKSASAEATHEIHYIPSVLLGPQARESFRSSRLQTHNSVIGVPI 75
RETPILDDYDYEEEEEPPRRANHVSREDEFGSQMTHALDSLGRPGEEKVEFEKKGGISFGRTKGTSGSEADDETQL 151
TFYTEQYRSRRRSKGLLKSPVNKTALTLIAVSSCILAMVCGNQMSCPLTVKVTLHVPEHFIADGSSFVVSEGSYLD 227
ISDWLNPAKLSLYYQINATSPWVRDLCGQRTTDACEQLCDPDTGECSCHEGYAPDPVHRHLCVRSDWGQSEGPWPY 303
TTLERGYDLVTGEQAPEKILRSTFSLGQGLWLPVSKSFVVPPVELSINPLASCKTDVLVTEDPADVREEAMLSTYF 379
ETINDLLSSFGPVRDCSRNNGGCTRNFKCVSDRQVDSSGCVCPEELKPMKDGSGCYDHSKGIDCSDGFNGGCEQLC 455
LQQTLPLPYDTTSSTIFMFCGCVEEYKLAPDGKSCLMLSDVCEGPKCLKPDSKFNDTLFGEMLHGYNNRTQHVNQG 531
QVFQMTFRENNFIKDFPQLADGLLVIPLPVEEQCRGVLSEPLPDLQFLTGDIRYDEAMGYPMVQQWRVRSNLYRVK 607
LSTITLSAGFTNVLKILTKESSRDELLSFIQHYGSHYIAEALYGSELTCIIHFPSKKVQQQLWLQYQKETTELGSK 683
KELKSMPFITYLSGLLTAQMLSDDQLISGVEIRCEEKGRCPSTCHLCRRPGKEQLSPTPVLLEINRVVPLYTLIQD 759
NGTKEAFKNALMSSYWCSGKGDVIDDWCRCDLSAFDASGLPNCSPLPQPVLRLSPTVEPSSTVVSLEWVDVQPAIG 835
TKVSDYILQHKKVDEYTDTDLYTGEFLSFADDLLSGLGTSCVAAGRSHGEVPEVSIYSVIFKCLEPDGLYKFTLYA 911
VDTRGRHSELSTVTLRTACPLVDDNQAEEIADKIYNLYNGYTSGKEQQTAYNTLMEVSASMLFRVQHHYNSHYEKF 987
GDFVWRSEDELGPRKAHLILRRLERVSSHCSSLLRSAYIQSRVDTIPYLFCRSEEVRPAGMVWYSILKDTKITCEE 1063
KMVSMARNTYGETKGR* 1079
Signal Sequence
MAC/Perforin Domain
Transmembrane Domain
Fibronectin III Domain
EGF Repeat
Positively Charged Residues

Figure 2.11

B

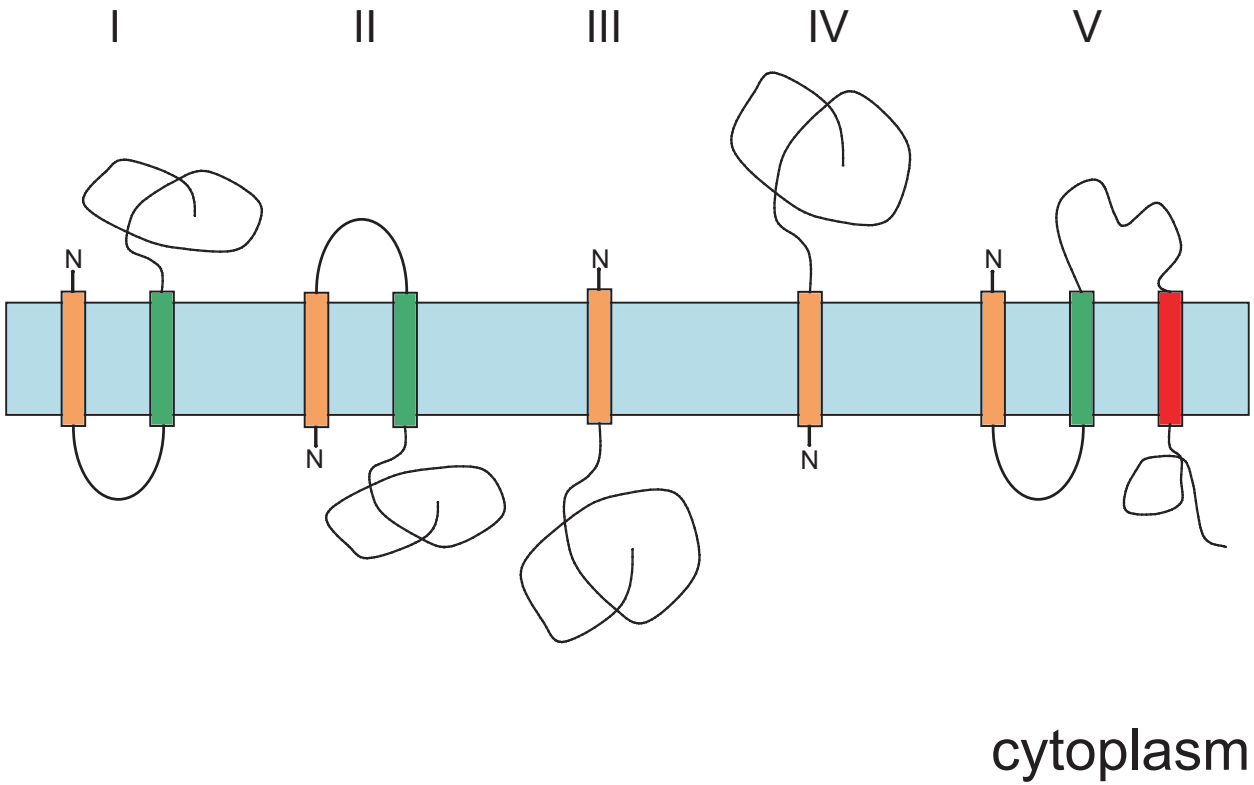

staining data, we have created several hypothetical models of the ASTN2 membrane topology (Figure 2.11 B).

In topology models I and II (Figure 2.11 B) we predict ASTN2 to have multiple membrane passes and illustrate two alternative orientations of the ASTN2 signal sequence and transmembrane domain. The presence of the positively charged residues after the signal sequence and before the transmembrane domain lead us to favor model I, which orients these regions of ASTN2 in the cytoplasmic loop between the membrane-spanning domains. In topology models III and IV we illustrate the case of ASTN2 having only one membrane pass, which is possible since the putative transmembrane domain is less hydrophobic and not as strongly conserved as the predicted signal sequence (G. von Heijne, personal communications). Due to the accumulation of positively charged residues after the signal sequence, we would favor orientation III over IV, since model III positions the positively charged residues at the cytosolic edge of the transmembrane pass. An additional plausible ASTN2 membrane topology is illustrated in model V, in which we predicts that, in addition to the signal sequence and transmembrane domain, ASTN2 may have a third membrane-spanning region. The membrane attack-complex (MAC) of the complement system is know to form transmembrane channels (http://smart.embl-heidelberg.de/smart/do_annotation.pl?DOMAIN=MACPF&START) and thus, we hypothesize that the MAC/PF domain may function as a role as a transmembrane domain in ASTN2.

Examinations of ASTN1 sequence (A. Sali and M.E. Hatten, unpublished observations) and surface staining experiments are consistent with ASTN1 have multiple transmembrane passes and the FNIII domain and carboxy-terminus

exposed on the cell surface. Although the topology of ASTN1 has yet to be experimentally confirmed, we strongly favor topology model I (Figure 2.11 B) for ASTN1. Live cell surface staining data for ASTN2 does not provide direct evidence for this topology, unless, as we outlined earlier, we interpret the negative surface staining results to mean that ASTN1 and ASTN2 are localized to different cellular compartments. Meaning that ASTN2 could have the exact same topology as ASTN1 (Figure 2.11 B, model I) but may not be exposed on the cell surface because it is not localized to the plasma membrane. Instead, ASTN2 expression could be restricted to membrane-bound intracellular compartments. In order for this to be true, the positive live staining we see with the ASTN2-Δ684-Venus construct would have to be due to mislocalization caused by the deletion of a required sorting motif, a possibility which is yet to be resolved. As noted previously, an alternative interpretation of our surface staining data is that ASTN1 and ASTN2 have different orientations in the membrane, and models for potential ASTN2 topologies were presented in Figure 2.11 B. Currently, work is ongoing to resolve the uncertainty of the topology of ASTN2 proteins and proposed studies and their implications on ASTN2 function are discussed in more detail in Chapter 6.

Chapter 3: ASTN1 and ASTN2 Interact

Introduction

Numerous studies established ASTN1 as a neuronal protein involved in glial-guided neuronal migration, however, the glial binding or signaling partner for the Astrotactin proteins has yet to be identified (Fishell and Hatten, 1991; Fishman and Hatten, 1993; Stitt and Hatten, 1990). Furthermore, the Astrotactin proteins have yet to be connected with a downstream signaling pathway. Protein sequence analysis of ASTN1 (Zheng et al., 1996) and ASTN2 (Figure 2.1 A) reveals that both of these proteins contain three EGF repeats, a MAC/PF domain, and a FNIII domain. EGF repeats are found in the extracellular domain of membrane-bound proteins (http://ca.expasy.org/cgi-bin/nicedoc.pl?PDOC 00021) and are involved in protein-protein interactions and receptor binding in other cell-surface receptors including laminin and LDL receptor (Appella et al., 1988). Similarly, FNIII domains are also present in many cell-surface receptors and serve as protein-protein interactions sites (http://ca.expasy.org/cgi-bin/ nicedoc.pl?PDOC50853). Thus, it is likely that the EGF repeats and FNIII domains in the Astn proteins also function as protein binding domains and may be required for interactions with proteins expressed on glial fibers to form the specialized adherence junctions characteristic of glial-guided neuronal migration. The MAC/PF domain is characterized as the signature conserved region amongst the complement components C6, C7, C8-α, C8-β, C9 and perforin, and likely represents a membrane-spanning region (http://ca.expasy.org/cgi-bin/nicedoc.pl?PDOC00251). Therefore the MAC/PF domains in the Astrotactin proteins may be membrane anchoring regions or additional transmembrane

domains. Currently the importance of these conserved domains and their functional significance in the Astrotactin proteins is unknown.

We have shown that both ASTN1 and ASTN2 are expressed in neurons in the developing cerebellum and are both integral membrane proteins (Figure 2.7 B and C) that form higher-order multimers (Figure 2.7 D). Along with the similar subcellular localizations, the multimerization experiments suggest that perhaps ASTN1 and ASTN2 might interact. A heterotypic interaction of ASTN2 with ASTN1 would suggest a role for ASTN2 in glial-guided neuronal migration.

ASTN1 and ASTN2 Interact *In Vitro*

The early postnatal expression of both ASTN1 and ASTN2 in the cerebellum during period of granule cell migration and the localization of these proteins in similar cerebellar cell types and cellular compartments suggests that these two proteins could interact *in vivo*. To determine if ASTN1 and ASTN2 interact, we overexpressed the Astrotactin proteins in HEK293T cells and performed *in vitro* co-immunoprecipitation experiments with the cell lysates. In these experiments we transiently cotransfected pGW1-Astn2-Myc and pGW1-Astn1, pulled down with the anti-ASTN1 antibody and probed for Myc. Figure 3.1 A (top panel, left lane) shows that ASTN2-Myc co-immunoprecipates and, therefore, interacts with ASTN1. The controls verify that the interaction is specific and illustrate that Myc alone does not interact anti-ASTN1 antibody (top panel, middle lane), and the anti-ASTN1 antibody does not interact with ASTN2-Myc in the absence of ASTN1 (top panel, right lane). Whole cell lysate input loading controls are shown in the bottom two panels. In combination with our previous protein localization results (Figure 2.7C), one interpretation is that the interaction between ASTN1 and ASTN2 could occur in the cell membrane and/or membranes of vesicles within the cell.

ASTN1:ASTN2 Binding is Independent of Conserved Domains

In order to determine the region responsible for the ASTN1:ASTN2 interaction, we generated pRK5-Astn2-Venus tagged constructs with deletions of the individual conserved domains of the protein (Figure 2.9). The Astn2-Venus tagged deletions and pGW1-Astn1-Myc were cotransfected in HEK293T cells and co-immunoprecipitations were performed by pulling down with anti-GFP

Figure 3.1. ASTN1 and ASTN2 Interactions.

Lysates from transfected HEK293T cells were prepared and co-IP was performed. (**A**) Co-IP with the anti-ASTN1 antibody reveals that ASTN1 and ASTN2 interact. (Top) Western blot of co-IP samples pulled down with the anti-ASTN1 antibody and probed with an anti-Myc antibody to detect ASTN2-Myc shows that ASTN1 and ASTN2 interact *in vitro*. (Bottom) Whole cell lysate loading controls. (**B**, **C**, **D**) Co-IP with an anti-GFP antibody demonstrates that (**B**) no individual conserved domain in ASTN2 is required for the ASTN1:ASTN2 interaction, (**C**) the ASTN1:ASTN2 interaction occurs in the membrane or in the membrane trafficking pathway and (**D**) the ASTN1:ASTN2 interaction is calcium independent. (Top) Western blot of co-IP samples pulled down with anti-GFP and probed with an anti-Myc antibody to detect ASTN1-Myc. (Bottom) Whole cell lysate loading controls. (IP=immunoprecipitation; A1=ASTN1; A2=ASTN2; M=Myc; V=Venus; SS=signal sequence).

Figure 3.1

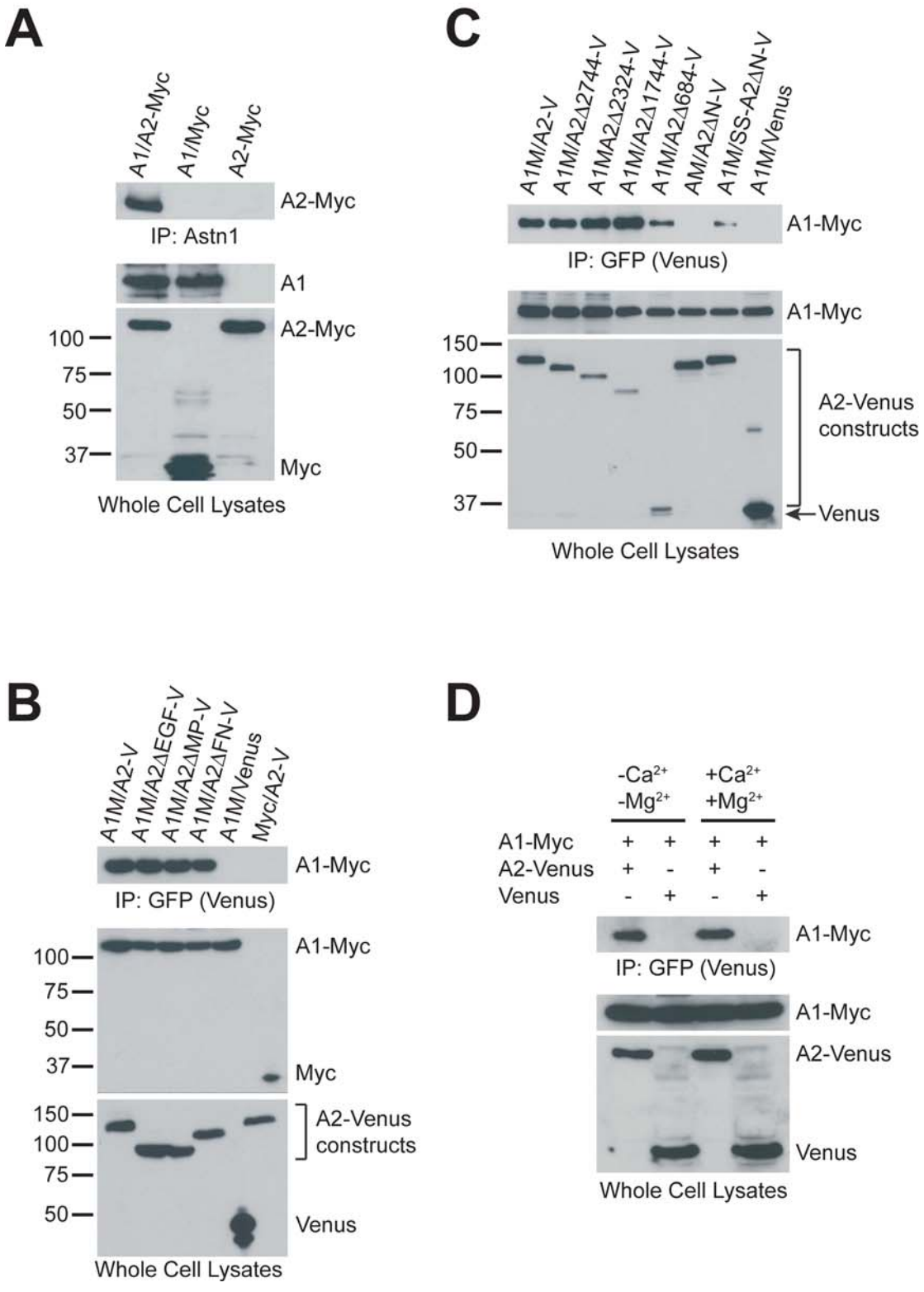
A
A1/A2-Myc
A1/Myc
A2-Myc
A2-Myc
IP: Astn1
A1
A2-Myc
100
75
50
37
Myc
Whole Cell Lysates
C
A1M/A2-V
A1M/A2Δ2744-V
A1MA2Δ2324-V
A1M/A2Δ1744-V
A1M/A2Δ684-V
AM/A2ΔN-V
A1M/SS-A2ΔN-V
A1M/Venus
A1-Myc
IP: GFP (Venus)
A1-Myc
150
100
75
50
37
A2-Venus constructs
Venus
Whole Cell Lysates
B
A1M/A2-V
A1M/A2ΔEGF-V
A1M/A2ΔMP-V
A1M/A2ΔFN-V
A1M/Venus
Myc/A2-V
A1-Myc
IP: GFP (Venus)
A1-Myc
100
75
50
37
Myc
150
100
75
50
A2-Venus constructs
Venus
Whole Cell Lysates
D
-Ca2+ -Mg2+
+Ca2+ +Mg2+
A1-Myc + + + +
A2-Venus + - + -
Venus - + - +
A1-Myc
IP: GFP (Venus)
A1-Myc
A2-Venus
Venus
Whole Cell Lysates

(ASTN2-Venus) and probing for Myc (ASTN1-Myc). As shown in Figure 3.1 B (top panel), the ASTN2-ΔEGF-Venus, ASTN2-ΔMP-Venus, and ASTN2-ΔFN-Venus deletion proteins all interact with ASTN1, demonstrating that no individual conserved domain is responsible for the ASTN1:ASTN2 interaction. Since the control immunoprecipitations show that the interactions are specific and Venus does not pull down ASTN1-Myc nor does ASTN2-Venus interact with Myc alone (Figure 3.1 B, top panel, right most lanes), we conclude that the binding between ASTN1 and ASTN2 is independent of the conserved domains. Loading controls of the whole cell lysates are shown in the bottom two panels.

ASTN1:ASTN2 Binding Requires Sorting of ASTN2 to the Membrane

In an effort to narrow down the region of interaction between ASTN1 and ASTN2, we generated Astn2-Venus tagged constructs containing serial deletions of the protein as illustrated in Figure 2.9. These Astn2 serial deletion constructs were then cotransfected with pGW1-ASTN1-Myc into HEK293T cells and co-immunoprecipitation experiments were performed as described for the conserved domain deletions. These experiments provide evidence to support our hypothesis that the ASTN1:ASTN2 interactions occur in the cell membrane or membrane compartments within the cell (Figure 3.1 C). ASTN1-Myc interacts with the ASTN2-Δ2744-Venus, ASTN2-Δ2324-Venus, ASTN2-Δ1744-venus, ASTN2-Δ684-Venus, and SS-ASTN2-ΔNterm-Venus deletion proteins (Figure 3.1 C, top). The only case in which the ASTN1:ASTN2 interaction does not occur is when ASTN1 is coexpressed with ASTN2-ΔNterm-Venus, an ASTN2 protein containing a deletion of the N-terminus and no signal sequence (Figure 3.1 C,

top, third lane from right). Without a signal sequence, the ASTN2-ΔNterm-Venus deletion protein is mislocalized and does not get targeted to the membrane/membrane compartments (Figure 3.2, right) like the full length ASTN2-Venus and the SS-ASTN2-ΔNterm-Venus deletion with the engineered conventional signal sequence (Figure 3.2 left and middle respectively). We conclude the mistargeting of the ASTN2-ΔNterm-Venus results in the elimination of the interaction between ASTN1 and ASTN2 since the ASTN2 amino-terminal deletion construct with an engineered conventional signal sequence is still able to bind the ASTN1 protein (Figure 3.1 C, lane 7). Thus our results suggest that the ASTN1 and ASTN2 interaction occurs in the membrane or in the membrane trafficking pathway.

Furthermore, this experiment demonstrates that the binding between ASTN1 and ASTN2 still exists even if only a single region of the ASTN2 protein is present as is the case with the ASTN2-Δ684-Venus (Figure 3.1 C, top panel, lane 5). This deletion contains only the amino-terminus of the ASTN2 protein (and no conserved domains) but is still sufficient to permit binding to ASTN1. The control immunoprecipitation (Figure 3.1 C, top panel, right most lane) verifies that the interactions are specific and not due to interactions of either the Myc or Venus tags. Loading controls of the whole cells lysates are shown in the bottom two panels. Taken together these results suggest a strong interaction exists between the ASTN1 and ASTN2 proteins and this interaction may have functional implications.

Figure 3.2. Without a Signal Sequence, ASTN2ΔNterm-Venus is Mislocalized.

In transfected HEK293T cells, expression of A2-Venus and SS-ASTN2ΔNterm-Venus is localized to membranes and vesicles while A2ΔNterm-Venus expression is cytoplasmic. Transfected cells were fixed after 36 hours *in vitro*, immunostained using an anti-GFP antibody, and imaged via confocal microscopy. Images shown are reconstructed 7 μm z-stacks. Expression of A2-Venus and SS-ASTN2ΔNterm-Venus is localized to membranes and vesicles while A2ΔNterm-Venus expression is cytoplasmic. Scale bar represents 10 μm. (A2=ASTN2; SS=signal sequence).

Figure 3.2

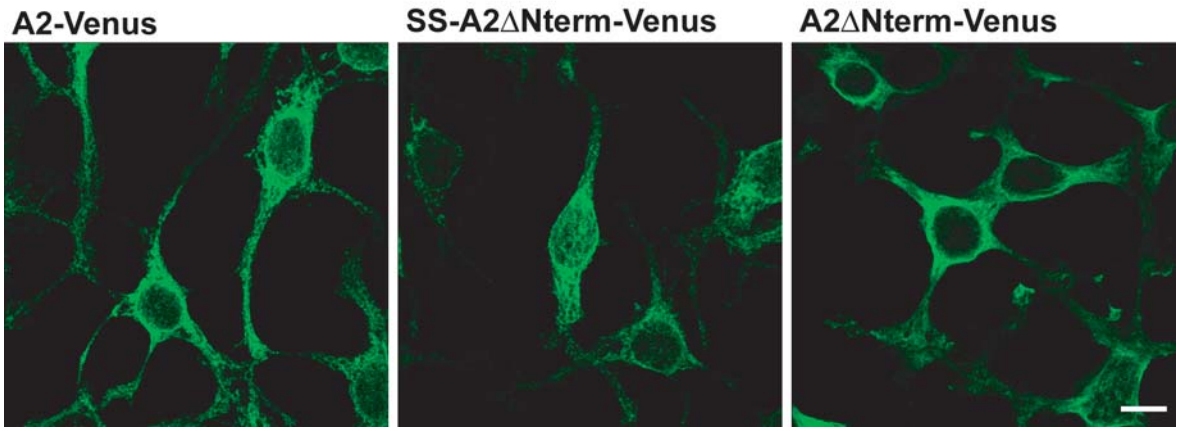

The ASTN1:ASTN2 Interaction is Calcium Independent

Previous data demonstrates that glial-guided neuronal migration is calcium independent. Both the binding of [^{35}S]-methionine-labeled granule cells to glial cells and the anti-ASTN1 FAB fragment inhibition of the binding of [^{35}S]-methionine-labeled plasma membranes to glial cells occur in a calcium independent manner (Stitt and Hatten, 1999). In order to determine if the interaction between ASTN1 and ASTN2 was also calcium independent we performed co-immunoprecipitations of transfected ASTN1-Myc and ASTN2-Venus in HEK293T cells in the presence and absence of calcium and magnesium in the immunoprecipitation buffer. The result of this experiment demonstrates that the interaction between ASTN1 and ASTN2 is also calcium independent (Figure 3.1 D). As shown by the intensity of the ASTN1-Myc signal in the immunoprecipitation lanes (Figure 3.1 D, top), the ASTN1 and ASTN2 interaction is equally as strong in the presence of 1mM $CaCl_2$ and 0.5mM $MgCl_2$ (no EDTA or EGTA) as it is in the absence of both cations (plus EDTA and EGTA) demonstrating that the interaction between ASTN1 and ASTN2 can occur under various conditions. Whole cell lysate loading controls are shown in the bottom panels.

The Stoichiometry of the ASTN1:ASTN2 Interaction is Important

Overexpression of ASTN1 and ASTN2 in granule neurons demonstrates the importance of the stoichiometry of the ASTN1:ASTN2 interaction. To look at the effects of overexpression in neurons, we electroporated purified cerebellar granule neurons with either pCIG-Astn1-Venus or pCIG-Astn2-Venus, or both, and then live stained with propidium iodide to determine cell viability. When

either ASTN1-Venus or ASTN2-Venus are overexpressed individually in granule cells, the Venus positive neurons die as indicated by the propidium iodide positive nuclei (Figure 3.3 A and B, arrowheads). Live imaging of neurons expressing either ASTN1-Venus or ASTN2-Venus reveals that these neurons are undergoing cell death as indicated by the limited cell process extension and membrane blebbing (data not shown).

However, when both ASTN1-Venus and ASTN2-Venus are overexpressed in granule cells, many of the coelectroporated neurons survive (Figure 3.3 C, stars). The positive neurons in the ASTN1-Venus and ASTN2-Venus co-overexpression have a similar morphology to the control Venus electroporated neurons (Figure 3.3 D), indicating that these neurons are differentiating normally. We quantified these results by scoring the Venus positive neurons in each condition as live or dead, based on the propidium iodide staining. The results of three independent experiments demonstrate that, on average, only 15+/-3% of ASTN1-Venus and 12+/-6% of ASTN2-Venus electroporated neurons survive when either construct is overexpressed alone (Figure 3.3 E). However, when these proteins are overexpressed together, the survival of the positively electroporated cells increases to 59+/-3%. The survival of the ASTN1-Venus and ASTN2-Venus coelectroporated cells is significant over the individual overexpressions as determined by Student t-test ($p<0.01$ and $p<0.05$ respectively, $n=3$). Although the overall survival of the coelectroporated cells is reduced as compared to the Venus control, this difference can be attributed to the limitations of the coelectroporation technique and it is likely that most of the dead cells were only singly transfected.

Figure 3.3. The Stoichiometry of the ASTN1:ASTN2 Interaction is Important.

Overexpression of (**A**) ASTN1-Venus, (**B**) ASTN2-Venus, (**C**) ASTN1-Venus and ASTN2-Venus, and (**D**) Venus reveals the importance of stoichiometry of the ASTN1:ASTN2 interaction. Purified granule neurons were electroporated and cultured *in vitro* for 16 hours. Cultures were live stained with propidium iodide, fixed, and then immunostained with an anti-GFP antibody. (**E**) Quantification of cell viability staining in **A**, **B**, **C**, and **D**. Average cell survival from three experiments was calculated and significance was determined by Student t-test. Scale bar represents 10 μm. (A1=ASTN1; A2=ASTN2; Ven=Venus).

Figure 3.3

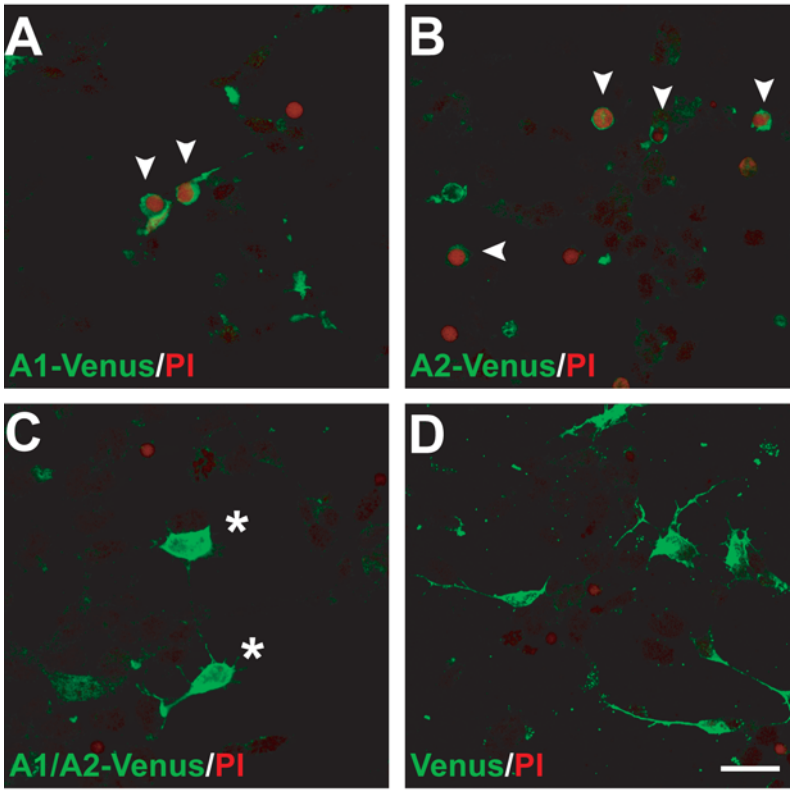
A
A1-Venus/PI
B
A2-Venus/PI
C
A1/A2-Venus/PI
D
Venus/PI

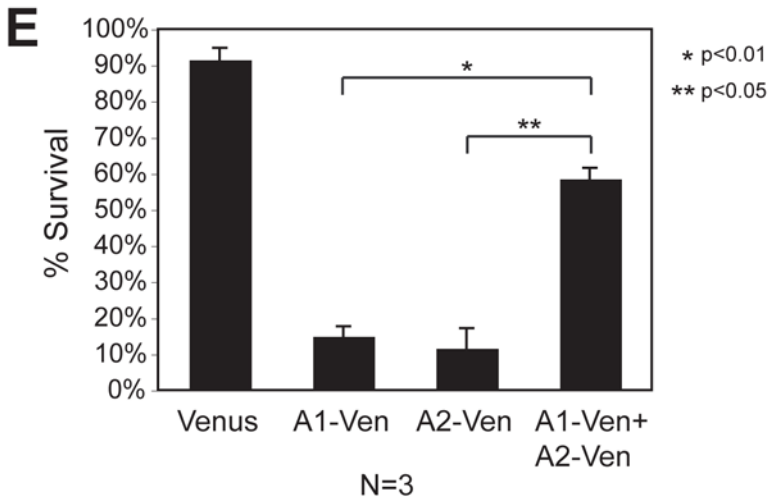
E
100%
90%
80%
70%
60%
50%
40%
30%
20%
10%
0%
% Survival
*
**
* p<0.01
** p<0.05
Venus
A1-Ven
A2-Ven
A1-Ven+
A2-Ven
N=3

In order to estimate the level of overexpression in electroporated neurons, pCIG2-Astn1-ires-EGFP and pCIG2-Astn2-ires-EGFP constructs were electroporated into granule neurons and immunostaining with the anti-ASTN1 and anti-ASTN2 antibodies was used to evaluate fluorescence intensity of transfected (Figure 3.4, arrows) vs. non-transfected neurons. The results reveal that transfected neurons express only 1.1-1.3 times the protein level of non-transfected neurons and suggest that a small imbalance in the stoichiometry of ASTN1 and ASTN2 can have significant cellular consequences. Together, these results demonstrate that the interplay between ASTN1 and ASTN2 is important and that the stoichiometry of this interaction has functional significance for the granule neurons.

Figure 3.4. Quantification of ASTN Overexpression in Granule Neurons.

Coelectroporation of (**A**, **B**) ASTN1-iresEGFP and ASTN2-Myc and (**C**, **D**) ASTN1-iresEGFP and ASTN1-Myc in cerebellar granule neurons reveals that the overexpression is at near physiological levels (arrows). Purified granule neurons were electroporated, cultured *in vitro* for 36 hours and immunostained with anti-GFP (shown in **A** and **C**) and anti-ASTN (shown in **B** and **D**) antibodies. Scale bar represents 10 μm.

Figure 3.4

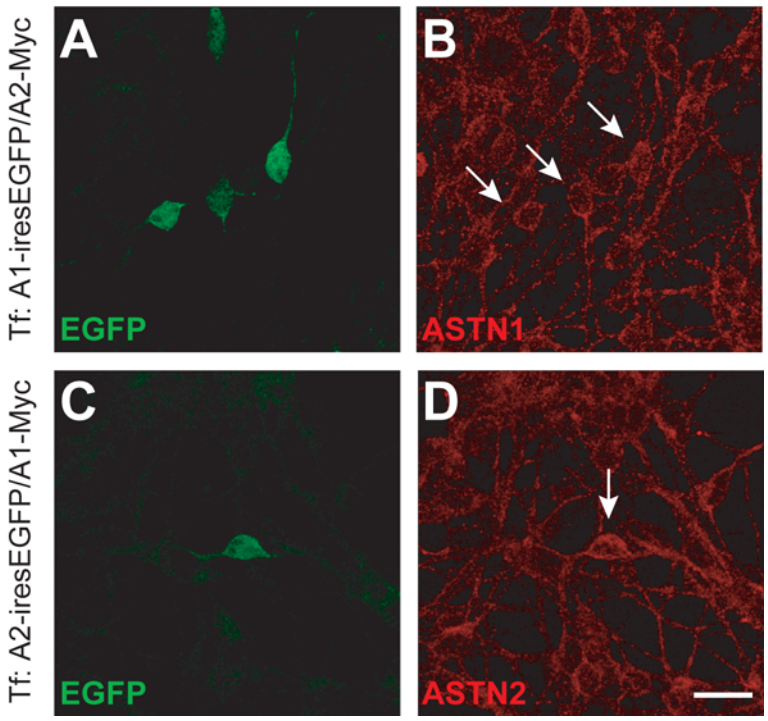
A
B
C
D
Tf: A1-iresEGFP/A2-Myc
Tf: A2-iresEGFP/A1-Myc
EGFP
EGFP
ASTN1
ASTN2

Chapter 4: Links Between ASTN1, ASTN2, and Endocytosis

Introduction

Endocytosis is a complex and tightly controlled process through which receptors, channels, transporters, and other integral membrane proteins are selectively internalized to control the composition of the plasma membrane, downregulate signaling, and recycle transmembrane proteins (Le Roy and Wrana, 2005; Maldonado-Baez and Wendland, 2006; Sorkin, 2004; Szymkiewicz et al., 2004). The endocytic clearance of proteins from the cell surface can be constitutive or ligand-induced, and occurs in a clathrin-dependent or clathrin-independent but lipid-raft-dependent manner (Le Roy and Wrana, 2005; Szymkiewicz et al., 2004). Furthermore, as noted by Szymkiewicz and colleagues (2004), the recruitment of receptors into specialized membrane domains, the formation of vesicles and the trafficking of receptors together with their ligands within endocytic compartments are regulated by reversible protein modifications, and multiple protein–protein and protein–lipid interactions.

Numerous studies reveal a role for endocytosis in growth cone collapse (Fournier et al., 2000) and motility (Kamiguchi et al., 1998) and the disassembly of adhesion sites at the rear of migrating neutrophils (Fan and Malik, 2003; Lawson and Maxfield, 1995; Pierini et al., 2000) and macrophages (Cao et al., 2006). Taken together, these studies demonstrate the importance of turnover of cell surface adhesion proteins in growth cone and cell motility and suggest a recycling mechanism by which receptors from adhesion sites in the rear of the cell or growth cone are removed from the surface via endocytosis and trafficked to the advancing edge, providing fresh adhesion receptors to these areas and permitting forward movement (Pellinen and Ivaska, 2006). The role of the

endo/exocytic cycle of integrins and other cell surface adhesion proteins including the L1 subfamily of CAMs and lipoprotein receptor related protein (LRP) receptor in cell adhesion and motility are becoming progressively better established (Cao et al., 2006; Pellinen and Ivaska, 2006; Thelen et al., 2002).

The release of adhesion sites at the rear of migrating cells and creation of new adhesion sites at the leading edge is essential for forward movement. Lawson and Maxfield (1995) and Pierini et al. (2000) demonstrated that integrins de-adhere from the substratum and are internalized into endocytic vesicles at the rear of motile neutrophils, and proposed that these adhesion molecules are then recycled forward to the advancing edge of the cell for the creation of new adhesion sites. Early studies by Bretscher (1989) on the fibronectin receptor of CHO cells (integrin $\alpha 5\beta 1$) illustrated that this receptor undergoes active endocytosis whereby the receptor is primarily recycled instead of degraded, supporting the theory that as neutrophils migrate, integrins are endocytosed at sites of detachment at the rear of the cells and trafficked to new sites of adhesion at the leading edge. In addition, the active endocytosis of surface adhesion molecules has also been shown to be important in the de-adhesion step of macrophage migration. The interaction of the LRP receptor/integrin/Mac-1 complex at the trailing edge of macrophages triggers a switch from cell adhesion to cell detachment, resulting in the internalization of the adhesion complex via endocytosis and de-adhesion at the rear of the cell (Cao et al., 2006). Zhang and colleagues (2006) suggested that the endocytosed adhesion complex is then recycled to the surface of the leading edge of the migrating cell, allowing for the formation of a new adhesion and forward movement of the macrophage, similar to the paradigm presented by Lawson and Maxfield (1995).

Similarly, the cell adhesion molecule L1 was shown to be internalized at the rear of growth cones, and this regulation of L1 surface expression is suggested to be important for axon growth and growth cone motility (Lemmon, 1998). In addition, Thelen et al. (2002) and Panicker et al. (2006) demonstrated a role for L1 in the potentiation of cell migration though β1 integrins, which is dependent on receptor-mediated endocytosis. Thelen et al. (2002) also illustrated that that antibody-induced endocytosis of L1 and β1 integrin had an inhibitory effect on migrating neurons in acute cerebellar slices suggesting a role for endocytosis in neuronal migration.

Interestingly, these L1 studies and additional investigations of the endocytosis of integrins (reviewed in Pellinen and Ivaska, 2006) demonstrated that the endocytosis of these cell surface adhesion molecules is dependent upon the cytoplasmic domain of the protein containing tyrosine-based endocytosis sorting signals of the type YXXΦ (where X is any residue and Φ is a hydrophobic residue). This motif is required for the binding of the clathrin adaptor protein, AP-2, which in turn recruits clathrin to the plasma membrane to induce the endocytosis of the receptors (Maldonado-Baez and Wendland, 2006; Marsh, 2001). Mutations or deletions of this motif significantly reduce/eliminate endocytosis of the receptors (Panicker et al., 2006; Thelen et al., 2002) or alters the trafficking of the receptors after internalization (Kamiguchi et al., 1998).

Although a role for endocytosis in glial-guided migration has just recently been considered, evidence suggestive of this phenomenon exists in early time-lapse video and EM studies. Video microscopy and correlated EM studies of migrating cerebellar granule neurons demonstrated the presence of coated

vesicles at the adherence junctions between migrating neuron and glial fiber (Gregory et al., 1988) and revealed a dynamic flow of vesicles into the leading process of migrating neurons (Edmondson and Hatten, 1987). Together, these results suggest that the endocytosis of cell surface adhesion proteins may also occur at the junctional adhesion sites that exist between neuronal cell soma and glial fiber during migration and perhaps this endocytosis is required for detachment of adhesion sites at the rear of the neuron and forward movement of the cell, much like the model proposed for the advancement of neutrophils.

The cell surface adhesion protein ASTN1 mediates neuron-glial adhesion and is required for glial-guided neuronal migration (Adams et al., 2002; Edmondson et al., 1988; Fishell and Hatten, 1991; Stitt and Hatten, 1990). However a role for the related protein ASTN2 in neuronal migration has not yet been defined. Based on the incomplete disruption of migration seen in the Astrotactin null mice, we originally hypothesized that ASTN2 had a redundant role to ASTN1; yet, our cell surface localization studies demonstrate that unlike ASTN1, the much of the ASTN2 protein is not exposed on the cell surface and, therefore, may ASTN2 may function differently. Still, the strong interaction between ASTN1 and ASTN2 suggests the interaction may be important for the function of these molecules.

Coexpression with ASTN2 Changes the Cell Surface Localization of ASTN1: Immunocytochemistry Evaluation

Due to the strong biochemical interaction we observed between ASTN1 and ASTN2, we hypothesized that coexpression of ASTN1 might be required for exposure of ASTN2 on the cell surface of HEK293T cells. We cotransfected pGW1-Astn1-Myc and pCIG-Astn2-Venus into HEK293T cells and then performed live cell immunostaining with an anti-GFP antibody to detect the cell surface expression of the carboxy-terminus of ASTN2. In this experiment, Venus-αTubulin (Figure 4.1 A, left panels) was used as a negative control for surface staining because it is a cytoplasmic protein and therefore contains no extracellular domains, and Neuroligin-1-EYFP (NLG1-EYFP), (Figure 4.1 A, second from left) was used as a positive control for surface staining because it is an integral membrane protein that contains domains which are expressed on the cell surface of neurons (Scheiffele et al., 2000). Our results demonstrate that the carboxy-terminus of ASTN2-Venus is not exposed to the surface in the absence or presence of ASTN1 (Figure 4.1 A, right most panels). To further investigate the functionality of the ASTN1:ASTN2 interaction we repeated the live staining experiment focusing on ASTN1-Venus cell surface localization. Previous results demonstrate that the carboxy-terminus of ASTN1 is exposed to the cell surface [(Fishell and Hatten, 1991) and Figure 2.8 K], and this result was further confirmed in this experiment. Figure 4.1 A (third from left) shows a discrete, speckled cell surface staining pattern in the cells cotransfected ASTN1-Venus and Myc. Unexpectedly, when pCIG-Astn1-Venus was cotransfected with pGW1-Astn2-Myc (Figure 4.1 A, third from right), the surface expression of ASTN1 was significantly diminished to levels close to that of the negative control (Venus-

Figure 4.1. Coexpression with ASTN2 Changes the Cell Surface Localization of ASTN1.

(**A**) Cell surface staining of transfected HEK293T cells demonstrates that when coexpressed with ASTN2, ASTN1 is no longer exposed on the cell surface (top panel, third from right). ASTN1 surface expression in the absence of ASTN2 is shown (top panel, third from left). Transfected cells were cultured 36 hours *in vitro* and live cell immunostained with an anti-GFP antibody. Top panel shows surface staining via recognition of the anti-GFP with an AlexaFluor 555 secondary antibody. Bottom panel illustrates Venus/EYFP expression and verifies the cells were transfected. Scale bar represents 20 μm. (**B**) Flow cytometry analysis of ASTN live staining confirms that coexpression with ASTN2 changes the cell surface localization of ASTN1. After 36 hours *in vitro*, transfected HEK293T cells were live stained with an anti-GFP antibody and surface expression was detected with a FACSort Analyzer. Surface labeling demonstrates that the carboxy-terminus of ASTN1 is exposed on the cell surface (top, middle), but when coexpressed with ASTN2, less ASTN1 is exposed on the cell surface (top, right). Dot plots of surface labeling represented as FL4 (Alexa 647 signal on X-axis) vs. FL1 (Venus/EYFP signal on Y-axis). Upper left quadrant values represent single/transfection (Venus/EYFP) positive cells, and upper right quadrant values represent double positive/surface labeled cells (Venus/EYFP expression positive and AlexaFluor 647 live stain positive). (**C**) Quantification of surface labeling from **B**. Average surface labeling from three experiments was calculated and Student t-test was performed to determine significance. (Ven, V=Venus; Tub=Tubulin; NLG1=Neuroligin-1; A1=ASTN1; A2=ASTN2).

Figure 4.1

A

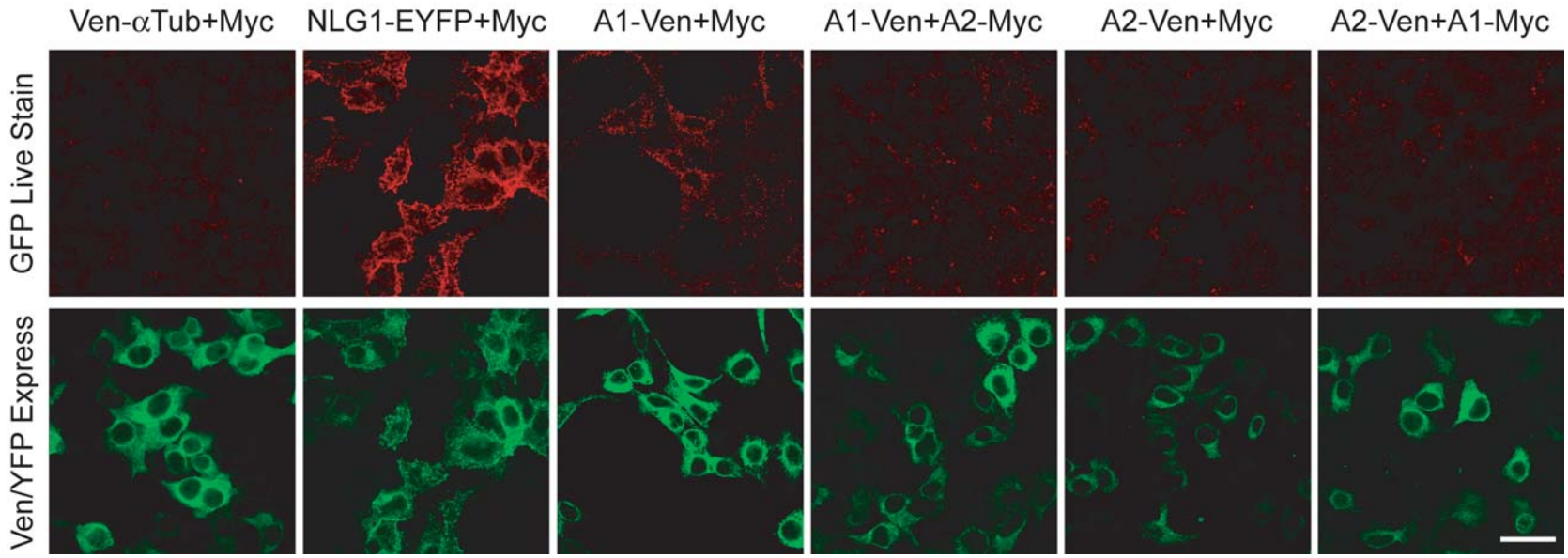
Ven-αTub+Myc
NLG1-EYFP+Myc
A1-Ven+Myc
A1-Ven+A2-Myc
A2-Ven+Myc
A2-Ven+A1-Myc
GFP Live Stain
Ven/YFP Express

Figure 4.1

B

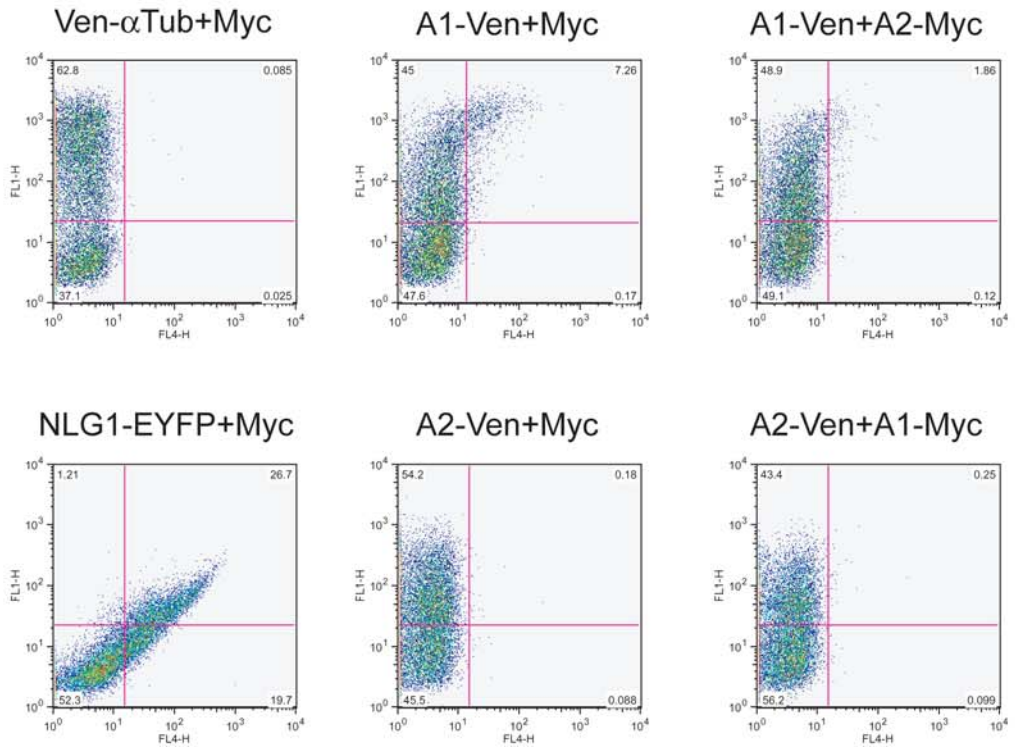
Ven-αTub+Myc
62.8
0.085
37.1
0.025
A1-Ven+Myc
45
7.26
47.6
0.17
A1-Ven+A2-Myc
48.9
1.86
49.1
0.12
NLG1-EYFP+Myc
1.21
26.7
52.3
19.7
A2-Ven+Myc
54.2
0.18
45.5
0.088
A2-Ven+A1-Myc
43.4
0.25
56.2
0.099
FL1-H
FL4-H

C

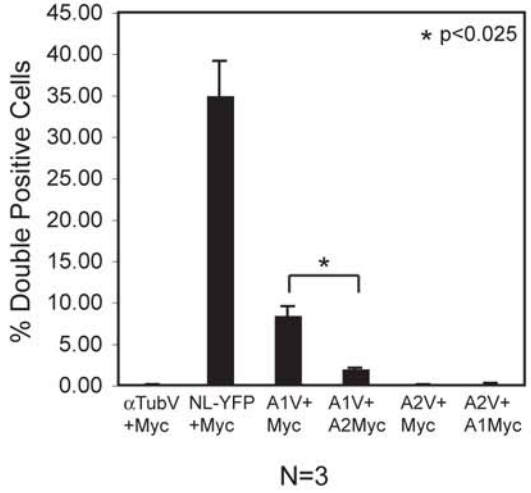
% Double Positive Cells
45.00
40.00
35.00
30.00
25.00
20.00
15.00
10.00
5.00
0.00
* p<0.025
*
αTubV +Myc
NL-YFP +Myc
A1V+ Myc
A1V+ A2Myc
A2V+ Myc
A2V+ A1Myc
N=3

αTubulin). The bottom panel of Figure 4.1 A shows Venus/EYPF expression, demonstrating the cultures were positively transfected. To equalize the amount of DNA during transfection and to ensure the Myc tag had no effect on localization, when examining individual surface expression, Venus-αTubulin, NLG1-EYFP, ASTN1-Venus, and ASTN2-Venus were cotransfected with Myc.

Flow Cytometry Quantification

We further verified and quantified the live cell immunostaining results by measuring the levels of surface staining via flow cytometry. The flow cytometry results confirm that coexpression of ASTN2 changes the cell surface localization of ASTN1 (Figure 4.1 B). When ASTN1-Venus is expressed with Myc (top middle), on average, 8.46+/-1.07% of cells have ASTN1-Venus on the cell surface (Figure 4.1 C). However, when coexpressed with ASTN2-Myc, ASTN1-Venus surface localization is decreased four-fold to only 2.02+/-0.115% of cells (B, bottom middle and C). The change in ASTN1-Venus cell surface localization is significant ($p<0.025$, $n=3$) based on the Student t-test. As shown by the immunostaining, coexpression of ASTN1 has no effect on the surface localization of ASTN2-Venus (Figure 4.1 B, right and C). In this experiment, Venus-αTubulin (cotransfected with Myc) serves as the negative control and on average showed only a negligible amount of surface labeling (B, top left and C). NL1-EYFP (cotransfected with Myc) served as the positive control and had an average 35+/-4.15% of double-labeled cells (Figure 4.1 C) and few transfected cells without surface labeling (B, bottom left). From these experiments we can conclude that the ASTN1:ASTN2 interaction has functional significance and serves to alter the

location of ASTN1 in the cell. Taken together, these results suggest that ASTN2 may stimulate the endocytosis of ASTN1, a process that could potentially impact the adherence junctions created between granule neurons and their glial support fibers during neuronal migration in the cerebellum.

Coexpression of ASTN2 Specifically Reduces the Cell Surface Localization of ASTN1

Flow cytometry analysis confirms that the reduction in cell surface localization induced by ASTN2 coexpression is specific for ASTN1. Figure 4.2 demonstrates that the cell surface localization of NLG1-EYFP does not change when coexpressed with ASTN2-Myc. When NLG1-EYFP is coexpressed with either Myc or ASTN2-Myc, on average 26% of cells reveal NLG-EYFP on the cell surface (Figure 4.1 C) with few transfected cells without surface staining (B). Venus-αTubulin (cotransfected with Myc) served as a negative control and on average showed only a negligible amount of surface staining. These results reveal that the ASTN2 reduction of ASTN1 surface localization is not a general phenomenon applicable to all proteins exposed on the cell surface, but rather a specific effect of ASTN2 on ASTN1.

ASTN1 and ASTN2 Contain Conserved Endocytosis Sorting Signals

To further investigate the possibility of a link between ASTN1, ASTN2, and endocytosis, we performed bioinformatics analysis of ASTN1 and ASTN2 protein sequence using the Eukaryotic Linear Motif Resource (ELM, http://elm.eu.org/). Through this analysis we identified two di-leucine based clathrin mediated endocytosis sorting signals in the amino-terminus, and three

Figure 4.2. ASTN2 Does Not Change the Surface Localization of Neuroligin-1.

(**A**) Flow cytometry analysis of Neuroligin-1-EYFP live staining reveals that coexpression with ASTN2 specifically changes the cell surface localization of ASTN1. After 36 hours *in vitro*, transfected HEK293T cells were live stained with an anti-GFP antibody and surface expression was detected with a FACSort Analyzer. Surface labeling demonstrates that Neuroligin-1-EYFP is equally expressed on the cell surface in the (A, middle) absence and (A, right) presence of ASTN2. Dot plots of surface labeling represented as FL4 (Alexa 647 signal on X-axis) vs. FL1 (Venus/EYFP signal on Y-axis). Upper left quadrant values represent single/transfection (Venus/EYFP) positive cells, and upper right quadrant values represent double positive/surface labeled cells (Venus/EYFP expression positive and AlexaFluor 647 live stain positive). (**B**) Quantification of surface labeling from **A**. Average surface labeling from three experiments was calculated and significance was assessed via Student t-test. (Ven, V=Venus; Tub=Tubulin; NLG1=Neuroligin-1; A2=ASTN2).

Figure 4.2

A

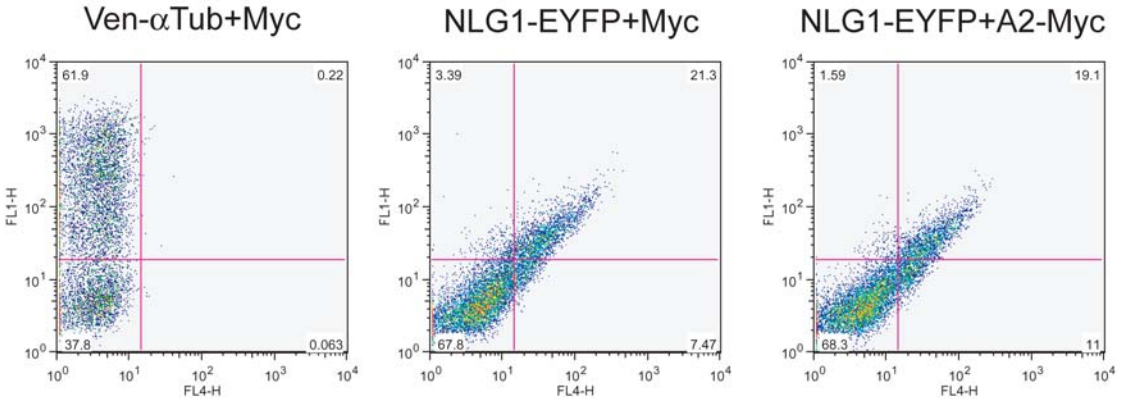
Ven-αTub+Myc
NLG1-EYFP+Myc
NLG1-EYFP+A2-Myc
61.9
0.22
37.8
0.063
3.39
21.3
67.8
7.47
1.59
19.1
68.3
11
FL1-H
FL4-H

B

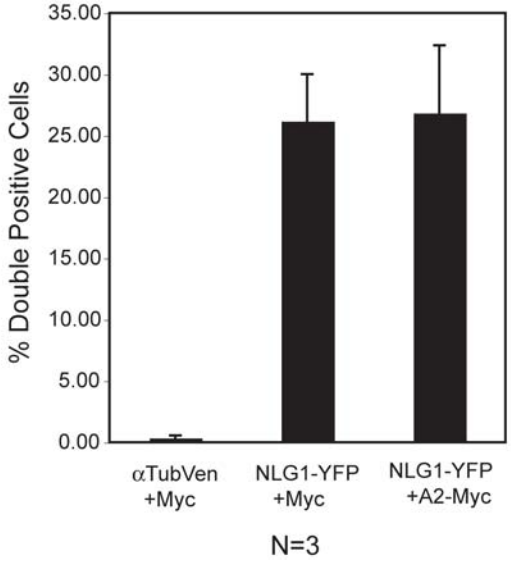
% Double Positive Cells
35.00
30.00
25.00
20.00
15.00
10.00
5.00
0.00
αTubVen +Myc
NLG1-YFP +Myc
NLG1-YFP +A2-Myc
N=3

tyrosine-based endocytosis sorting signals in the carboxy-terminus of ASTN2 (Figure 4.3, yellow). In other proteins, di-leucine motifs have been shown to act similarly as the tyrosine-based signals and both of these motifs have been shown to serve as interaction sites with adaptor protein complexes that function in clathrin mediated endocytosis (Maldonado-Baez and Wendland, 2006; Marsh, 2001). The endocytosis sorting motifs in ASTN2 are located in the amino-terminus of the protein in the region between the signal sequence and transmembrane domain (Figure 4.3 orange and green respectively), which is predicted to be an intracellular domain of the protein (The UK HGMP Protein Transmembrane Prediction Resource, http://www.biologie.uni-hamburg.de/b-online/library/genomeweb/GenomeWeb/prot-transmembrane.html; G. von Heijne, unpublished communications). Thus, this region of the protein could potentially interact with endocytosis adaptor proteins inside the cell to signal the clathrin-mediated endocytosis of the ASTN protein complex.

Unlike ASTN2, the sequence analysis of ASTN1 shows no extended intracellular domains (The UK HGMP Protein Transmembrane Prediction Resource, http://www.biologie.uni-hamburg.de/b-online/library/genomeweb/GenomeWeb/prot-transmembrane.html), however, bioinformatics analysis revealed the presence of tyrosine-based endocytosis motifs in the carboxy-terminus. As shown by immunostaining and flow cytometry, the ASTN1 protein changes localization with coexpression of ASTN2, suggesting these motifs may be functional upon interaction with ASTN2. In addition, both ASTN1 and ASTN2 contain sorting/internalization signals, which are generally found in the cytoplasmic juxtamembrane region of the type I transmembrane proteins and function to target proteins from the *trans*-Golgi network to the

Figure 4.3. ASTN2 Contains Potential Endocytosis Sorting Signals.

Bioinformatics analysis revealed two potential di-leucine clathrin mediated endocytosis sorting signals in the amino-terminus, and three tyrosine-based endocytosis sorting signals in the carboxy-terminus of ASTN2 (yellow). Locations of conserved domains are shown: orange, signal sequence; green, transmembrane domain; blue, EGF Repeat; red, MAC/Perforin Domain; purple, Fibronectin III Domain.

Figure 4.3

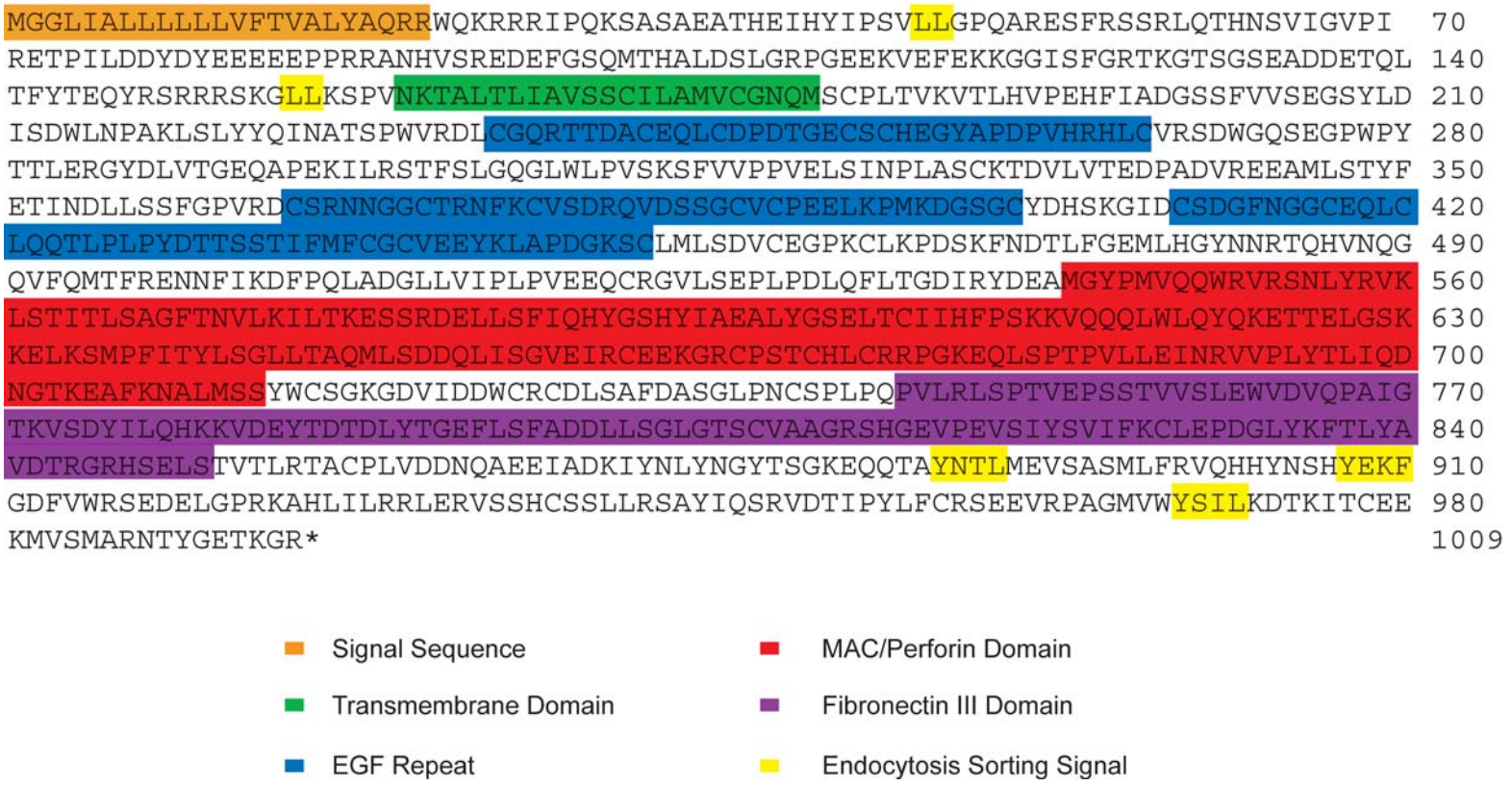
MGGLIALLLLLLVFTVALYAQRRWQKRRRIPQKSASAEATHEIHYIPSVLLGPQARESFRSSRLQTHNSVIGVPI 70
RETPILDDYDYEEEEEPPRRANHVSREDEFGSQMTHALDSLGRPGEEKVEFEKKGGISFGRTKGTSGSEADDETQL 140
TFYTEQYRSRRRSKGLLKSPVNKTALTLIAVSSCILAMVCGNQMSCPLTVKVTLHVPEHFIADGSSFVVSEGSYLD 210
ISDWLNPAKLSLYYQINATSPWVRDLCGQRTTDACEQLCDPDTGECSCHEGYAPDPVHRHLCVRSDWGQSEGPWPY 280
TTLERGYDLVTGEQAPEKILRSTFSLGQGLWLPVSKSFVVPPVELSINPLASCKTDVLVTEDPADVREEAMLSTYF 350
ETINDLLSSFGPVRDCSRNNGGCTRNFKCVSDRQVDSSGCVCPEELKPMKDGSGCYDHSKGIDCSDGFNGGCEQLC 420
LQQTLPLPYDTTSSTIFMFCGCVEEYKLAPDGKSCLMLSDVCEGPKCLKPDSKFNDTLFGEMLHGYNNRTQHVNQG 490
QVFQMTFRENNFIKDFPQLADGLLVIPLPVEEQCRGVLSEPLPDLQFLTGDIRYDEAMGYPMVQQWRVRSNLYRVK 560
LSTITLSAGFTNVLKILTKESSRDELLSFIQHYGSHYIAEALYGSELTCIIHFPSKKVQQQLWLQYQKETTELGSK 630
KELKSMPFITYLSGLLTAQMLSDDQLISGVEIRCEEKGRCPSTCHLCRRPGKEQLSPTPVLLEINRVVPLYTLIQD 700
NGTKEAFKNALMSSYWCSGKGDVIDDWCRCDLSAFDASGLPNCSPLPQPVLRLSPTVEPSSTVVSLEWVDVQPAIG 770
TKVSDYILQHKKVDEYTDTDLYTGEFLSFADDLLSGLGTSCVAAGRSHGEVPEVSIYSVIFKCLEPDGLYKFTLYA 840
VDTRGRHSELSTVTLRTACPLVDDNQAEEIADKIYNLYNGYTSGKEQQTAYNTLMEVSASMLFRVQHHYNSHYEKF 910
GDFVWRSEDELGPRKAHLILRRLERVSSHCSSLLRSAYIQSRVDTIPYLFCRSEEVRPAGMVWYSILKDTKITCEE 980
KMVSMARNTYGETKGR* 1009
Signal Sequence
Transmembrane Domain
EGF Repeat
MAC/Perforin Domain
Fibronectin III Domain
Endocytosis Sorting Signal

lysosomal-endosomal compartments (ELM, http://elm.eu.org/). Furthermore, these motifs are known interaction sites with adaptor protein complexes. Although we have demonstrated that neither ASTN1 nor ASTN2 bind directly with Clathrin light chain or the classical adaptors proteins Numb, Dab1 or Dab2 (data not shown), it is possible, based on our bioinformatics analysis, that the Adaptor Protein-1 (AP-1) or Adaptor Protein-2 (AP-2) proteins bind to ASTN1 or ASTN2 and experiments to verify this hypothesis are ongoing.

ASTN1 and ASTN2 Colocalize with Golgi and Endosome Markers

To determine if ASTN1 and ASTN2 colocalizes with structures in the Golgi network and endocytosis pathways, we utilized known cell compartment markers as well as the GFP-Endo Living Colors expression vector (pAC-GFP1-Endo, Clontech) to image endocytic vesicles. As shown by Figure 4.4, in transfected HEK293T cells both ASTN1 and ASTN2 partially colocalize with GM130, a Golgi-matrix protein, signifying the presence of both ASTN proteins in the Golgi Network, which was expected presuming all membrane proteins must pass through the Golgi Network during their processing. To further investigate the sub-cellular localization, we coexpressed ASTN1 and GFP-Endo (RhoB fusion) and ASTN2 and GFP-Endo in HEK293T cells and imaged single optical sections of fixed cells to localize the transfected proteins. Our results demonstrate that both ASTN1 and ASTN2 are expressed on a subset of RhoB positive endosomes as well as in other vesicles that are not RhoB positive (Figure 4.5 A). Also, cotransfection reveals that the coexpression of both ASTN1 and ASTN2 with GFP-Endo does not change the partial colocalization of either protein with RhoB positive endosomes (Figure 4.5 A, bottom panels).

Figure 4.4. ASTN1 and ASTN2 Colocalize with Golgi Markers.

Expression of ASTN1 (top) and ASTN2 (bottom) in transfected HEK293T cells reveals that ASTN proteins colocalize with GM130, a marker of the Golgi network. Transfected cells were cultured 36 hours *in vitro*, fixed, and immunostained with an anti-GM130 and anti-ASTN antibodies. Images shown represent single optical confocal sections and scale bar represents 10 μm.

Figure 4.4

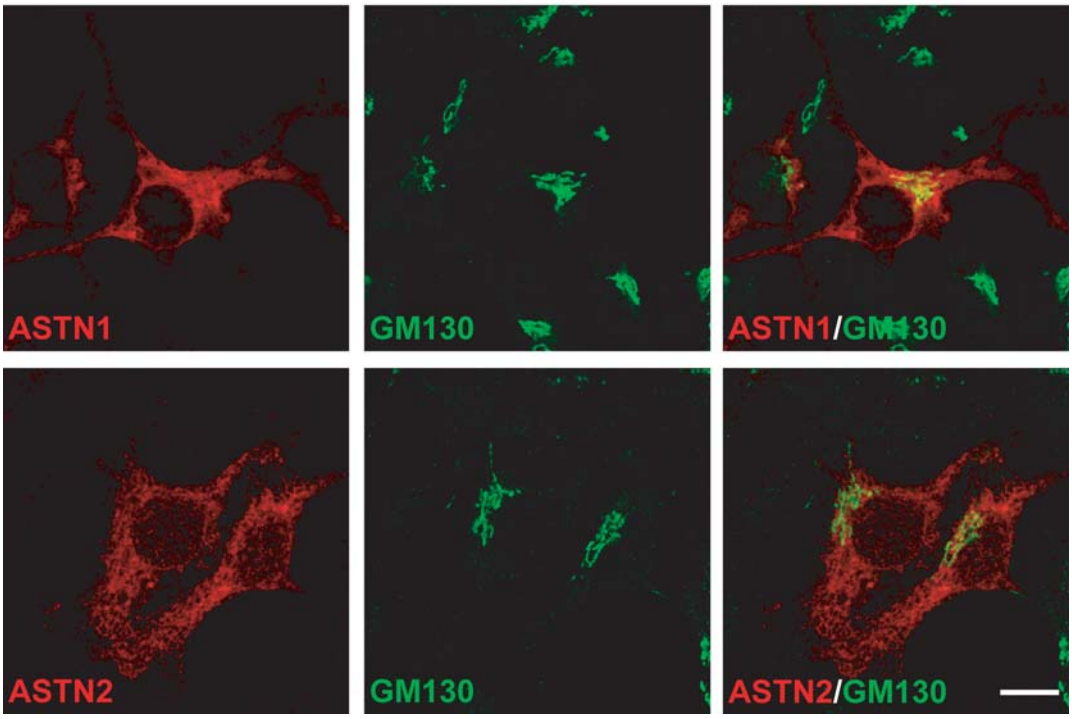

Figure 4.5. ASTN1 and ASTN2 Colocalize with Endosome Markers.

Expression of ASTN1 and ASTN2 in transfected HEK293T cells demonstrates that the ASTN proteins colocalize with (**A**) GFP-Endo and (**B,** arrowheads) early endosome marker, EEA1. (**A**) Cells were transfected with (top) ASTN1 and GFP-Endo, (middle) ASTN2 and GFP-Endo, or (bottom) ASTN1, ASTN2, and GFP-Endo, cultured 24 hours *in vitro*, fixed, and immunostained with anti-GFP and anti-ASTN antibodies. (**B**) Cells were transfected with (top) ASTN1, (middle) ASTN2, or (bottom) ASTN1 and ASTN2, cultured for 36 hours *in vitro*, fixed, and immunostained with anti-EEA1 and ASTN antibodies. Images shown represent single optical confocal sections and scale bars represent 10 μm.

Figure 4.5

A

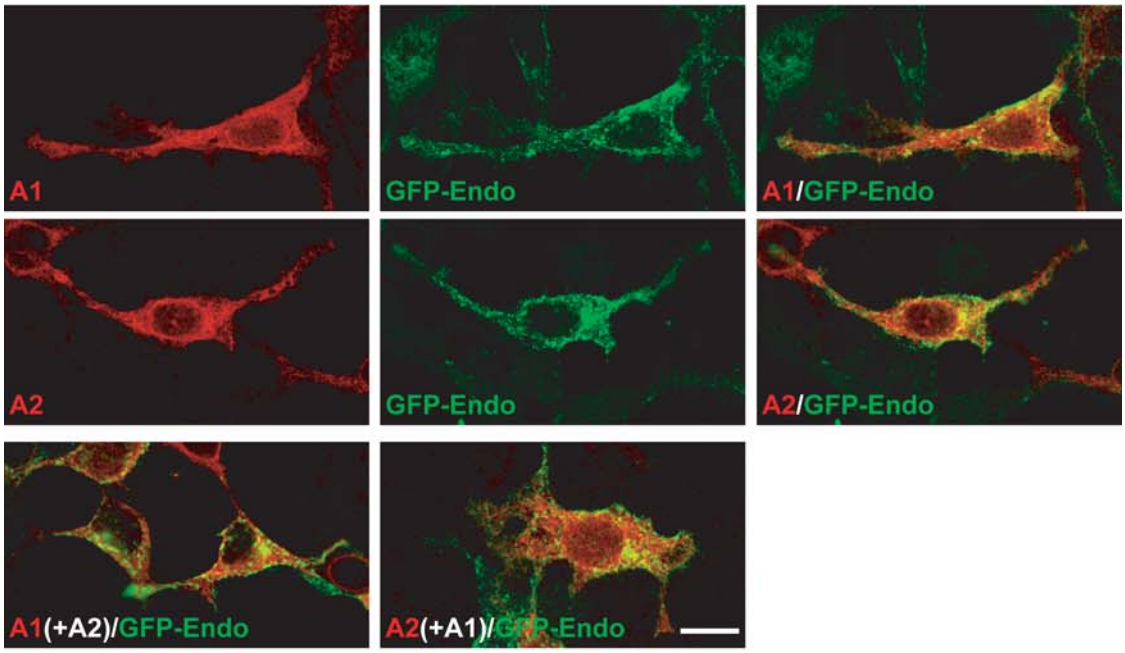
A1
GFP-Endo
A1/GFP-Endo
A2
GFP-Endo
A2/GFP-Endo
A1(+A2)/GFP-Endo
A2(+A1)/GFP-Endo

B

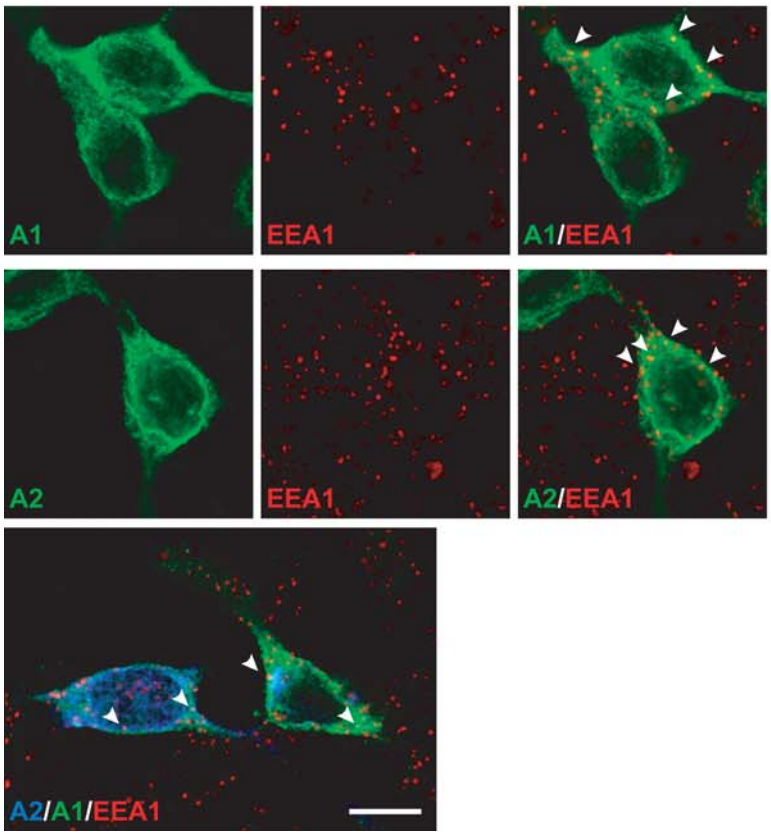
A1
EEA1
A1/EEA1
A2
EEA1
A2/EEA1
A2/A1/EEA1

Since RhoB is a maker for both early and late endosomes we utilized Early Endosome Antigen 1 (EEA1) antibodies to illustrate that both ASTN1 and ASTN2 are expressed on a subset of early endosomes in transfected cells (Figure 4.5 B, arrowheads). Cotransfection of ASTN1-Venus and ASTN2 and triple immunostaining with anti-ASTN2, anti-GFP, and anti-EEA1 antibodies revealed the presence of several triple labeled endosomes (Figure 4.5 B, bottom panel, arrowheads). Together, these data imply that both ASTN1 and ASTN2 are expressed on early and late endosomes in transfected cells and support the hypothesis that endocytosis of ASTN1 and ASTN2 may occur in migrating neurons. Although these costaining experiments provide some evidence in support of our hypothesis, we acknowledge that there are several drawbacks of using overexpression in heterologous cells to model ASTN function. With overexpression there is increased protein turnover, which complicates our interpretation of ASTN localization in membrane compartments. In addition, cellular factors in the HEK293T cells may differ from those in neurons and therefore, we recognize that there may be alternate mechanisms involved in targeting the endogenous ASTN proteins in neurons.

ASTN1 and ASTN2 Colocalize with Clathrin Light Chain in Migrating Cerebellar Granule Neurons

After demonstrating that the ASTN proteins are associated with endosomes in transfected cells, we next wanted to look at the association of endogenous ASTN1 and ASTN2 and endosomes in cerebellar granule neurons. Due to the small size of and limited cytoplasm in these neurons, classical endosome markers are extremely difficult to visualize. Additionally, GFP-Endo

visualization was not possible because RhoB overexpression is toxic to the granule neurons. Since our previous bioinformatics analysis of ASTN2 showed the presence of di-leucine motifs for clathrin-mediated endocytosis, we infected the purified cerebellar small cell fraction (95% granule neurons, 5% glia) with Venus tagged Clathrin light chain retrovirus and imaged the colocalization of Clathrin and endogenous ASTN proteins in migrating granule neurons in single optical confocal sections. Figure 4.6 illustrates that in granule neurons, both ASTN1 (top) and ASTN2 (middle) are highly colocalized with Clathrin light chain-Venus. Moreover, in granule neurons that are migrating on glial fibers (shown via GFAP immunostaining) a significant colocalization of ASTN2 and Venus tagged Clathrin light chain is detected. The staining pattern of both ASTN proteins and Clathrin light chain-Venus is speckled, with an accumulation of protein localized at the base of the leading process as well as in the edge of the neuron opposite the adhesion site. These results demonstrate that there is a close association of ASTN1 and ASTN2 with Clathrin light chain in migrating granule neurons, providing further support that the ASTN proteins may actively undergo clathrin-mediated endocytosis in migrating granule neurons.

High Power Live Imaging Shows the Dynamics of ASTN1 in Migrating Granule Neurons

Using spinning disc video microscopy we imaged the protein dynamics in live, electroporated cerebellar granule neurons coexpressing ASTN1-Venus and ASTN2-Cherry. In migrating granule neurons, ASTN1-Venus is expressed in discrete speckles (Figure 4.7, arrowheads) that move throughout the leading process of the migrating neuron and in a mass at the base of the cell soma and

Figure 4.6. ASTN1 and ASTN2 Colocalize with Clathrin Light Chain in Migrating Cerebellar Granule Neurons.

Endogenous (top) ASTN1 and (middle and bottom) ASTN2 colocalize with labeled Venus-tagged Clathrin light chain (expressed via retrovirus infection). Purified percoll small cell fraction cells (95% neurons, 5% glia) were cultured with retrovirus supernatant for 36 hours *in vitro*, fixed, and immunostained with anti-GFP and (top) anti-ASTN1, (middle) anti-ASTN2, (bottom) anti-ASTN2 and anti-GFAP. GFAP staining confirms migration of the granule neuron on a glial fiber. Images shown represent single optical confocal sections and scale bar represents 5 μm.

Figure 4.6

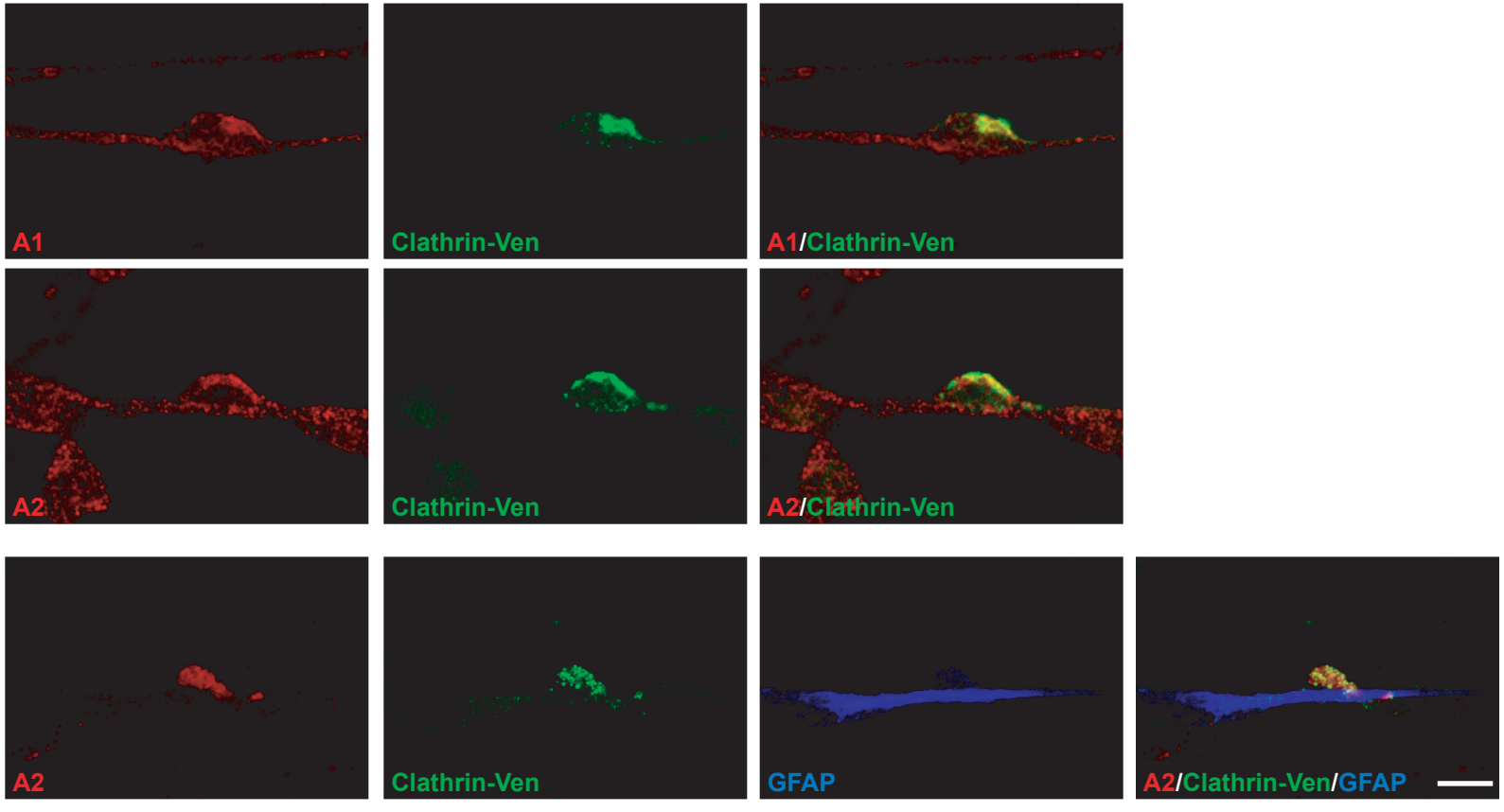
A1
Clathrin-Ven
A1/Clathrin-Ven
A2
Clathrin-Ven
A2/Clathrin-Ven
A2
Clathrin-Ven
GFAP
A2/Clathrin-Ven/GFAP

Figure 4.7. ASTN1-Venus Dynamics in the Leading Process.

In migrating granule neurons, ASTN1-Venus is expressed in discrete speckles (arrowheads) that move throughout the leading process of the migrating neuron and in a mass at the base of the cell soma and leading process (stars). Purified cerebellar granule neurons were electroporated with ASTN1-Venus and ASTN2-Cherry and cocultured with the cerebellar small cell fraction containing 5% glia for 36 hours on low poly-D-lysine coated dishes. Migrating neurons were imaged with a spinning disk confocal microscope with a *z*-stack acquired once per minute. Eight panels depicting the dynamics of ASTN1-Venus in the leading process as the neuron migrates along the glial process are maximum projections of the respective *z*-stack for each time point. Scale bar represents 5 μm.

Figure 4.7

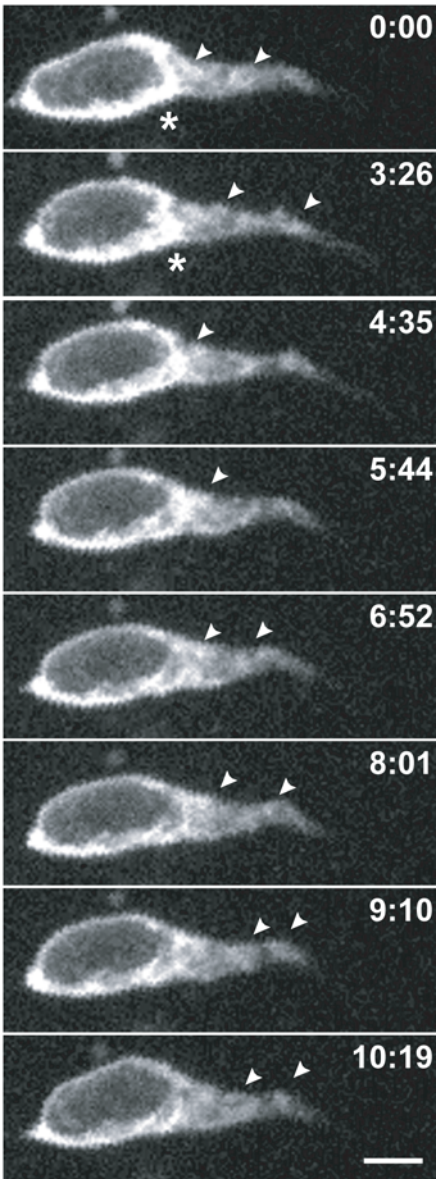

leading process (Figure 4.7, stars) where adhesions with the glial fiber would exist. The kymograph in Figure 4.7 reveals waves of ASTN1-Venus protein movement (arrowheads), which begins with ASTN1-Venus accumulating at the base of the leading process and continuing down the length of the process over a ten-minute time span. This result is consistent with previous ASTN1 immunostaining of cerebellar granule neurons (Fishell and Hatten, 1991; P.M. Wilson and M.E. Hatten, unpublished observations), which showed ASTN1 is expressed in an overall speckled pattern with an accumulation at one edge of the cell.

To further examine ASTN1 dynamics in vitro we imaged additional ASTN1-Venus/ASTN2-Cherry coexpressing cells over longer time periods (80-90 minutes) to capture entire migration sequences. The top panel in Figure 4.8 is a representative DIC frame from the imaging sequence and illustrates the location of the ASTN1-Venus expressing neuron (green, green arrowhead) on a radial glial fiber. Live imaging revealed an accumulation of ASTN1-Venus along the front edge of the migrating neuron (Figure 4.8, arrows) during the stage of migration when the cell has a tear shaped morphology and the back of the cell begins to detach from the glial fiber. These results are consistent with the ASTN1 and Clathrin light chain-Venus colocalization studies where we showed a buildup of ASTN1 and Clathrin immunoreactivity at the front edge of the migrating neuron. As illustrated by Figure 4.8, once the front of the neuron begins to move forward and there is an advancement of the leading process, ASTN1-Venus accumulates in the base of the leading process (closed arrow heads) suggestive of a new adhesion site between the base of the leading process and the glial fiber. As the neuron continues to migrate, there is a burst of

Figure 4.8. ASTN1-Venus Dynamics in Actively Migrating Granule Neurons.

The top panel is a representative DIC frame from the imaging sequence and illustrates the location of the ASTN1-Venus expressing neuron (green, green arrowhead) on a radial glial fiber. In migrating granule neurons, ASTN1-Venus accumulates along the front edge as the cell begins to move forward along the glial process (arrows) and at the base of the cell once the neuron has stepped forward (filled arrowheads), flows throughout the base of the leading process when the neuron is in the stationary phase of its migration (open arrowheads), and amasses at the base of the cell after the neuron moves forward again (star). Granule neurons were purified, electroporated with ASTN1-Venus and ASTN2-Cherry, and cocultured with the cerebellar small cell fraction containing 5% glia for 36 hours. Migrating neurons were imaged with a spinning disk confocal and a *z*-stack was acquired once every 3.5 minutes; each panel represents a maximum *z*-stack projection. Scale bar represents 10 μm in top panel and 5 μm in all other panels.

Figure 4.8

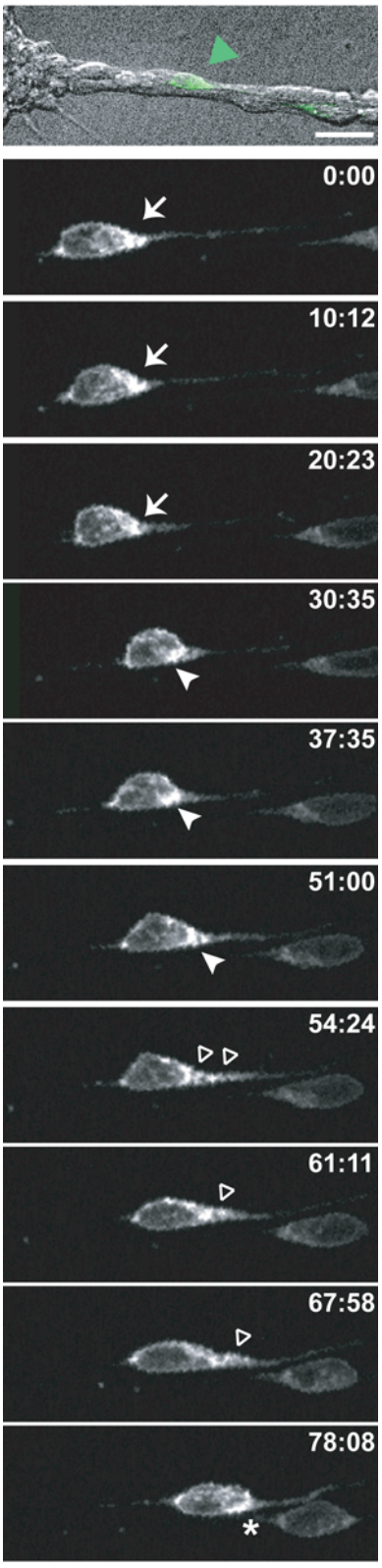

ASTN1-Venus proteins into the leading process (open arrow heads). The streaming of ASTN1-Venus protein down the leading process continues while the neuron remains in the stationary phase of its two-stoke migration movement (Figure 4.8, middle panel), and ends with an accumulation of ASTN1-Venus at the front edge of the cell (bottom panel, star) after the cell body has completed its salutatory jump forward. The deposit of ASTN1-Venus created at the front of the cell is suggestive of a newly established adhesion site between the neuron and glial fiber. Together with the Clathrin light chain colocalization results, these data suggest a vesicular cycling of ASTN1-Venus through the migrating granule neuron.

Chapter 5: Discussion

Central nervous system migrations fall within a three-step program of development, which includes the establishment of neuronal identity, directed migration, and assembly into compact neuronal layers (Hatten, 1999). The orchestrated, wide-ranging migrations of precursor cells and differentiated neurons are critical steps in the formation of proper neuronal circuitry and function to establish the complex cytoarchitecture of the vertebrate brain (Galaburda and Christen, 1997; Hatten and Heintz, 1995). The cerebellar granule neuron provides a unique model system for examining key issues in nervous system development (Rakic, 1971) and the radial migration of granule neurons along the glial-fiber system has been extensively described. Numerous studies have identified Astrotactin as a principal receptor system in glial-guided neuronal migration in the cerebellum and have demonstrated a role for ASTN1 in neuron-glial adhesion and the locomotion of neurons along the glial fibers (Adams et al., 2002; Edmondson et al., 1988; Fishell and Hatten, 1991; Stitt and Hatten, 1990).

Although recent advances have been made in understanding the mechanics of somal translocation during glial-guided neuronal migration, the mechanism of formation and release of the specialized adhesion sites formed between the neurons and Bergmann glial fibers is yet to be determined. This thesis work characterizes the newly identified member of the *Astn* family, *Astn 2* and indicates a key role for ASTN2 in the localization of ASTN1. Based on our findings we present a new model for glial-guided neuronal migration, which

puts forth the processes of receptor turnover and endocytosis as a means for releasing the adhesion sites between the glial fiber and the rear of the neuronal cell soma to permit forward movement of the neuron.

ASTN1 and ASTN2: A Comparative Examination

This work details the cloning and characterization of the newly identified astrotactin family member, *Astn2*. The role of ASTN1 in neuron-glial adhesion and glial-guided migration has been described in detail in the mouse. We found that putative homologs for both *Astn* genes in *Homo sapiens* (human), *Pan troglodytes* (chimp), and *Canis familaris* (dog), and similar transcribed sequences in other vertebrates including *Gallus gallus* (chicken) and *Xenopus tropicalis* (frog). Our results show that although mouse *Astn1* and *Astn2* have different genomic structures, the mouse ASTN1 and ASTN2 proteins are highly homologous and contain all the same conserved domains. *In situ* hybridization reveals that *astn2* is highly expressed in the brain, particularly in cerebellar granule neurons during their course of radial migration into the IGL. Using an anti-ASTN2 specific antibody, we demonstrate that like ASTN1, ASTN2 is an integral membrane protein and is expressed in neurons and not astroglia. In light of the considerable homology between the ASTN1 and ASTN2 proteins, the temporal-spatial pattern of ASTN2 expression suggests that, like ASTN1, ASTN2 may also play a role in glial-guided neuronal migration in the developing cerebellum.

However, we note that the overall expression pattern of *astn2* differs from that of *astn1*. *In situ* hybridization demonstrates that at early postnatal ages *astn1* is more widely expressed throughout the brain as compared to *astn2*, which is markedly most highly expressed in the olfactory bulb and the granule neurons of

the hippocampus and cerebellum. In addition, developmental Western blot analysis demonstrates that ASTN1 is consistently expressed during embryogenesis, particularly during the phase of migration of the granule cell precursors along the surface of the rhombic lip. Although ASTN1 expression is slightly unregulated postnatally, expression is greatly diminished by P14 when migration of granule neurons along glial fibers is still ongoing. In comparison, embryonic expression of ASTN2 is very weak, and the pinnacle of ASTN2 expression in the cerebellum spans from P0 to P14, the time period in which glial-guided migration is occurring. Moreover, our investigation of ASTN surface expression indicates that despite their homology and conservation, ASTN1 and ASTN2 are differentially exposed on the cell surface. Surface staining experiments reveal that little or no ASTN2 protein may actually be exposed to the surface, and while the carboxy-terminus of ASTN1 can be visualized with extracellular antisera, the carboxy-terminus of ASTN2 cannot. This divergence as well as the differential expression during development calls into question the original hypothesis that ASTN2 functions redundantly with ASTN1 (Adams et al., 2002), and suggests that ASTN2 may actually perform a unique role in glial-guided neuronal migration. We acknowledge that the interpretation our surface staining results is limited based on the use of heterologous cells systems, and experiments are underway to verify these findings in granule neurons. In addition, experiments are ongoing to determine the exact topology of both ASTN molecules (possible topologies are illustrated in Figure 2.11 B) and the functionality and signaling capabilities of the predicted intracellular domains.

ASTN1 and ASTN2 as Interaction Partners

Previous work established ASTN1 as a neuronal protein involved in glial-guided neuronal migration but little is know about how ASTN1 mediates adhesion. Despite exhaustive searches (M.E. Hatten, unpublished data), the glial binding/signaling partner for the Astrotactin proteins has yet to be identified (Fishman and Hatten, 1993; Stitt and Hatten, 1990). Likewise, to date ASTN1 has not been connected to any downstream signaling cascades through which these proteins may signal that regulate the formation and/or collapse of adhesion sites as the neuron moves along the glial fiber. This work provides the first evidence of an *in vitro* interaction involving ASTN1 and describes the interaction between ASTN1 and ASTN2. In doing so, we imply a role for ASTN2 in glial-guided neuronal migration as a binding partner of ASTN1.

Interestingly, the ASTN1:ASTN2 interaction is not dependent on an individual domain/region of the ASTN2 protein, and the binding occurs even when the ASTN2 protein is truncated to a single domain. Moreover, our data indicate that the ASTN1:ASTN2 interaction occurs in the membrane or in the membrane trafficking pathway, the sub-cellular region to which these proteins are targeted *in vivo*. The heterotypic interaction between the Astrotactin proteins is calcium independent, a result consistent with previous data (Stitt and Hatten, 1990) that demonstrated that ASTN1-mediated adhesion during glial-guided neuronal migration is a calcium independent process. Overexpression studies in cerebellar granule neurons confirmed the biological significance of the ASTN1:ASTN2 interaction and demonstrated that the stoichiometry of ASTN protein expression is important, and, since all of our interaction studies were performed via overexpression in a heterologous cell system, we are currently

carrying our immunoprecipitations using granule cell lysate to evidence the ASTN1:ASTN2 interaction in these cells. However, as a whole, our current results indicate that an interaction exists between the ASTN1 and ASTN2 proteins and that this interaction likely has functional implications for the neuron during migration.

Multiple regions in ASTN1, including the FNIII domain (Zheng, 1996) and carboxy-terminus (Figure 2.8 K), are exposed on the cell surface and therefore available to function in mediating neuron-glial adhesion during migration. However, investigations of transfected ASTN2 in heterologous cells reveal that the localization of ASTN2 is different from that of ASTN1 and only a limited portion of the ASTN2 protein may be exposed on the cell surface. We hypothesized that since the interaction between the ASTN proteins occurred in the membrane/membrane compartments perhaps this interaction was required to more fully expose ASTN2 to the cell surface. Although we proved this theory to be untrue, we did establish that coexpression with ASTN2 alters the cell surface localization of ASTN1. We show that ASTN2 does not change the localization other neuronal cell surface proteins such as NLG1, thus demonstrating the specificity of the ASTN1 phenomenon.

In metazoan cells, the mechanism of disassembly of adhesion sites at the rear of the cell involves the removal of adhesion receptors from the cell surface via endocytosis (Lawson and Maxfield, 1995). The endocytosed receptors passage through early endosomes, after which some endosomes are targeted to lysosomes for degradation, while others are trafficked back to the plasma membrane (Le Roy and Wrana, 2005; Maxfield and McGraw, 2004), resulting in the cycling of these adhesion systems from the adhesion junction to the front of

the cell to provide a continuous supply of receptors as the cell moves forward (Lawson and Maxfield, 1995). The results of this study suggest that ASTN2 performs a unique function in neuronal migration and may be responsible for regulating the surface expression of ASTN1, which ultimately may impact the formation and release of adherence junctions created between the granule neurons and their glial support fibers during neuronal migration.

Regulating Surface Expression:
ASTN1, ASTN2, Vesicle Dynamics, and Clathrin-Mediated Endocytosis in Glial-guided Neuronal Migration

The modulation of surface expression of membrane proteins is important in the processes of axon guidance, growth cone motility, and cell migration. In *Drosophila melanogaster*, commissureless, a short transmembrane protein, controls axon guidance across the midline by regulating surface levels of the roundabout receptor (Keleman et al., 2005). Similarly, studies by Lemmon and colleagues demonstrate that regulation of surface expression of the cell adhesion protein L1 is a key step in the advancement of growth cones (Kamiguchi and Lemmon, 2000; Kamiguchi et al., 1998). In the process of cell migration, the control of surface expression of adhesion receptors including integrins (Lawson and Maxfield, 1995), LRP (Cao et al., 2006), and CAMs (Kamiguchi and Lemmon, 2000), and signaling receptors such as the chemokine receptors (Fan and Malik, 2003), is required for the advancement of the cell and the fine-tuning of directed migrations. The modulation of surface expression of these receptors occurs via intracellular trafficking events such as sorting at the *trans*-Golgi network in the

case of commissureless:roundabout and clearance/internalization via endocytosis in the other cases.

Since our results establish that ASTN2 specifically controls the surface expression of ASTN1, we performed bioinformatics analysis to determine if the ASTN proteins contained any conserved sorting motifs. Our analysis indicates that ASTN2 contains both di-leucine and tyrosine-based endocytosis sorting signals in predicted intracellular domains of the protein. These motifs are binding sites of the clathrin adaptor protein, AP-2, which in turn recruits clathrin to the plasma membrane to induce endocytosis (Maldonado-Baez and Wendland, 2006; Marsh, 2001). Di-leucine and tyrosine-based motifs have been identified in a number of cell surface adhesion proteins that are known to be cleared from the membrane via endocytosis including L1 (Kamiguchi et al., 1998), integrin β2 (Pellinen and Ivaska, 2006), and E-cadherin (Miyashita and Ozawa, 2007). Based on this evidence, we hypothesized that perhaps the ASTN2 regulation of ASTN1 surface expression is mechanistically due to ASTN2 induced endocytosis of the ASTN1:ASTN2 complex.

Although time-lapse video microscopy and correlated electron microscopy studies performed nearly twenty years ago (Gregory et al., 1988) have described the presence of coated endo/exocytic figures and coated vesicles along the interstitial densities in migrating neurons, until now, little attention has been paid to this observation. Our characterization of ASTN2 expression reveals that like ASTN1, ASTN2 is associated with membranes and is expressed in a speckled pattern in the cerebellar granule neuron. Additional investigations in transfected cells indicate that in addition to the plasma membrane, both ASTN1 and ASTN2 are partially localized to the Golgi network and early and late

endosomes (as evidenced by colocalization with known markers including GM130, RhoB, and EEA1) linking the ASTN proteins with these key intracellular trafficking networks. Most interestingly, this work shows that in migrating granule neurons both ASTN1 and ASTN2 colocalize with retrovirusly expressed Clathrin light chain. Taken together with the early descriptions of coated vesicles in the neuron adjacent to neuron/glial apposition site, these localization studies further support a link between adhesion, clathrin-mediated endocytosis, receptor recycling, and ASTN function in glial-guided neuronal migration.

Video microscopic studies on the dynamics of granule cell migration in real time reveal a flow of intracellular vesicles within the migrating neuron, from the nuclear indentation into the leading process (Edmondson and Hatten, 1987). Imaging studies presented in this work describe an accumulation of ASTN1-Venus protein along the front edge of the migrating neuron and at the edge of the leading process during forward movement as well as a dynamic flow of ASTN1 protein along the length of the leading process during stationary phases. We show here, for the first time, the dynamics of ASTN1 protein within a migrating neuron. Based on previous reports, we correlate the movement of ASTN1 protein within the neuron to the flow and cycling of intracellular vesicles. Our description of an accumulation of ASTN1 at the front edge of the neuron and base of the leading process are consistent with the known function of ASTN1 in mediating neuron-glial adhesion during glial-guided neuronal migration (Adams et al., 2002; Edmondson et al., 1988; Fishell and Hatten, 1991; Fishman and Hatten, 1993; Stitt and Hatten, 1990).

One current model of neuronal migration is based on studies of the cell polarity protein, mPar6α, and propose that mPar6α signaling at the neuronal

centrosome functions to maintain the integrity of the tubulin cage around the nucleus and drives somal translocation along the glial fiber (Solecki et al., 2004). However the key question of the means by which the specialized adhesion junctions between the neurons and glial fibers are created and released during migration still remains. Based on the overall findings of this study we present a new, integrated model for neuronal migration (Figure 5.1) whereby the ASTN based adhesion at the rear of the neuron is disassembled and released via clathrin-mediated endocytosis (Figure 5.1, step 1) allowing for forward movement of the neuron along the glial fiber. Similarly, our model suggests that new adhesion sites at the front of the neuron and along the leading process (Figure 5.1, pink) are created, in part, by the recycling of these adhesion receptors from the rear of the cell through intracellular endosomes (yellow, bright pink; steps 2-3), which are then transported via microtubules (green; step 4) to plasma membrane where adhesion proteins could be placed back onto the cell surface via exocytosis (step 5).

Our proposed model is supported by the extensive work of Fred Maxfield, among others, which clearly indicates a role for endocytosis in the de-adhesion steps of migration and recycling of adhesion receptors to the leading edge of cells that undergo crawling migratory movements (Lawson and Maxfield, 1995; Pierini et al., 2000). This study demonstrates that although it appears that the mechanism of force generation at the leading edge of these crawling cells is different from that of the neuron advancing along a glial fiber (D.J. Solecki and M.E. Hatten, unpublished observations), the mechanism for the release and formation of adhesion sites in cells undergoing migratory movements may, in fact, be conserved. Likewise it appears that conservation extends to the adhesion

Figure 5.1. Model for Endocytosis and Receptor Recycling in Glial-Guided Neuronal Migration.

Integrated model for neuronal migration demonstrates that Par6α signaling at the neuronal centrosome (blue) functions to maintain integrity of the perinuclear tubulin cage (green) and drives somal translocation. ASTN based adhesion at the rear of the neuron (purple) is disassembled and released via clathrin-mediated endocytosis permitting forward movement along the glial fiber. ASTN proteins are recycled from the rear of the cell via endosomes (yellow, dark pink) and intracellular compartments, including the *trans*-Golgi network, and are trafficked in vesicles (pink circles) along microtubules (green) back onto the surface of the plasma membrane via exocytosis, resulting in the creation of new adhesion sites at the front of the migrating neuron (pink).

Figure 5.1

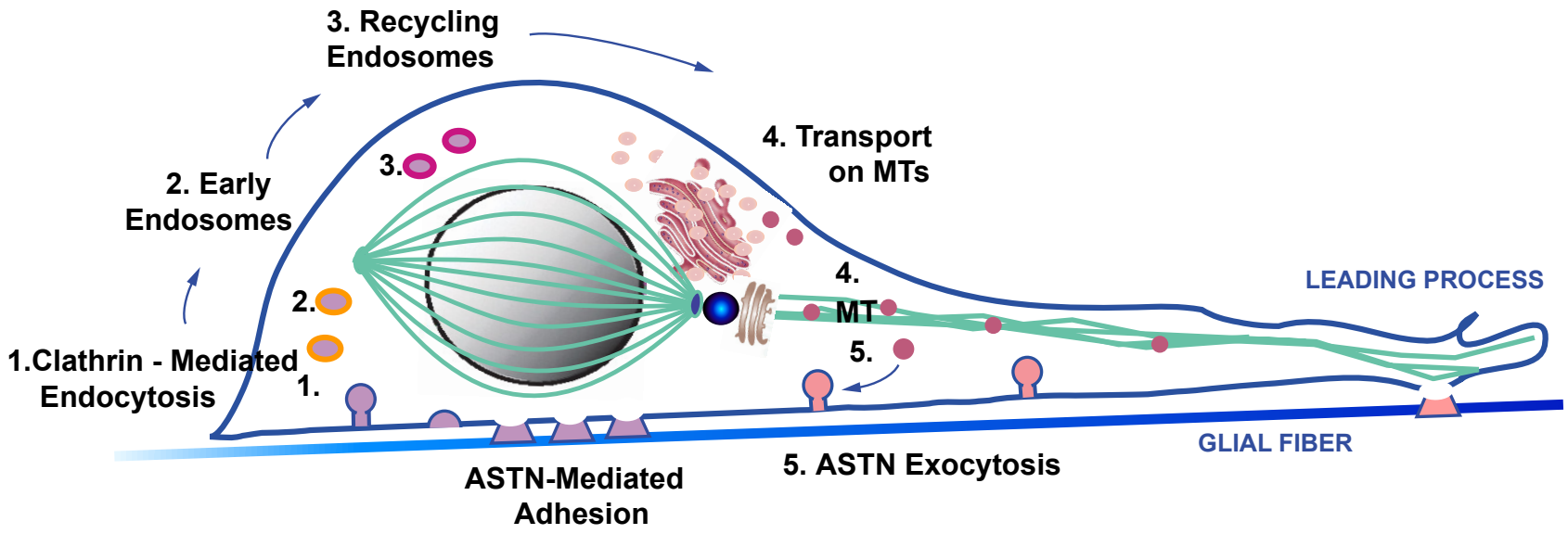
3. Recycling
Endosomes
4. Transport
on MTs
2. Early
Endosomes
3.
2.
1.Clathrin - Mediated
Endocytosis
1.
4.
MT
5.
LEADING PROCESS
GLIAL FIBER
ASTN-Mediated
Adhesion
5. ASTN Exocytosis

sites formed during the advancement of the neuronal growth cone (Kamiguchi and Lemmon, 2000). As of yet we do not know which motifs function in initiating the endocytic removal of the ASTN adhesion proteins from the cell surface or which motifs may direct their intracellular cycling, nor do we know the signaling pathways that trigger and regulate this process. However, investigations are underway to resolve these details. Understanding the regulation of adhesion formation and release during glial-guided neuronal migration and the coordination of these events with centrosome and microtubule dynamics at the front of the cell will elucidate new mechanisms and signaling pathways involved in the development of laminar brain regions.

Controlling Directed Cell Migrations: Mechanisms and Pathways

Cell migration is a complex and highly coordinated process that plays a key role in embryonic morphogenesis, tissue repair and regeneration, and central nervous system development (Hatten, 1999; Ridley et al., 2003). The classic models for cell movement are based on the pioneer studies of Abercrombie (1961), which described the locomotion of metazoan cells (i.e. fibroblasts) and proposed that the polarization of the cytoskeleton in the direction of an external cue, and the extension of a specialized motile structure, termed the "leading edge", directs this type of cell motility (Abercrombie, 1961). Figure 5.2 A illustrates the characteristic subcellular organization of migrating fibroblasts. The leading edge (consisting of a broad actin-rich lamellipodium (orange) and a more internal myosin-rich lamellum) is at the front of the cell, the nucleus (grey) is positioned in the rear of the cell behind the centrosome (purple) and Golgi apparatus (brown), and the microtubules (green) are orientated in the direction

Figure 5.2. Structure of Migrating Cells.

Subcellular and cytoskeletal organization of a migrating fibroblast (**A**) and granule neuron (**B**). Grey, nucleus; purple, centrosome; brown, Golgi apparatus, green, microtubules; lamellipodium=orange; brown circles, vesicles.
(**A** from Jaffe and Hall. Annu. Rev. Cell. Dev. Biol. 2005)

Figure 5.2

A

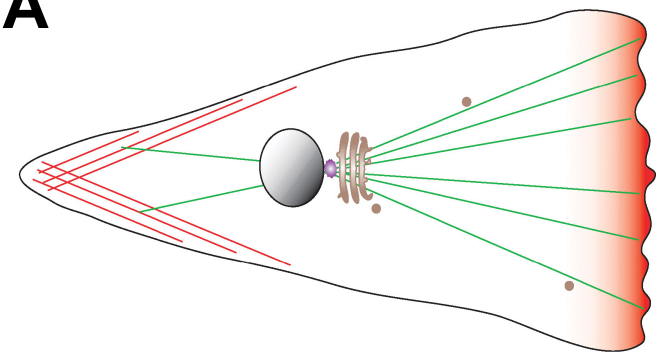

B

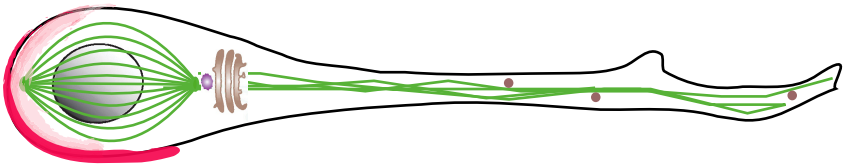

of migration (Jaffe and Hall, 2005; Ridley et al., 2003). This polarized cellular organization necessary for directed cell motility requires coordinated cytoskeletal rearrangements, including assembly and disassembly of the actin cytoskeleton and orientation of the microtubule organizing center (MTOC) in the direction of migration.

While it has been known for some time (decades) that the major driving force of migration of many non-neuronal cells depends upon the extension of a large, broad lamellipodium, the mechanism of glial-guided neuronal migration has only recently been examined. It is clear that the short range migrations of fibroblasts, epithelial cells, and astrocytes, such as in wound healing, function to protrude and spread to fill and cover a lesion (Redd et al., 2004). In contrast, the directed, radial migrations of neurons along glial fibers play a much different role. Rather than functioning to spread cells over an area, glial-guided neuronal migrations cover long distances and function to physically reposition the cell bodies of these neurons to regions where they will go on to establish neuronal circuitry (Hatten, 1999). Migrating neurons share some similarities with motile fibroblasts, such as the polarization of the cytoskeleton, but strikingly, they lack a leading edge protrusion in the leading process that they extend along the glial fiber in the direction of migration (Edmondson and Hatten, 1987). The subcellular organization of a migrating neuron is illustrated in Figure 5.2 B. The centrosome (purple) and Golgi apparatus (brown) are polarized in the direction of migration and located at the base of the leading process, and the nucleus (grey) is positioned at the rear of the cell. During migration, a specialized tubulin cage (green) forms around the nucleus and microtubules (green) project to the tip of the leading process (Rivas and Hatten, 1995). In addition, the

cellular machinery required to move the cell soma, including f-actin and myosin, is localized at the base of the leading process (D.J. Solecki and M.E. Hatten, unpublished observations). Recent work by Solecki, Hatten, and colleagues has shown that directed neuronal migration occurs in a coordinated "two-stroke" manner, with forward movement of the centrosome preceding that of the nucleus (Solecki et al., 2004).

In both non-neuronal and neuronal cells, the centrosome is a key indicator of polarity. The centrosome localizes forward of the nucleus in the direction of migration, and reorientation of the centrosome and microtubules allows for efficient transport of cargo to front edge of the cell and leading process (Zmuda and Rivas, 1998). Centrosome reorientation in the direction of migration is regulated by a highly conserved polarization signaling complex and pathway. During directed, non-neuronal migration centrosome reorientation involves the Rho GTPase Cdc42 and the mPar6 polarity signaling complex (Cau and Hall, 2005; Etienne-Manneville and Hall, 2001; Gomes et al., 2005; Lee et al., 2005; Palazzo et al., 2001; Tzima et al., 2003). Similarly, studies of migrating cerebellar granule neurons have shown that mPar6α localizes to the centrosome, and overexpression of mPar6α disrupts the perinuclear tubulin cage, retargets other mPar6α complex members and core centrosomal components away from the centrosome, and inhibits centrosomal movement and neuronal migration (Solecki et al., 2004).

An integral step in the migration of both polarized fibroblast cells and neurons is the establishment and dissolution of adhesions, which also likely involves conserved molecular players. Adhesions form between the migrating

cell and the extracellular matrix or adjacent cells via cell surface adhesion proteins (Ridley et al., 2003), and serve to anchor the cell as it locomotes along its substrate. Studies by Gupton and Waterman-Storer (2006) demonstrate that myosin contractility is important for the assembly and refinement of adhesion sites between migrating epithelial cells and the cell substrate. This work suggests that a balance between adhesion strength and myosin II contractility is required for optimal migration: if there is too little myosin contractility, the adhesions formed are too small to support migration, and likewise, if the contractility is too great, the adhesions are too large to be efficiently released (Gupton and Waterman-Storer, 2006). Interestingly, recent time-lapse video microscopy studies have implicated a role for myosin IIB in glial-guided neuronal migration (D.J. Solecki and M.E. Hatten, unpublished observations). These studies show that myosin IIB accumulates at the front edge of the migrating neuron and demonstrate that myosin IIB contractility is responsible for driving the forward movement of the neuron along the glial fiber during migration (D.J. Solecki and M.E. Hatten, unpublished observations). In light of the work of Waterman-Storer, we speculate that, in addition to providing the force to move the centrosome and cell soma forward, myosin IIB contractility might also play a key role in regulating the formation and refinement of adhesions and adhesion strength during glial-guided neuronal migration.

How might a neuron coordinate these actin and microtubule cytoskeleton rearrangements necessary for neuronal migration? While a large number of signaling molecules have been implicated in the process of migration, the Rho family members of small GTPases (including RhoA, Rac1, and Cdc42) stand out as key regulators of this important process [reviewed in (Etienne-Manneville,

2004; Raftopoulou and Hall, 2004; Watanabe et al., 2005)]. The Rho GTPases are guanine nucleotide-binding proteins that function as molecular switches by cycling between an active GTP-bound state and an inactive GDP-bound state. They are best known for their involvement in organization of the actin cytoskeleton. During the migration of non-neuronal cells, Rac and Cdc42 are required at the front of the cell for actin polymerization, and RhoA regulates focal adhesion assembly, cell contraction and rear cell retraction. In addition to their regulation of the actin cytoskeleton, recent studies show that these Rho GTPases regulate the microtubule cytoskeleton [reviewed in (Etienne-Manneville, 2004; Raftopoulou and Hall, 2004; Watanabe et al., 2005)]. RhoA stabilizes microtubules, Rac likely facilitates microtubule elongation, and, as mentioned above, Cdc42 reorients the centrosome and microtubules in the direction of migration. In addition, Rac and Cdc42 often antagonize RhoA activity, and vice versa, to coordinate or modulate cellular changes. Thus it is plausible that Cdc42, through the mPar6α complex, is acting to orient the centrosome and microtubules to optimize trafficking, while RhoA regulates acto-myosin contractility to establish and refine permissive cell adhesions and generate force to pull the neuron forward.

In addition to likely crosstalk and feedback between the Rho GTPase pathways, there is also accumulating evidence that cytoskeletal elements regulate each other and the Rho GTPases. Actin and microtubule organization and movements appear to be linked together, and there is evidence that microtubules can regulate actin dynamics through regulation of the Rho GTPases (Etienne-Manneville, 2004; Raftopoulou and Hall, 2004; Watanabe et al., 2005). Microtubule growth has also been shown to regulate focal adhesion turnover

and RhoA activity (Etienne-Manneville and Hall, 2001). Indeed, in addition to its effects on centrosomal movement, mPar6α is capable of regulating myosin phosphorylation in cerebellar granule neurons (D.J. Solecki and M.E. Hatten, unpublished observations). It will be interesting to determine which signaling pathway(s) regulates mPar6α function with respect to these findings and the potential interactions between the actin and microtubule cytoskeletons in migrating neurons.

It is evident that migration is a highly complex and dynamic process that involves the integration of numerous signaling pathways to coordinate a variety of cellular processes to bring about directed locomotion. One of these cellular processes, namely the regulation of adhesion sites formed between the migrating neuron and the glial fiber, is a critical step in the process of forward migration. Investigations of glial-guided neuronal migration have illustrated that as the neuron migrates, the Golgi apparatus is polarized at the front of the neuron (Rivas and Hatten, 1995) and there is a dynamic flow of vesicles through the neuron and leading process (Edmondson and Hatten, 1987). The finding that ASTN1 is critical for the interaction of neurons with glia during migration (Edmondson et al., 1988; Fishell and Hatten, 1991; Zheng, 1996), and that ASTN2 regulates the surface levels of ASTN1 (Figure 4.1), suggests a model (Figure 5.1) by which ASTN1 promotes the formation of adhesions, while ASTN2 promotes the dissolution of adhesions by inducing the clathrin-mediated endocytosis of ASTN1. The cyclical formation and dissolution of adhesions would permits the neuron to move forward along the glial process, and the hypothesized

endocytosis of ASTN1 in our model would undoubtedly require coordination between the actin and microtubule cytoskeletons and the signaling molecules discussed above that regulate their organization.

Once internalized into the cell via endocytosis, receptors enter the early endosome where they are sorted and, from there, they are either degraded in the late endosome/lysosome or are recycled back to the plasma membrane (Le Roy and Wrana, 2005). Thus, reorientation of intracellular transport pathways (the microtubule cytoskeleton) in the direction of migration is important to facilitate the trafficking and recycling of cell surface receptors to the front of the cell and leading process in order to establish new adhesion sites and stabilize the neuron as it moves forward along the glial guide (Figure 5.1, step 4; Figure 5.2 B, brown circles). The centrosome, reoriented by Cdc42 and mPar6α complex signaling, plays a role in polarizing the Golgi apparatus in the direction of migration (Cau and Hall, 2005; Solecki et al., 2004), and coordinating the directed flow of vesicles through proteins such as Rab11 (Emery et al., 2005). In addition, studies in fibroblasts have revealed that Rab11, a component of the centrosome, works in coordination with Arf6 to bring adhesion proteins to the leading edge of motile cells, a process which is required to establish new focal adhesions at the front of the cell (Matafora et al., 2001). It is important to note that the Rho GTPases play a variety of roles in endocytosis in different cell types (Symons and Rusk, 2003) and thus, may also play multiple roles in the regulation of ASTN1 surface expression/endocytosis.

Extensive studies including genetic studies and live cell imaging have demonstrated that actin polymerization serves a key function in generating the force necessary to deform the plasma membrane during endocytic internalization (Kaksonen et al., 2006). Adaptor proteins bind to membrane proteins to recruit clathrin to the plasma membrane to initiate the endocytosis events (Marsh, 2001). Once the clathrin coat is formed under the region of the plasma membrane that will be internalized, a number of actin-associated proteins, including linkers (such as Eps15), dynamin, Arp2/3 complex, Apr2/3-complex activators (such as N-WASP), and myosins are assembled at the membrane (Kaksonen et al., 2006; Marsh, 2001). The EPS15 and myosin proteins function to link and anchor the actin-filaments to the plasma membrane respectively and activated Apr2/3 complexes enable the formation of branched actin-filaments at the plasma membrane and regulate actin dynamics; together these proteins are required for the invagination and membrane scission events that occur during the uptake process (Kaksonen et al., 2006). Dynamin plays an important role membrane deformation and in regulating actin assembly to endocytic sites, and may function as a regulatory GTPase during endocytosis (Kaksonen et al., 2006; Kruchten and McNiven, 2006). The Arp2/3-complex activators are themselves regulated by a number of signaling proteins, including Cdc42 (Kaksonen et al., 2006), which further links signaling pathways controlling cell polarity and microtubule organization at the front of the migrating neuron with the disassembly of adhesion sites at the rear. Although the precise signaling events directing the endocytosis of ASTN1 remain to be determined, we plan to more thoroughly characterize these events in order to further our understanding of the molecular mechanisms underlying glial-guided neuronal migration.

Chapter 6: Perspectives and Future Directions

Work in this thesis presents the cloning and biochemistry of the newly identified *Astn* family member, *Astn2*. We demonstrate that, like ASTN1, ASTN2 is expressed in the developing brain and in granule neurons of cerebellum during the period of their migration along radial glial fibers (Figure 2.7). However, we show that although the peptide sequence of ASTN1 and ASTN2 is highly conserved (Figure 2.2), these proteins are differently exposed to the cell surface (Figure 2.8 L-M and Figure 4.1). Thus two of the main questions that remain to be answered are the issues of the topology of ASTN2 in the membrane (possible topologies are modeled in Figure 2.11B) and the membrane localization of ASTN2.

Live cell staining experiments have demonstrated that unlike ASTN1, the carboxy-terminus of ASTN2 is not exposed on the cell surface (Figure 2.10 and 4.1). This result can be explained in two ways: 1) either the topology of ASTN2 in the plasma membrane differs from that of ASTN1 and the carboxy-terminus of ASTN2 is an intracellular domain, or 2) ASTN2 has the exact same topology but resides only in membrane-bound intracellular compartments and not in the plasma membrane, therefore, is not exposed on the cell surface. A number of studies could be performed to investigate and distinguish between these possibilities. Currently we are evaluating the glycosylation pattern of ASTN2 to determine which regions of the protein are exposed to the luminal side of the endoplasmic reticulum (ER), which would provide insight into the membrane topology of this protein. Alternatively, we could also examine the topology of

ASTN2 via glycosylation mapping and engineer additional glycosylation sites near conserved domains or within the carboxy-terminus to investigate if these regions are exposed in the lumen of the ER.

In addition to glycosylation studies, we could perform mass spectrometry to evaluate the insertion of ASTN2 into the membrane. Using our anti-ASTN2 specific antibody, endogenous ASTN2 protein could be immunoprecipitated from cerebellar lysate and run on an SDS-PAGE gel to isolate the ASTN2 protein. The isolated ASTN2 band could then be analyzed through amino-terminal sequencing via mass spectrometry to determine if the signal sequence remains intact or is cleaved. These results would provide insight into how ASTN2 inserts into the membrane and whether or not the stretch of sequence between the signal sequence and transmembrane domain is a true intracellular domain, capable of interacting with signaling molecules, adaptor proteins, or scaffold proteins within the cell.

Surface staining and flow cytometry analysis of the expression of the Venus-tagged ASTN2 serial deletions in HEK293T cells performed in this study revealed that a portion of the ASTN2 protein may be exposed on the cell surface (Figure 2.10). Exposure of the ASTN2-Δ684-Venus deletion protein was positively detected on the cell surface, and this result can be interpreted in one of two ways: 1) a portion of ASTN2 is actually localized to the plasma membrane and exposed on the cell surface, or 2) the deletion eliminated potential localization signals and resulted in the mislocalization of the ASTN2 protein. In order to differentiate between these possibilities and positively confirm the exposure of ASTN2 on the cell surface (and therefore the localization of this protein in the plasma membrane) we could engineer tags within the ASTN2

protein and perform surface staining to analyze whether or not particular stretches of the ASTN2 protein are on the cell surface. By engineering tags within the full-length protein, we would eliminate the possible mistargeting of the protein, which was a significant caveat of our deletion strategy. In addition, by using very small tags such as Myc, we would minimally affect the folding and secondary structure of the protein. Positive identification of ASTN2 on the cell surface would confirm the sorting of ASTN2 to the plasma membrane as well as internal membrane compartments, and would imply that like ASTN1, ASTN2 may also play a key role in adhesion during glial-guided neuronal migration. In contrast, negative surface staining results would indicate that ASTN2 expression is restricted to internal cell membrane compartments and would suggest that ASTN2 does not directly mediate adhesion during migration and rather functions by controlling the localization of ASTN1.

Another key finding in this thesis was the interaction between ASTN1 and ASTN2 (Figure 3.1). We have shown that ASTN1 and ASTN2 likely interact through multiple domains and that the stoichiometry of this interaction has biological relevance in granule neurons. Interestingly, we found that coexpression with ASTN2 changes the surface localization of the carboxy-terminus of ASTN1 in transfected HEK293T cells (Figure 4.1), indicating a role for ASTN2 in regulating the specific removal of ASTN1 from the cell surface. Based on bioinformatics analysis revealing the presence of endocytosis sorting signals in ASTN2 (Figure 4.3) and immunostaining studies illustrating the colocalization of the ASTN proteins with endosome markers and clathrin light chain (Figure 4.5 and Figure 4.6, respectively), we propose that the ASTN2-induced removal of ASTN1 from the cell surface occurs via endocytosis. Our

model (Figure 5.1) is founded on the motility paradigm provided by Lawson and Maxfield (1995), whereby the endocytosis of cell-surface adhesion receptors from adhesion sites at the rear of the migrating neuron initiates disassembly of these junctions and results in the de-adhesion required for forward movement. However, we acknowledge that additional experiments are required to confirm this assertion.

Since many of our studies of ASTN localization and ASTN1/2 function were performed in a heterologous cell system, we plan to recapitulate some of these experiments in granule neurons. Using labeled cell uptake markers such as dextran and transferrin, we could perform uptake assays to localize ASTN proteins. We could incubate granule neurons with either labeled dextran or transferrin, fix the cells, and then perform immunocytochemistry with the anti-ASTN1 or anti-ASTN2 antibodies to determine if ASTN proteins are endocytosed from the plasma membrane into internal membrane compartments along with these labeled uptake indicators. By incubating the cells for various time periods, we could label different membrane compartments, including both early and late endosomes and recycling endosomes. These experiments would provide key insight into how ASTN1 surface expression is regulated and could provide critical evidence in support of our proposed model for endocytosis-induced de-adhesion in migrating granule neurons.

Additionally we would like to distinguish whether or not ASTN proteins are internalized in a clathrin-mediated fashion. For these experiments we would likely turn back to the heterologous cell system and our surface expression analysis of ASTN1, utilizing tools such as dominant negative clathrin (Marsh, 2001) to inhibit clathrin function in these cells. The most direct and informative

experiment would be the coexpression of ASTN1 and ASTN2 in HEK293T cells in the presence of dominant negative clathrin to determine if the ASTN2-induced change in cell surface localization of ASTN1 is a clathrin-dependent or independent process. If the change in cell surface localization of ASTN1 was not blocked by inhibiting clathrin, we would then test other lipid based internalization mechanisms. If however, the ASTN2-induced alteration of ASTN1 surface exposure is reliant on clathrin function, it would provide further support of our theorized model for the disassembly of adhesion sites via clathrin-mediated endocytosis. If the results of these experiments support a role for clathrin-mediated endocytosis in regulating ASTN1 surface expression in the heterologous cell system, our model could be further tested by transfecting dominant negative clathrin into granule neurons and measuring the resulting effect on glial-guided neuronal migration via *in vitro* migration assays. If our model holds true, we would expect that inhibiting clathrin would prevent the release of adhesion sites at the rear of the migrating neurons and, as a result, the migration of these neurons along the glial fibers would be significantly reduced or eliminated entirely.

Along the same lines, we intend to investigate the functionality of the endocytosis sorting signals in the ASTN2 protein. Studies of other cell surface adhesion molecules have demonstrated that the mutation or deletion of these motifs eliminates their internalization into intracellular compartments (Kamiguchi et al., 1998; Panicker et al., 2006; Thelen et al., 2002). Therefore, we would like to utilize deletions of the ASTN2 protein (specifically the amino- and carboxy-terminal deletions which would eliminate the di-leucine and tyrosine-based sorting motifs, respectively) and study whether the cotransfection of these

deletions affects the exposure of ASTN1 on the cell surface. These experiments could provide key support for our model, which suggests that ASTN2 specifically induces the endocytosis of ASTN1, and could provide a basic mechanism for recruitment of adaptor protein complexes to the plasma membrane by ASTN2 to trigger the clathrin-mediated endocytosis of the ASTN protein complex. Looking back to the issue of ASTN2 localization in the cell, if ASTN2 is in fact located on the plasma membrane, it could simply recruit these adaptor proteins to the cell membrane if either the amino- or carboxy-terminal regions are intracellular and accessible for binding cytoplasmic proteins. However, if the ASTN2 protein is restricted to intracellular membrane compartments, the regulation of ASTN1 surface expression becomes more complex and requires further experimentation and investigation.

Recent work, which was not discussed in this thesis, has demonstrated that both ASTN1 and ASTN2 bind Nischarin (R.H. Fryer, P.M. Wilson, and M.E. Hatten, unpublished observations), a cytoplasmic protein that binds α5 integrin and modulates actin dynamics in fibroblasts (Alahari et al., 2000). Studies in cerebellar granule neurons shows that overexpression of Nischarin inhibits both glial-guided neuronal migration (via inhibition of PAK1 kinase activity) and actin dynamics in growth cones (R.H. Fryer and M.E. Hatten, unpublished observations). Interestingly, human Nischarin (IRAS) is localized to endosomes and overexpression of IRAS redistributes surface α5 integrin to intracellular endosomal compartments, suggesting that IRAS may also function as a sorting nexin (Lim and Hong, 2004). We hypothesize that perhaps Nischarin acts via a similar mechanism to regulate the surface expression of ASTN proteins in

granule neurons. In order to further examine this possibility, experiments including co-immunoprecipitation assays with ASTN and Nischarin deletion constructs are currently underway to characterize the interaction between the ASTN proteins and Nischarin. Once the interaction domains are identified, we propose to do surface staining analysis of ASTN1 in granule neurons to determine if ASTN1 exposure to the cell surface is diminished when Nischarin is overexpressed. The results of these experiments could further our understanding of the regulation of ASTN expression and may support a key role for Nischarin in controlling ASTN-mediated adhesion during glial-guided neuronal migration. Such a finding would providing a link between the ASTN proteins and intracellular signaling molecules, including PAK1, which are known to regulate migration [(Alahari et al., 2004) (R.H. Fryer and M. E. Hatten, unpublished observations)].

In this thesis work, we characterize the expression of the newly identified ASTN family member, ASTN2, and describe the interaction between ASTN1 and ASTN2 in detail. Most importantly, our analysis reveals a unique role for ASTN2 in regulating the surface expression of ASTN1 and implies a novel role for receptor turnover and endocytosis in glial-guided neuronal migration. Our study of ASTN2 has led us to ask additional questions, many of which have been discussed in this chapter. The answers to these questions will be essential to enhancing our understanding the complex process of glial-guided neuronal migration in molecular terms.

Chapter 7: Materials and Methods

Construction of the Full-length Astrotactin 2 Mouse cDNA and Expression Vectors

The full-length *Astn2* mouse sequence was generated by assembling sequence data from the UCSC Genome Browser (http://www.genome.ucsc.edu), the TIGR Gene Indices (now The Dana Farber Gene Index Project, http://compbio.dfci.harvard.edu/tgi/cgi-bin/tgi/gimain.pl?gudb=mouse), and Celera (http://www.celera.com) databases. The upstream region of *Astn2* mouse cDNA was amplified by PCR from E17 brain first strand marathon ready cDNA (BD Biosciences) and Advantage DNA polymerase (BD Biosciences) using the following primers:
mA2exon1-B4-XmaI-S: 5′-gtctccttctctttgtgcg-3′
mA2exon1-EcoRV-AS: 5′-ggcgaggtggcattgatc-3′.
This insert was subsequently digested with *XmaI* and *EcoRV* and subcloned into the *XmaI* and *EcoRV* sites of the pRK5-Astn2 existing partial cDNA to fuse the newly acquired upstream sequence in frame with the existing cDNA. The resulting full-length *Astn2* cDNA was then subcloned into the *SmaI* and *SalI* sites of the pGW1 expression vector.

We generated pGW1-Astn2-Myc, the carboxy-terminal *Astn2* Myc fusion, by re-amplifying the carboxy-terminus of *Astn2* using an anti-sense primer that contained the Myc coding sequence. The insert was then swapped into the *XhoI* and *SalI* sites of pGW1-Astn2 expression vector replacing the untagged carboxy-terminal region with the Myc tagged version. The pGW1-Astn2-Venus carboxy-terminal fusion was created by fusing the Venus cDNA in frame with the 3′ end of the Astn2 coding sequence by joining PCR. The carboxy-terminal Astn2-

Venus fusion insert was subcloned into the *XhoI* and *SalI* sites of pGW1-Astn2 expression vector replacing the untagged carboxy-terminal region with the Venus tagged version.

To generate the pCIG2-Astn2-ires-EGFP construct, the Astn2 cDNA was subcloned into the *SmaI* and *NotI* (*blunted*) sites of the pCIG2 expression vector. To produce pCIG-Astn2-Venus and pCIG-Astn2-Cherry carboxy-terminal fusions, the Venus and Cherry cDNAs were fused in frame with the 3′ end of *Astn2* coding sequence by joining PCR. The resulting Astn2-Venus fusion inserts (*XhoI*/*NotI*) were subcloned along with the rest of the Astn2 cDNA (*XmaI*/*XhoI*) into pCIG expression vector by three-way ligation into the *XmaI* and *NotI* sites.

Construction of Astrotactin 2 Individual Domain Deletion Expression Vectors

The pRK5-Astn2-ΔEGF-Venus construct was created through several subcloning steps. First the region of *Astn2* downstream of the EGF Repeats was engineered by PCR to contain an *EcoRV* site at the 5′ end using the following primers:

A2afterEGFs-EcoRV-S: 5′-ggatatcctaatgctctcagatgtctg-3′

A2-Cterm-AS: 5′-ccggcctttggtttcccc-3′.

Next, the pRK5-Astn2 cDNA was digested with *EcoRV* and *XhoI* to eliminate Astn2 coding sequence containing the EGF Repeats (the *EcoRV* is located just 5′ of the EGF Repeats). The PCR engineered insert was then subcloned into the digested pRK5-Astn2 vector, creating a construct that contained the amino-terminus, MAC/PF domain, FN domain and carboxy-terminus, but not the EGF Repeats. Finally to make a carboxy-terminal Venus fusion, the Venus cDNA was fused in frame with the 3′end of the coding sequence by joining PCR. The

resulting Astn2-Venus fusion insert was subcloned into the *XhoI* and *SalI* sites of the pRK5-Astn2-ΔEGF construct described above, replacing the untagged carboxy-terminal region with the Venus tagged version.

The pRK5-Astn2-ΔMACPF-Venus construct was generated by several subcloning steps. First, the region of *Astn2* downstream of the MAC/PF domain was engineered by PCR to contain an *Acc651* site at one end and a *SalI* site at the other using the following primers:

A2-afterMP-Acc651-S: 5′-gggtacccctactggtgttctggtaaagg-3′

A2-Cterm-SalI-AS: 5′-acgcgtcgacggatccatgaaagtcgtgc-3′.

Subsequently, the pRK5-Astn2 cDNA was digested with *Acc651* and *SalI* to eliminate *Astn2* coding sequence from the MAC/PF domain to the stop codon (the *Acc651* site is conveniently located just 5′ of the MAC/PF domain). The PCR engineered insert was then subcloned into the digested pRK5-Astn2 vector, creating a construct that contained the amino-terminus, EGF Repeats, FN domain, and carboxy-terminus, but not the MAC/PF domain. Finally, to make a carboxy-terminal Venus fusion, the Astn2-Venus insert from the joining PCR reaction described above was subcloned into the *XhoI* and *SalI* sites of the newly created pRK5-Astn2-ΔMACPF vector to replace the untagged carboxy-terminal region with the Venus tagged version.

The pRK5-Astn2-ΔFN-Venus construct was created by the following subcloning steps: First, the region of *Astn2* upstream of the FN domain was engineered by PCR to contain an *XhoI* site at one end using the following primers:

A2-beforeEcoRV-S: 5′-gcagtcgccgccgcagcaaaggtttac-3′

A2-B4-FN-XhoI-AS: 5′-cgctcgagtccagtaagaactcatcagtgc-3′.

Next, the pRK5-Astn2 cDNA was digested with *EcoRV* and *XhoI* to eliminate Astn2 coding sequence including the FN domain (the *XhoI* site is conveniently located just 3′ of the FN domain sequence). The PCR engineered insert was then subcloned into the digested pRK5-Astn2 vector, creating a construct that contained the amino-terminus, EGF Repeats, MAC/PF domain, and carboxy-terminus, but not the FN domain. Finally to make a carboxy-terminal Venus fusion, the Astn2-Venus fusion insert was subcloned to replace the untagged carboxy-terminal region as previously described.

Construction of Astrotactin 2 Serial Deletion Expression Vectors

The pCIG-Astn2-Δ2744-Venus construct was generated by fusing, by restriction digest, the Venus cDNA to the *XhoI* site in the *Astn2* coding sequence located at nucleotide 2744. The construct was created by subcloning nucleotides 1-2744 of Astn2 (*XmaI*/*XhoI)* and Venus (*XhoI*/*NotI*) into the *XmaI* and *NotI* sites of pCIG by 3-way ligation.

The pCIG-Astn2-Δ2324-Venus expression vector was created by fusing Venus to nucleotide 2324 of *Astn2* by joining PCR. The resulting insert was subcloned into the *XmaI* and *NotI* sites of pCIG.

The pCIG-Astn2-Δ1774-Venus construct was generated by fusing the Venus cDNA to the *Acc651* site in the Astn2 coding sequence located at nucleotide 1774. The construct was created by subcloning nucleotides 1-1744 of

Astn2 (*XmaI*/*Acc651)* and Venus (*Acc651*/*NotI*) into the *XmaI* and *NotI* sites of pCIG by 3-way ligation.

The pCIG-Astn2-Δ684-Venus vector was created by fusing the Venus cDNA to the *EcoRV* site in the *Astn2* coding sequence located at nucleotide 684. The construct was created by subcloning nucleotides 1-684 of *Astn2* (*XmaI*/*EcoRV)* and Venus (*EcoRV*/*NotI*) into the *XmaI* and *NotI* sites of pCIG by 3-way ligation.

The pCIG-Astn2-ΔNterm-Venus construct was generated in two steps. First the region of *Astn2* after the amino-terminus was engineered to contain an *EcoRI* site and ATG start site by PCR using the following primers:
A2-EcoRI-ATG-684-S: 5′-ggaattcgcatggatatctccgattggcta-3′
A2-afterAcc651-AS: 5′-gtgacaggtagatggacagcg-3′.
The resulting insert was then subcloned into the *EcoRI* and *Acc651* sites of the existing pCIG-Astn2-Venus construct effectively replacing the original amino-terminus with the new deleted version. The engineered pCIG-Astn2-ΔNterm-Venus construct contains a deletion of the *Astn2* amino-terminal region but retains all functional domains and the carboxy-terminal Venus fusion.

The pFLAG-SS-Astn2-ΔNterm-Venus construct was created by subcloning the *EcoRV*/*SalI* fragment of the pGW1-Astn2-Venus into the *EcoRV* and *SalI* sites of the pFLAG-CMV1 expression vector. The digested Astn2-Venus *EcoRV*/*SalI* fragment contains all functional domains and a carboxy-terminal Venus fusion, but lacks the amino-terminus, thus, the resulting construct is an amino-terminal Flag fusion of the Astn2 coding sequence containing a deletion of the amino-terminal *Astn2* region. Since the pFLAG-CMV1 vector (Sigma) contains a

constitutive preprotrypsin signal sequence, the expressed protein will be targeted to the membrane.

Construction of Astrotactin 1 Expression Vectors

We generated pGW1-Astn1-Myc, a carboxy-terminal Myc fusion, by re-amplifying the carboxy-terminus of *Astn1* using an anti-sense primer that contained the Myc coding sequence. The insert was then swapped into the *EcoRI* and *SalI* sites of pGW1-Astn1 expression vector replacing the untagged carboxy-terminal region with the Myc tagged version.

To generate the pCIG2-Astn1-ires-EGFP construct, the *Astn1* cDNA was subcloned into the *SmaI* and *NotI* (*blunted*) sites of the pCIG2 expression vector. To produce the pCIG-Astn1-Venus and pCIG-Astn1-Cherry carboxy-terminal fusions, the Venus and Cherry cDNAs were fused in frame with the 3′ end of the *Astn1* coding sequence by joining PCR. The resulting Astn1-Venus fusion inserts (*EcoRI*/*NotI*) were subcloned, along with the rest of the *Astn1* cDNA (*XmaI*/*EcoRI*), into pCIG expression vector by three-way ligation into *XmaI* and *NotI* sites.

RT-PCR Analysis

RNA was extracted from E8.5 and E10 embryos and E10 brain using Tri-Reagent (Molecular Research Center). First strand cDNA was generated via the Superscript RT-PCR kit (Invitrogen) using equal amounts of RNA per sample (5 μg). The resulting cDNA was used in PCR reactions with the following primer sets:

Astn2-rtpcr-sense: 5′-gatggctttaatggagggtg-3′

Astn2-rtpcr-AS: 5′-gtgacaggtagatggacagcg-3′

GAPDH-rtpcr-sense: 5′-agtggagattgttgccatca-3′

GAPDH-rtpcr-AS: 5′-tccaccaccctgttgctgta-3′,

which spanned intron/exon junctions in the *Astn2* and GAPDH genes respectively.

Northern Blot Analysis

RNA was extracted from embryonic and postnatal mouse tissue using Tri-Reagent (Molecular Research Center). Equal amounts (15 μg) of each RNA sample were run on a 1X MES buffered agarose gel containing formaldehyde. The gel was transferred overnight onto Hybond-XL membrane (Amersham) and UV cross-linked. Northern blot was performed using a 634 base pair Astn2 probe derived from restriction digest of the *Astn2* cDNA to isolate nucleotides 61-741 of the open reading frame of *Astn2* (Figure 2.1 A, pink). Riboprobes were prepared with a [P^{32}] labeling kit (Strategene) and purified over a G50 mini quick spin column (Roche) and the membrane was hybridized overnight in hybridization solution (6X SSPE, 5X Denhardts, 0.5% sodium dodecyl sulfate, and 50 mg single stranded salmon sperm DNA). After numerous washes, the membrane was exposed to film (Kodak) overnight at -80°C and the film was developed using an X-OMAT developer (Ewen Parker X-Ray). The membrane was then stripped in boiling 0.1% sodium dodecyl sulfate and re-hybridized with a 1.2 kB GAPDH riboprobe (derived from 5′ UTR, full coding sequence, and 3′UTR) as previously described.

In situ Hybridization

Postnatal (P6 and P10) and Adult mice were transcardially perfused with 4% paraformaldehyde and the brains were dissected, equilibrated in 30% sucrose overnight at 4ºC, and sectioned on a Leica SM2000R freezing sledge microtome. *In situ* hybridization was performed on 60 μm thick sections using the 634 base pair *Astn2* probe previously described (Figure 2.1 A, pink). For comparison, *in situ* hybridization was also performed using an *Astn1* probe (a 1749 base pair region derived from the 3' UTR of the *Astn1* gene). Sense and anti-sense riboprobes were prepared with a digoxygenin-labeling kit (Roche) and either T3 or T7 RNA polymerase (New England Biolabs). Hybridization was performed overnight at 70ºC in hybridization solution (50% formamide, 2% sodium dodecyl sulfate, 5X SSC, 500 μg/ml tRNA, and 2% BBR powder). Tissue sections were then washed, blocked in 10% sheep serum in TBS-Tween, and incubated overnight at 4ºC in TBS-Tween containing 1% sheep serum and anti-digoxygenin antibody (1:5000, Roche). After antibody incubation, sections were washed with TBS-Tween containing 2 mM levamisole and then incubated with color reaction solution containing 3.5 μl NTMT and 3.5 μl BCIP (X-phosphate) per mL at room temperature for 4.5-24 hours. After numerous washes in TBS-Tween, tissue sections were mounted in 80% glycerol.

Generation and Purification of Anti-ASTN2 Antibodies

The ASTN2 carboxy-terminal peptide (KITCEEKMVSMARNTYGETKGR) was synthesized (RU Protein Facility Ref) and coupled to bovine thyroglobulin (Sigma). The coupled peptide was then used for the immunization of a female

New Zealand white rabbit to raise an ASTN2 specific polyclonal antibody (Covance Inc.). The rabbit anti-serum was subsequently immunoaffinity purified on a column containing ASTN2 peptide coupled to Affi-Gel-15 resin (BioRad). Bound antibodies were removed from the column with both low pH glycine and high salt $MgCl_2$ elutions and the eluates were tested for specific immunoreactivity with ASTN2 via immunoblotting and immunostaining.

Cell Lines and Transfections

HEK293T cells were obtained from American Type Tissue Culture (ATTC) and grown at 37°C + 5% CO_2 in Dulbecco's modified Eagles medium (Gibco) supplemented with 10% fetal bovine serum, glutamine (4 mM), penicillin-streptomycin (20U/ml). In preparation for live and fixed cell immunostaining procedures for microscopy, HEK293T cells were transiently transfected with Lipofectamine™ 2000 in poly-D-lysine and matrigel coated 8 well glass tissue culture chamber/slides (BD Biosciences) with 0.2 μg of DNA per construct as per the manufacturer's instructions. For immunoblotting of transfected cell lysate and live cell staining for flow cytometry, HEK293T cells were transiently transfected with Lipofectamine™ 2000 (Invitrogen) in 6 cm dishes (Corning) with 8 μg of DNA per construct. For co-immunoprecipitation experiments, the 6 cm dish transient transfection protocol previously described was varied slightly such that 4 μg of the Astn1-Myc, control Venus, and control Myc constructs were cotransfected with 8 μg of Astn2-Venus constructs in order to ensure equal

amounts of protein expression. In all cases, the transiently transfected HEK293T cells were harvested for immunoblotting or processed for immunostaining 24-48 hours later.

Retrovirus Production

Recombinant ecotropic replication-incompetent retroviruses were produced as previously described (Tomoda et. al., 1999; Solecki et. al., 2001). Briefly, HEK293T cells were cotransfected with a retroviral construct and pCL-Eco, an ecotropic packaging construct. Twenty-four hours post-transfection, medium was replaced with granule cell medium lacking glucose and the resulting culture supernatant containing retroviruses was harvested 24 and 48 hours later. The retrovirus supernatant was then supplemented with glucose (6 mM) and filtered through a 0.22-μm pore.

Preparation of Brain/Cerebellar Homogenate

Mouse E10, E12, E14, and E16 brain, and P0, P2, P4, P6, P10, P14, and adult cerebellum were dissected in CMF-PBS. The tissue was then placed in a PBS based homogenization buffer containing 1 mM EDTA, 1 mM EGTA, and protease inhibitors (Roche) and homogenized using a PT 1200CL polytron (Kinematica) and dounce homogenizer. The tissue homogenate was then spun in a benchtop microcentrifuge at 4ºC at top speed for 15 minutes to eliminate any insoluble/nuclear material. The protein concentration of the soluble fraction was measured on a spectrophotometer (Biorad) by Coomassie (Bradford) Assay (Pierce) as per the manufacturer's instructions.

For cell fractionation experiments, the P10 cerebella homogenate soluble fraction was ultracentrifuged in a TLA-45 rotor (Beckman) at 100,000 g for 50 minutes at 4ºC to separate the cytosolic (supernatant) and crude membrane (pellet) fractions. The crude membrane fraction was resuspended in homogenization buffer and the concentration of both sub-cellular fractions was measured by Bradford Assay. A portion of the membrane fraction was then further sub-fractionated into integral and peripheral membrane fractions; a portion of the membrane pellet was resuspended in 0.1 M Na_2Co_3 pH 11.5, 1 mg/ml saponin, 5 mM EDTA, and protease inhibitors, incubated on ice 30 minutes, and ultracentrifuged at 100,000 g for 1 hour. The peripheral membrane fraction (supernatant) was separated and the integral membrane fraction (pellet) was resuspended in homogenization buffer. The concentration of both membrane sub-fractions was measured by Bradford Assay.

SDS-PAGE Gel Electrophoresis and Immunoblotting

Transiently transfected HEK293T cells were washed twice with cold PBS, lysed in ice cold 1% Triton-X-PBS with 1 mM EDTA, 1 mM EGTA, and protease inhibitors (Roche), and solubilized on ice for 20 minutes. The cell lysate was then centrifuged at top speed for 15 minutes in a bench top microcentrifuge at 4ºC to remove any insoluble material. The soluble fraction was combined with a Tris based sample buffer containing 6% sodium dodecyl sulfate and 3% β–mercaptoethanol and boiled for 5 minutes. For experiments involving tissue homogenate or cell fractionation samples, the prepared protein samples were combined with sample buffer and boiled for 5 minutes. For the developmental western blot and cell fractionation immunoblotting experiments, we loaded an

equal amount of protein (5 μg and 20 μg respectively) per sample to allow a direct comparison of protein levels.

In all experiments, protein samples were separated on 7.5 or 10% SDS-polyacrylamide electrophoresis gels and transferred to PVDF membrane (Millipore) in 20% methanol in Tris/glycine buffer at 22 volts overnight. Membranes were blocked in 5% non-fat milk in TBS-Tween and proteins were detected by primary antibody incubation for 1 hour at room temperature in blocking buffer using the following antibodies: rabbit anti-ASTN2 (1:200), rabbit anti-ASTN1 (1:200), mouse anti-Flag M2 (1:400, Sigma), ErbB4 (1:400, Santa Cruz), MMP9 (1:500, Torrey Pines Biolabs), mouse anti-GAPDH (1:1000, Chemicon), mouse anti-c-Myc (1:50, Calbiochem), mouse anti-JL8 GFP (1:2000, Clontech). Then, membranes were incubated for one hour with a horse radish peroxidase (HRP)-conjugated secondary antibody using the following antibodies: Sheep-anti-mouse IgG (1:10,000, Jackson ImmunoResearch) or Donkey-anti-rabbit IgG-HRP (1:50,000, Amersham). HRP-antibody signals were detected with enhanced chemiluminescence reagents, ECL or ECL+ (Amersham), and membranes were exposed to Biomax film (Kodak). For experiments that required blots to be reprobed with additional antibodies, membranes were stripped in a Tris based buffer containing 2% SDS and 0.7% β–mercaptoethanol and blocking and antibody probing was repeated as described.

For the investigation of ASTN2 expression in P7 mouse tissues, a custom made tissue blot from ProSci Inc. containing P7 mouse brain, eye, heart, lung, liver, kidney, spleen, and skin tissues was used. Briefly, 50 μg of protein per sample was run on a 4-20% gradient SDS-polyacrylamide electrophoresis gel and

transferred to nitrocellulose membranes as per the manufacturer's protocol. Immunoblotting was performed as described for PVDF membranes.

Co-Immunoprecipitation

Transiently transfected cells were lysed in ice cold 1% Triton-X immunoprecipitation (IP) buffer (PBS, 1 mM EDTA, 1 mM EGTA, and protease inhibitors), solubilized 20 minutes on ice, and spun down in a benchtop microcentrifuge at top speed for 15 minutes at 4°C to remove any insoluble material. After reserving a portion of the supernatant for an input loading control, the remaining 500 μl of the soluble cell lysate was incubated with 50 μl of Protein A/G beads (Calbiochem) and 2 μg of either anti-ASTN1 or rabbit anti-GFP antibodies (Invitrogen) for 3 hours at 4°C. The beads were washed once with 1% Triton-X IP buffer, twice with 1% Triton-X IP buffer with 500 mM NaCl, and then twice with IP buffer, and eluted in 30 μl of sample buffer. Protein samples were boiled for 5 minutes and separated on SDS-polyacrylamide electrophoresis gels and immunoblotted as previously described. Note: for the co-immunoprecipitations performed to test calcium dependence, one set of transiently transfected cells was lysed in an alternative cation-containing IP buffer containing 1 mM $CaCl_2$, 0.5 mM $MgCl_2$ (in the absence of EDTA and EGTA).

Preparation of Mixed Cerebella Cultures for Immunostaining and Retrovirus Infection

Mixed cerebella cultures were prepared as previously described (Hatten, 1985). Briefly, whole cerebella were removed from C57Bl/6J postnatal day 5-7 (P5-P7) mice. After the meninges were dissected away, the tissue was dissociated into a single cell suspension in trypsin using fine-bore Pasteur pipettes. The cell suspension was then applied to a two-step (35%-65%) Percoll gradient and separated by centrifugation. The small cell fraction, containing 90% neurons and 10% astroglia was collected and washed once in cold CMF-PBS. The purified small cell fraction was then resuspended in granule cell medium (BME (Gibco) supplemented with 10% horse serum, glucose (6 mM), glutamine (4 mM) and penicillin-streptomycin (20U/ml)) and preplated once on a bacterial dish (Applied Scientific) for 15 minutes at 35ºC + 5% CO_2. For immunostaining experiments, cells were counted and plated in 16 well LabTek glass tissue culture chamber/slides (Nunc) coated with low concentrations of poly-D-lysine (0.001-0.01 mg/ml) at a density of 175-225,000 cells/well. For immunostaining experiments involving retrovirus infection, retroviral supernatants (100 μl/well) were added to 200 μl of the purified cells at the time of plating.

Preparation of Granule Cell Cultures and Electroporation of Granule Neurons

Granule cell cultures were prepared as previously described (Hatten, 1985). Briefly, the small cell fraction was isolated and preplated on a bacterial dish as described above. Then, to isolate a pure population of granule neurons, the cells were preplated an additional 2 hours on a 0.1 mg/ml poly-D-lysine

coated 6 cm tissue culture dish (Corning) to remove the contaminating glial cell population. For immunostaining experiments, purified granule neurons were plated in 16 well LabTek tissue culture chamber/slides (Nunc) coated with 0.5 mg/ml poly-D-lysine and matrigel at a density of 175-225,000 cells/well.

For the experiments illustrating the effects of ASTN1 or ASTN2 overexpression, purified granule neurons were electroporated with 4 μg of pCIG-Astn1-Venus, 4 μg of pCIG-Astn2-Venus, or 4 μg of both pCIG-Astn1-Venus and pCIG-Astn2-Venus in 100 μl of Mouse Neuron Nucleofector solution (Amaxa) on setting A-30. After electroporation, cells were incubated at 35ºC + 5% CO_2 for 15 minutes in RPMi (Gibco) supplemented with glucose (6 mM). Cells were then spun down, resuspended in granule cell media, and plated in 8 well LabTek plastic tissue culture chamber/slides (Nunc) coated with 0.5 mg/ml poly-D-lysine and matrigel at a density of 600,000 neurons/well.

Preparation of Migration Cultures and Live Imaging

Migration cultures were prepared as previously described (Edmonson and Hatten, 1987). Briefly, the Percoll purified small cell fraction was isolated and preplated as described for mixed cerebella cultures. A portion of the purified cells were plated in movie dishes (Mattex) coated with low concentrations of poly-D-lysine in BME supplemented with 10% horse serum, glucose (6 mM), glutamine (4 mM), penicillin-streptomycin (20 U/ml), and 0.01 M HEPES at a density of 1 million cells/dish. In the meantime, purified granule neurons were isolated from the remaining small cell fraction via the 2 hour preplating as described for purified granule neuron cultures. The granule

neurons were electroporated with 30 μg of pCIG-Astn1-Venus and 30 μg pCIG-Astn2-Cherry using the Mouse Neuron Nucleofector solution as described. Electroporated neurons (resuspended in granule cell medium) were then plated (225,000/dish) on top of the mixed cerebella culture already plated in the Mattex dishes. Migration cultures were imaged after 48 hours of incubation using a Carl Zeiss Axiovert 200M equipped with a 40x, 1.3-NA, Plan-Neofluar objective and a PerkinElmer Wallac UltraView confocal head with 514-nm excitation filter and Orca ER cooled CCD camera (Hamamatsu) for high resolution. Cells were imaged for 20-80 minutes and 9 μm *z*-stacks (7 sections per stack) were taken every 1-3.25 minutes during imaging. Images were processed and analyzed using MetaMorph (Universal Imaging Corp.).

Immunocytochemistry of Transfected HEK293T Cells and Primary Cerebellar Cultures

After incubation for 24-36 hours, cultures were fixed with 4% paraformaldehyde, blocked with 10% normal goat serum in PBS, and permeabilized with 0.05% Triton-X. Primary antibody incubations were performed overnight at 4ºC in 1% normal goat serum in PBS, using the following antibodies: rabbit anti-ASTN2 (1:200), rabbit anti-ASTN1 (1:200, Covance), mouse anti-c-Myc (1:50, Calbiochem), mouse anti-Flag M2 (1:400, Sigma), mouse anti-Tag-1 IgM (1:2, 4D7), mouse anti-GFAP (1:500, Sigma), rabbit anti-GFP (1:2000, Invitrogen), mouse anti-EEA1 (1:100, abcam), mouse anti-GM130 (1:50, BD Biosciences). After numerous washes, secondary antibody incubations were performed at room temperature for 45 minutes in 1% normal goat serum in PBS

using the following antibodies: goat anti-rabbit IgG-488 Alexa Fluor, goat anti-rabbit IgG-555 Alexa Fluor, goat anti-mouse IgG-488 Alexa Fluor, goat anti-mouse IgG-555 Alexa Fluor, goat anti-chicken IgG-488 Alexa Fluor (all at 1:500, Invitrogen Molecular Probes). For ASTN1 and ASTN2 overexpression experiments in granule neurons where propidium iodide was used as a cell death indicator, propidium iodide (2.5 μg/ml final concentration, Sigma) live staining was performed at 37°C + 5% CO_2 for 10 minutes followed by numerous washes with culture media and then immunostaining was performed as described above. Slides were mounted in Mowoil (Calbiochem) and imaged using a Radiance 2000 confocal laser-scanning microscope.

Live Cell Immunostaining for Microscopy

Forty-eight hours post-transfection, HEK293T cell cultures were washed once with warm culture media and incubated with rabbit anti-GFP antibodies (1:2000, Invitrogen) for 10 minutes at 37°C + 5% CO_2. Cultures were then washed with cold media, fixed with 4% paraformaldehyde on ice for 15 minutes to prevent antibody internalization, and incubated with goat anti-rabbit IgG-555 Alexa Fluor (1:500, Molecular Probes) in 10% normal goat serum. Slides were mounted in Mowoil (Calbiochem) and imaged using a Radiance 2000 confocal laser-scanning microscope.

Live Cell Immunostaining for Flow Cytometry

Forty-eight hours post-transfection, HEK293T cell cultures were washed once with warm PBS and harvested in 1 mM EDTA-PBS. Cells were spun down at 1000 rpm in a swinging bucket centrifuge and incubated in a single cell

suspension with rabbit anti-GFP antibodies (1:20,000, Invitrogen) for 10 minutes at 37ºC + 5% CO_2 in warm culture media. After antibody incubation, cells were washed once with cold culture media, once with cold 10% normal goat serum in PBS, and then incubated in a single cell suspension with goat anti-rabbit IgG-647 Alexa Fluor (1:5000, Molecular Probes) for 25 minutes on ice. Cells were then washed once with cold 10% normal goat serum in PBS, once with ice cold PBS and were then resuspended to a single cell suspension in 1 mL of PBS. Propidium iodide (100 ng/ml, Sigma) was added for dead cell exclusion and cells were incubated on ice for 15 minutes before flow cytometry analysis.

Flow Cytometry Analysis of Surface Staining

Flow cytometry analysis was performed on the FACSort Analyzer (BD Biosciences) using CellQuest Pro 5.2 software (BD Biosciences). Detectors, compensation levels, and acquisition gates were set based on non-transfected and single color controls and a total of 20,000 cells were analyzed per condition. The resulting data were analyzed using FlowJo 8.3.3 (Tree Star Inc.). The analysis included a gating for live cells (PI-negative) and cell size, and the resulting cell population was presented in a dot plot as FL4 (Alexa 647 signal on X-axis) vs. FL1 (Venus/EYFP signal on Y-axis). Quadrants were fitted based on background signal and identical quadrants were applied to each condition in the experiment to allow for comparisons. Upper left quadrant values represent single/transfection (Venus/EYFP) positive cells, whereas upper right quadrant values represent double positive/surface labeled cells (Venus/EYFP expression

positive and Alexa 647 live stain positive) in each experimental condition. In addition, results were graphically displayed as the average percentage of surface labeled cells.

References

Abercrombie, M. (1961). The bases of the locomotory behaviour of fibroblasts. Exp Cell Res *Suppl 8*, 188-198.

Adams, N. C., Tomoda, T., Cooper, M., Dietz, G., and Hatten, M. E. (2002). Mice that lack astrotactin have slowed neuronal migration. Development *129*, 965-972.

Alahari, S. K., Lee, J. W., and Juliano, R. L. (2000). Nischarin, a novel protein that interacts with the integrin alpha5 subunit and inhibits cell migration. J Cell Biol *151*, 1141-1154.

Alahari, S. K., Reddig, P. J., and Juliano, R. L. (2004). The integrin-binding protein Nischarin regulates cell migration by inhibiting PAK. Embo J *23*, 2777-2788.

Alberts, B. (1994). Molecular biology of the cell, 3rd edn (New York: Garland Pub.).

Alder, J., Cho, N. K., and Hatten, M. E. (1996). Embryonic precursor cells from the rhombic lip are specified to a cerebellar granule neuron identity. Neuron *17*, 389-399.

Alvarez Otero, R., Sotelo, C., and Alvarado-Mallart, R. M. (1993). Chick/quail chimeras with partial cerebellar grafts: an analysis of the origin and migration of cerebellar cells. J Comp Neurol *333*, 597-615.

Anton, E. S., Marchionni, M.A., Lee, K-F., Rakic, P. (1997). Role of GGF/neuregulin signaling in interactions between migrating neurons and radial glia in the developing cerebral cortex. Development *124*, 3501-3510.

Appella, E., Weber, I. T., and Blasi, F. (1988). Structure and function of epidermal growth factor-like regions in proteins. FEBS Lett *231*, 1-4.

Blaess, S., Graus-Porta, D., Belvindrah, R., Radakovits, R., Pons, S., Littlewood-Evans, A., Senften, M., Guo, H., Li, Y., Miner, J. H., *et al.* (2004). Beta1-integrins are critical for cerebellar granule cell precursor proliferation. J Neurosci *24*, 3402-3412.

Boyden, E. S., Katoh, A., and Raymond, J. L. (2004). Cerebellum-dependent learning: The Role of Multiple Plasticity Mechanisms. Annu Rev Neurosci *27*, 581-609.

Cao, C., Lawrence, D. A., Li, Y., Von Arnim, C. A., Herz, J., Su, E. J., Makarova, A., Hyman, B. T., Strickland, D. K., and Zhang, L. (2006). Endocytic receptor LRP together with tPA and PAI-1 coordinates Mac-1-dependent macrophage migration. Embo J *25*, 1860-1870.

Cau, J., and Hall, A. (2005). Cdc42 controls the polarity of the actin and microtubule cytoskeletons through two distinct signal transduction pathways. J Cell Sci *118*, 2579-2587.

De Zeeuw, C. I., and Yeo, C. H. (2005). Time and tide in cerebellar memory formation. Curr Opin Neurobiol *15*, 667-674.

Dobyns, W. B., and Truwit, C.L. (1995). Lissencephaly and other malformations of cortical development. update. 1995 update Neuropediatrics *26*, 132-147.

Eccles, J., Ito, M., and Szentagothai, J. (1967). The Cerebellum as a neuronal machine: Springer-Verlag).

Edmondson, J. C., and Hatten, M. E. (1987). Glial-guided granule neuron migration in vitro: a high-resolution time-lapse video microscopic study. J Neurosci *7*, 1928-1934.

Edmondson, J. C., Liem, R. K., Kuster, J. E., and Hatten, M. E. (1988). Astrotactin: a novel neuronal cell surface antigen that mediates neuron- astroglial interactions in cerebellar microcultures. J Cell Biol *106*, 505-517.

Emery, G., Hutterer, A., Berdnik, D., Mayer, B., Wirtz-Peitz, F., Gaitan, M. G., and Knoblich, J. A. (2005). Asymmetric Rab 11 endosomes regulate delta recycling and specify cell fate in the Drosophila nervous system. Cell *122*, 763-773.

Etienne-Manneville, S. (2004). Actin and microtubules in cell motility: which one is in control? Traffic *5*, 470-477.

Etienne-Manneville, S., and Hall, A. (2001). Integrin-mediated activation of Cdc42 controls cell polarity in migrating astrocytes through PKCzeta. Cell *106*, 489-498.

Fan, J., and Malik, A. B. (2003). Toll-like receptor-4 (TLR4) signaling augments chemokine-induced neutrophil migration by modulating cell surface expression of chemokine receptors. Nat Med *9*, 315-321.

Fiez, J. A. (1996). Cerebellar contributions to cognition. Neuron *16*, 13-15.

Fishell, G., and Hatten, M. E. (1991). Astrotactin provides a receptor system for CNS neuronal migration. Development *113*, 755-765.

Fishman, R. B., and Hatten, M. E. (1993). Multiple receptor systems promote CNS neural migration. J Neurosci *13*, 3485-3495.

Fournier, A. E., Nakamura, F., Kawamoto, S., Goshima, Y., Kalb, R. G., and Strittmatter, S. M. (2000). Semaphorin3A enhances endocytosis at sites of receptor-F-actin colocalization during growth cone collapse. J Cell Biol *149*, 411-422.

Galaburda, A. M., and Christen, Y. (1997). Normal and abnormal development of the cortex (Berlin ; New York: Springer).

Gao, W. O., Heintz, N., and Hatten, M. E. (1991). Cerebellar granule cell neurogenesis is regulated by cell-cell interactions in vitro. Neuron *6*, 705-715.

Gao, W. Q., and Hatten, M. E. (1993). Neuronal differentiation rescued by implantation of Weaver granule cell precursors into wild-type cerebellar cortex. Science *260*, 367-369.

Gasser, U. E., and Hatten, M. E. (1990). Central nervous system neurons migrate on astroglial fibers from heterotypic brain regions in vitro. Proc Natl Acad Sci U S A *87*, 4543-4547.

Gleeson, J. G., Lin, P. T., Flanagan, L. A., and Walsh, C. A. (1999). Doublecortin is a microtubule-associated protein and is expressed widely by migrating neurons. Neuron *23*, 257-271.

Gomes, E. R., Jani, S., and Gundersen, G. G. (2005). Nuclear movement regulated by Cdc42, MRCK, myosin, and actin flow establishes MTOC polarization in migrating cells. Cell *121*, 451-463.

Gonzalez-Gaitan, M., and Stenmark, H. (2003). Endocytosis and signaling: a relationship under development. Cell *115*, 513-521.

Graus-Porta, D., Blaess, S., Senften, M., Littlewood-Evans, A., Damsky, C., Huang, Z., Orban, P., Klein, R., Schittny, J. C., and Muller, U. (2001). Beta1-class integrins regulate the development of laminae and folia in the cerebral and cerebellar cortex. Neuron *31*, 367-379.

Gregory, W. A., Edmondson, J. C., Hatten, M. E., and Mason, C. A. (1988). Cytology and neuron-glial apposition of migrating cerebellar granule cells in vitro. J Neurosci *8*, 1728-1738.

Gupton, S. L., and Waterman-Storer, C. M. (2006). Spatiotemporal feedback between actomyosin and focal-adhesion systems optimizes rapid cell migration. Cell *125*, 1361-1374.

Hatten, M. E. (1990). Riding the glial monorail: a common mechanism for glial-guided neuronal migration in different regions of the developing mammalian brain. Trends Neurosci *13*, 179-184.

Hatten, M. E. (1993). The role of migration in central nervous system neuronal development. Curr Opin Neurobiol *3*, 38-44.

Hatten, M. E. (1999). Central nervous system migration. AnnuRev Neurosci *22*, 511-539.

Hatten, M. E., Alder, J., Zimmerman, K., and Heintz, N. (1997). Genes involved in cerebellar cell specification and differentiation. Curr Opin Neurobiol *7*, 40-47.

Hatten, M. E., and Heintz, N. (1995). Mechanisms of neural patterning and specification in the developing cerebellum. Annu Rev Neurosci *18*, 385-408.

Hatten, M. E., Liem, R. K., and Mason, C. A. (1984). Two forms of cerebellar glial cells interact differently with neurons in vitro. J Cell Biol *98*, 193-204.

Hatten, M. E., and Mason, C. A. (1990). Mechanisms of glial-guided neuronal migration in vitro and in vivo. Experientia *46*, 907-916.

Hatten, M. E. a. C. A. M. (1986). Neuron-astroglia interactions *in vitro* and *in vivo*. Trends Neurosci, 1-7.

Hirotsune, S., Fleck, M. W., Gambello, M. J., Bix, G. J., Chen, A., Clark, G. D., Ledbetter, D. H., McBain, C. J., and Wynshaw-Boris, A. (1998). Graded reduction of Pafah1b1 (Lis1) activity results in neuronal migration defects and early embryonic lethality. Nat Genet *19*, 333-339.

Husmann, K., Faissner, A., and Schachner, M. (1992). Tenascin promotes cerebellar granule cell migration and neurite outgrowth by different domains in the fibronectin type III repeats. J Cell Biol *116*, 1475-1486.

Ito, M. (1984). Cerebellum and Neural Control: Raven Press).

Jaffe, A. B., and Hall, A. (2005). Rho GTPases: biochemistry and biology. Annu Rev Cell Dev Biol *21*, 247-269.

Kaksonen, M., Toret, C. P., and Drubin, D. G. (2006). Harnessing actin dynamics for clathrin-mediated endocytosis. Nat Rev Mol Cell Biol *7*, 404-414.

Kamiguchi, H., and Lemmon, V. (2000). Recycling of the cell adhesion molecule L1 in axonal growth cones. J Neurosci *20*, 3676-3686.

Kamiguchi, H., Long, K. E., Pendergast, M., Schaefer, A. W., Rapoport, I., Kirchhausen, T., and Lemmon, V. (1998). The neural cell adhesion molecule L1 interacts with the AP-2 adaptor and is endocytosed via the clathrin-mediated pathway. J Neurosci *18*, 5311-5321.

Keleman, K., Ribeiro, C., and Dickson, B. J. (2005). Comm function in commissural axon guidance: cell-autonomous sorting of Robo in vivo. Nat Neurosci *8*, 156-163.

Kruchten, A. E., and McNiven, M. A. (2006). Dynamin as a mover and pincher during cell migration and invasion. J Cell Sci *119*, 1683-1690.

Kuhar, S. G., Feng, L., Vidan, S., Ross, M. E., Hatten, M. E., and Heintz, N. (1993). Changing patterns of gene expression define four stages of cerebellar granule neuron differentiation. Development *117*, 97-104.

Kuzniecky, R. I. (1994). Magnetic resonance imaging in developmental disorders of the cerebral cortex. Epilepsia *35 Suppl 6*, S44-56.

Lawson, M. A., and Maxfield, F. R. (1995). Ca(2+)- and calcineurin-dependent recycling of an integrin to the front of migrating neutrophils. Nature *377*, 75-79.

Le Roy, C., and Wrana, J. L. (2005). Clathrin- and non-clathrin-mediated endocytic regulation of cell signalling. Nat Rev Mol Cell Biol *6*, 112-126.

Lee, J. S., Chang, M. I., Tseng, Y., and Wirtz, D. (2005). Cdc42 mediates nucleus movement and MTOC polarization in Swiss 3T3 fibroblasts under mechanical shear stress. Mol Biol Cell *16*, 871-880.

Lim, K. P., and Hong, W. (2004). Human Nischarin/imidazoline receptor antisera-selected protein is targeted to the endosomes by a combined action of a PX domain and a coiled-coil region. J Biol Chem *279*, 54770-54782.

Maldonado-Baez, L., and Wendland, B. (2006). Endocytic adaptors: recruiters, coordinators and regulators. Trends Cell Biol *16*, 505-513.

Marsh, M. (2001). Endocytosis (Oxford: Oxford University Press).

Mason, C. A., Edmondson, J. C., and Hatten, M. E. (1988). The extending astroglial process: development of glial cell shape, the growing tip, and interactions with neurons. J Neurosci *8*, 3124-3134.

Matafora, V., Paris, S., Dariozzi, S., and de Curtis, I. (2001). Molecular mechanisms regulating the subcellular localization of p95-APP1 between the endosomal recycling compartment and sites of actin organization at the cell surface. J Cell Sci *114*, 4509-4520.

Maxfield, F. R., and McGraw, T. E. (2004). Endocytic recycling. Nat Rev Mol Cell Biol *5*, 121-132.

Millet, S., Bloch-Gallego, E., Simeone, A., and Alvarado-Mallart, R. M. (1996). The caudal limit of Otx2 gene expression as a marker of the midbrain/hindbrain boundary: a study using in situ hybridisation and chick/quail homotopic grafts. Development *122*, 3785-3797.

Miyashita, Y., and Ozawa, M. (2007). Increased internalization of p120-uncoupled E-cadherin and a requirement for a dileucine motif in the cytoplasmic domain for endocytosis of the protein. J Biol Chem.

Morales, D., and Hatten, M. E. (2006). Molecular markers of neuronal progenitors in the embryonic cerebellar anlage. J Neurosci *26*, 12226-12236.

O'Shea, K. S., Rheinheimer, J.S.T. , Dixit, V.M. (1990). Deposition and role of thromobospondin in the histogenesis of the cerebellar cortex. J Cell Biol *110*, 1275-1283.

Palay, S. L., and Chan-Palay, S. (1974). The Cerebellar Cortex: cytology and organization (New York: Springer-Verlag).

Palazzo, A. F., Joseph, H. L., Chen, Y. J., Dujardin, D. L., Alberts, A. S., Pfister, K. K., Vallee, R. B., and Gundersen, G. G. (2001). Cdc42, dynein, and dynactin regulate MTOC reorientation independent of Rho-regulated microtubule stabilization. Curr Biol *11*, 1536-1541.

Panicker, A. K., Buhusi, M., Erickson, A., and Maness, P. F. (2006). Endocytosis of beta1 integrins is an early event in migration promoted by the cell adhesion molecule L1. Exp Cell Res *312*, 299-307.

Pellinen, T., and Ivaska, J. (2006). Integrin traffic. J Cell Sci *119*, 3723-3731.

Pierini, L. M., Lawson, M. A., Eddy, R. J., Hendey, B., and Maxfield, F. R. (2000). Oriented endocytic recycling of alpha5beta1 in motile neutrophils. Blood *95*, 2471-2480.

Powell, S. K., Rivas, R. J., Rodriguez-Boulan, E., and Hatten, M. E. (1997). Development of polarity in cerebellar granule neurons. J Neurobiol *32*, 223-236.

Raftopoulou, M., and Hall, A. (2004). Cell migration: Rho GTPases lead the way. Dev Biol *265*, 23-32.

Rakic, P. (1971). Neuron-glia relationship during granule cell migration in developing cerebellar cortex. A Golgi and electronmicroscopic study in Macacus Rhesus. J Comp Neurol *141*, 283-312.

Rakic, P., Stensas, L. J., Sayre, E., and Sidman, R. L. (1974). Computer-aided three-dimensional reconstruction and quantitative analysis of cells from serial electron microscopic montages of foetal monkey brain. Nature *250*, 31-34.

Ramon y Cajal, S. (1911). Histology of the Nervous System, Vol I (New York: Oxford University Press).

Redd, M. J., Cooper, L., Wood, W., Stramer, B., and Martin, P. (2004). Wound healing and inflammation: embryos reveal the way to perfect repair. Philos Trans R Soc Lond B Biol Sci *359*, 777-784.

Ridley, A. J., Schwartz, M. A., Burridge, K., Firtel, R. A., Ginsberg, M. H., Borisy, G., Parsons, J. T., and Horwitz, A. R. (2003). Cell migration: integrating signals from front to back. Science *302*, 1704-1709.

Rio, C., Rieff, H. I., Qi, P., Khurana, T. S., and Corfas, G. (1997). Neuregulin and erbB receptors play a critical role in neuronal migration. Neuron *19*, 39-50.

Rivas, R. J., and Hatten, M. E. (1995). Motility and cytoskeletal organization of migrating cerebellar granule neurons. J Neurosci *15*, 981-989.

Scheiffele, P., Fan, J., Choih, J., Fetter, R., and Serafini, T. (2000). Neuroligin expressed in nonneuronal cells triggers presynaptic development in contacting axons. Cell *101*, 657-669.

Shirasaki, R., and Pfaff, S. L. (2002). Transcriptional codes and the control of neuronal identity. Annu Rev Neurosci *25*, 251-281.

Sidman, R. L., Rakic, P. (1973). Neuronal migration with special reference to developing human brain: a review. Brain Res *62*, 1-35.

Smith, D. S., Niethammer, M., Ayala, R., Zhou, Y., Gambello, M. J., Wynshaw-Boris, A., and Tsai, L. H. (2000). Regulation of cytoplasmic dynein behaviour and microtubule organization by mammalian Lis1. Nat Cell Biol *2*, 767-775.

Solecki, D. J., Model, L., Gaetz, J., Kapoor, T. M., and Hatten, M. E. (2004). Par6alpha signaling controls glial-guided neuronal migration. Nat Neurosci *7*, 1195-1203.

Sorkin, A. (2004). Cargo recognition during clathrin-mediated endocytosis: a team effort. Curr Opin Cell Biol *16*, 392-399.

Stitt, T. N., and Hatten, M. E. (1990). Antibodies that recognize astrotactin block granule neuron binding to astroglia. Neuron *5*, 639-649.

Symons, M., and Rusk, N. (2003). Control of vesicular trafficking by Rho GTPases. Curr Biol *13*, R409-418.

Szymkiewicz, I., Shupliakov, O., and Dikic, I. (2004). Cargo- and compartment-selective endocytic scaffold proteins. Biochem J *383*, 1-11.

Thelen, K., Kedar, V., Panicker, A. K., Schmid, R. S., Midkiff, B. R., and Maness, P. F. (2002). The neural cell adhesion molecule L1 potentiates integrin-dependent cell migration to extracellular matrix proteins. J Neurosci *22*, 4918-4931.

Tzima, E., Kiosses, W. B., del Pozo, M. A., and Schwartz, M. A. (2003). Localized cdc42 activation, detected using a novel assay, mediates microtubule organizing center positioning in endothelial cells in response to fluid shear stress. J Biol Chem *278*, 31020-31023.

Watanabe, T., Noritake, J., and Kaibuchi, K. (2005). Regulation of microtubules in cell migration. Trends Cell Biol *15*, 76-83.

Wingate, R. J. (2001). The rhombic lip and early cerebellar development. Curr Opin Neurobiol *11*, 82-88.

Wingate, R. J., and Hatten, M. E. (1999). The role of the rhombic lip in avian cerebellum development. Development *126*, 4395-4404.

Zheng, C. (1996). Astrotactin and Glial-Guided Neuronal Migration. Doctoral Dissertation, The Rockefeller University.

Zheng, C., Heintz, N., and Hatten, M. E. (1996). CNS gene encoding astrotactin, which supports neuronal migration along glial fibers. Science *272*, 417-419.

Zmuda, J. F., and Rivas, R. J. (1998). The Golgi apparatus and the centrosome are localized to the sites of newly emerging axons in cerebellar granule neurons in vitro. Cell Motil Cytoskeleton *41*, 18-38.